SANDIA REPORT

SAND96–0561 • UC–721
Unlimited Release
Printed April 1997

Modeling Brine Inflow to Room Q: A Numerical Investigation of Flow Mechanisms

Geoff A. Freeze, Tracy L. Christian-Frear, Stephen W. Webb

Approved for public release; distribution is unlimited.

Sandia National Laboratories

SF2900Q(8-81)

Modeling Brine Inflow To Room Q: A Numerical Investigation of Flow Mechanisms

Geoff A. Freeze
INTERA Inc.
1650 University Blvd. NE, Suite 300
Albuquerque, New Mexico 87102

Tracy L. Christian-Frear
Stephen W. Webb
Geohydrology Department
Sandia National Laboratories
P.O. Box 5800
Albuquerque, New Mexico 87185-1324

ABSTRACT

A hydrologic modeling study was performed to gain insight into the flow mechanisms around Room Q. A summary of hydrologic and structural data and of predictive fluid flow models from Room Q are provided. Six years of measured data are available from the time of excavation. No brine accumulation in Room Q was measured in the first two years following excavation. However, there is considerable uncertainty associated with this early-time data due to inadequate sealing of the room. Brine may have been lost to evaporation or it may have flowed into newly created disturbed rock zone (DRZ) porosity resulting from excavation. Non-zero brine accumulation rates were measured from 2-5 years, but brine accumulation within the room dropped to zero after 5.5 years. A conceptual model for brine inflow to Room Q was developed which assumes far-field Darcy flow combined with an increasing DRZ pore volume. Numerical simulations employed TOUGH28W and used predictive DRZ porosity increase with time from SPECTROM-32 rock deformation simulations. Simulated brine inflow showed good agreement with measured brine accumulation rates for the first five years. Two important conclusions were drawn from the simulation results: (1) early-time brine inflow to the room can be reduced to zero if the DRZ pore volume increases with time, and (2) brine accumulation (inflow) rates from 2 to 5 years suggest a far-field permeability of 5×10^{-22} m^2 with a bulk rock compressibility of 5.4×10^{-12} Pa^{-1}. The early-time brine inflow to the

room is very sensitive to the DRZ pore volume. However, because of uncertainty in the measured brine accumulation rates and the DRZ pore volume, it is not possible to make specific conclusions regarding the volume of brine that fills newly created DRZ porosity relative to the volume of brine that is lost to evaporation. Both mechanisms are capable of eliminating all early-time brine accumulation in the room. The reduction in brine accumulation after 5.5 years was not simulated. The most plausible explanation for the observed reduction in brine accumulation after 5.5 years is that the brine is leaking out of the room through fractures under the seal before it can be measured. Leakage beneath the seal was confirmed by recent dyed-brine tracer testing. The method for increasing DRZ porosity with time used in the TOUGH28W simulations may be too computationally intensive for use in WIPP Performance Assessment calculations. However, a simplified representation of this phenomena can be implemented in Performance Assessment calculations through the use of a fixed porosity DRZ region with a reduced initial brine saturation.

DISCLAIMER

Portions of this document may be illegible in electronic image products. Images are produced from the best available original document.

DISCLAIMER

ACKNOWLEDGEMENTS

CONTENTS

Figures

Tables

1.0 INTRODUCTION

The presence of brine in and around WIPP waste disposal rooms has several potential effects on repository performance. Most importantly, brine may enhance gas generation and repository pressurization, resulting in an increased driving force for radionuclide and/or VOC-bearing gas movement away from the repository. It is therefore important to properly characterize the mechanisms for brine movement around the repository.

For the purposes of performance assessment, brine inflow must be predicted on a disposal-room and repository scale over a 10,000-year time period. Uncertainties in the brine inflow mechanisms, including the applicability of a Darcy flow model to flow in low permeability salt, have been described in previous reports (Nowak et al., 1988; Lappin et al., 1989). Some of these uncertainties are:

- The effect of the disturbed rock zone (DRZ)
- Uncertainty in the flow parameters (permeability, far-field pore pressure)
- The effect of host rock heterogeneity
- The effect of excavation scale (upscaling flow from borehole- to room-scale)

Room Q testing (Nowak, 1990) was designed to address some of these uncertainties. Room Q is a 109 m long cylindrical room with a 2.9 m diameter which was drilled horizontally in the WIPP underground. Brine accumulation volumes in the room and room humidity were measured to estimate brine inflow. Geophysical measurements of fluid saturation and porosity, and room closure measurements of mechanical deformation were made to characterize the DRZ. Hydraulic tests were performed to determine permeability and near- and far-field pore pressures. Room Q barometric pressure, temperature, relative humidity, closure, resistivity, and brine accumulation measurements are presented in Jensen et al. (1993a), Jensen et al. (1993b), Jensen et al. (1996). Domski et al. (1996) present hydraulic test interpretations to determine permeability and pore pressures. A discussion of the geophysical surveys is presented in Borns (Appendix A1). Preliminary flow model analyses for Room Q were presented by McTigue (Appendix A2) and McTigue (Appendix A3).

This report reviews the available Room Q data and previous model interpretations to develop a conceptual model for brine inflow to Room Q. Structural and hydrologic data and observations

1

are examined and correlated to develop the conceptual model. Numerical simulations of brine inflow based upon the conceptual model are compared with measured brine accumulation in the room. Simulation results help to identify relevant mechanisms and parameters which influence brine inflow to Room Q or any similar excavation. Finally, recommendations are made for brine flow modeling in performance assessment calculations.

1.1 Background

The WIPP is located in southeastern New Mexico in the Delaware Basin, which contains several Permian-age sedimentary deposits. The WIPP repository lies in the lower portion of the Salado Formation at a depth of approximately 655 m below land surface (Figure 1-1). The Salado Formation consists of a large number of beds of relatively pure halite and impure halite containing interspersed clay and polyhalite. Thin interbeds of anhydrite, with associated underlying clay seams, are present in laterally continuous layers. The thicker, laterally extensive anhydrite interbeds have been designated as numbered Marker Beds (MB). Thinner units are designated as numbered Map Units (MU). The repository horizon is separated by a few meters of halite from the overlying Anhydrite a (MU-8), Anhydrite b (MU-11), and Marker Bed 138 and the underlying Marker Bed 139 (Figure 1-1). Repository excavation follows a single stratigraphic horizon, using the orange marker band (OMB), a distinctive stratum, as a reference. As a result, the repository dips gently (generally less than 1° slope) to the southeast, following the regional dip of the Salado Formation.

The underground facility consists of a waste storage area at the south end and an experimental area at the north end (Figure 1-2). The waste storage area is designed to have eight waste disposal panels, each of which will contain seven rooms. Each rectangular disposal room is approximately 4 m high, 10 m wide, and 91 m long. Room Q is a cylindrical test room, 109 m in length with a 2.9 m diameter. The excavated volume of Room Q is about one fifth of the excavated volume of a disposal room. Room Q was excavated in an isolated, undisturbed portion of the experimental area (Figure 1-2), and follows the same stratigraphy as the waste panels (Figure 1-3). The orange marker band (OMB), a distinctive reference stratum, was used to establish the grade for the boring operations.

A disturbed rock zone (DRZ) is present around WIPP excavations (Nowak and McTigue, 1987; Stormont et al., 1987; Borns and Stormont, 1988; 1989; Beauheim et al., 1993). Within the DRZ, time-dependent deformation of the salt occurs as it creeps toward an excavation, resulting in

W   E

Santa Rosa
and Gatuña
Formations

Ground
Surface

Feet   Meters

Dewey Lake
Red Beds

500

200

Rustler Formation

1000

Upper Member

400

Salado
Formation

McNutt Potash Zone

1500

2000

600

WIPP

Lower Member

2500

800

3000

WIPP
Repository
Horizon

MB138
Anhydrite a
Anhydrite b

Sea
Level

MB139

3500

1000

Anhydrite c

Castile Formation

MB140

4000

1200

0   5000'

Bell Canyon Formation

4500

1400

0   1500m

Horizontal Scale
Note 7.5x Vertical Exaggeration

Figure 1-1. Regional WIPP stratigraphy.
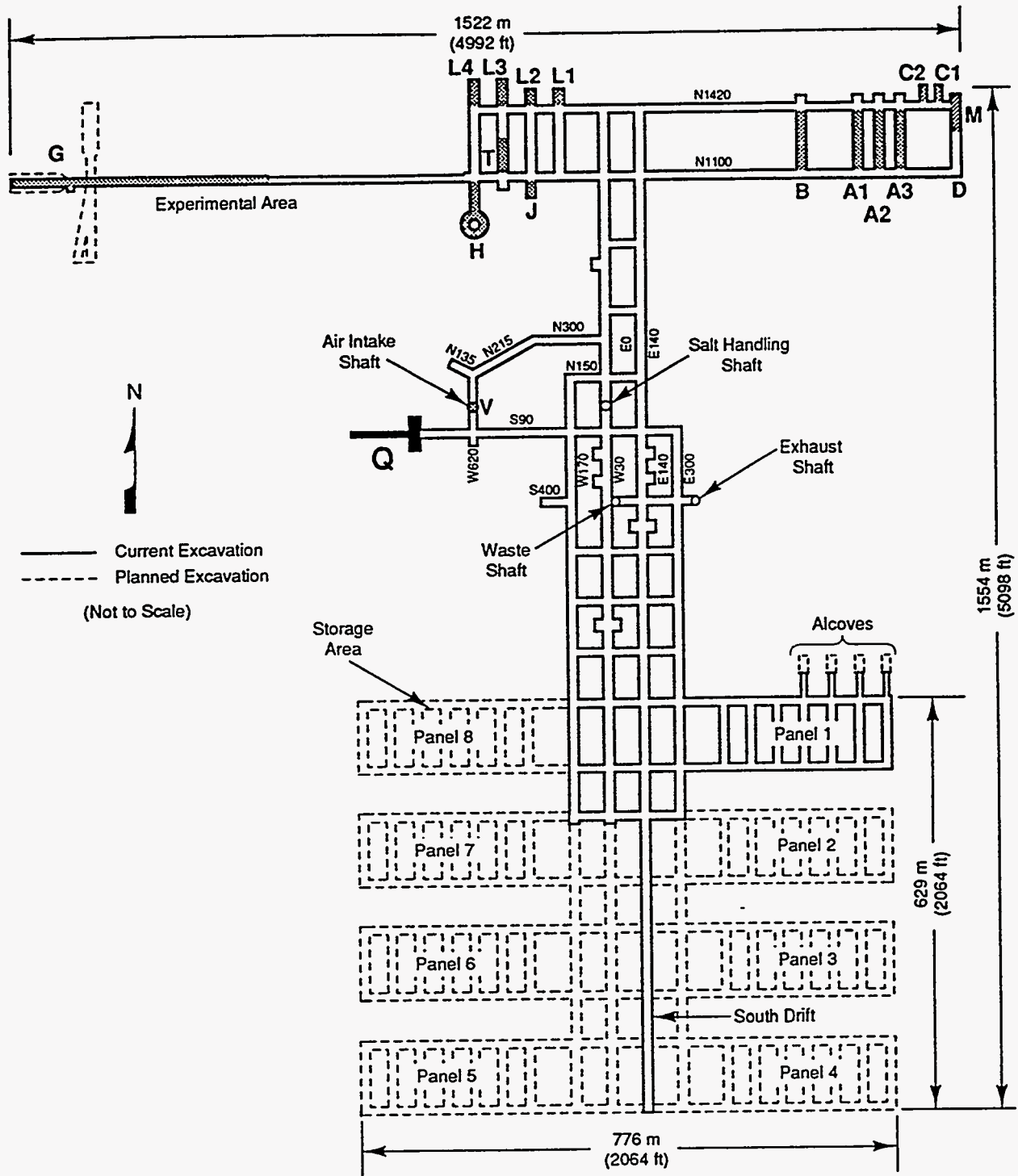
Figure 1-2. Location of Room Q.

TRI-6330-129-6

4.
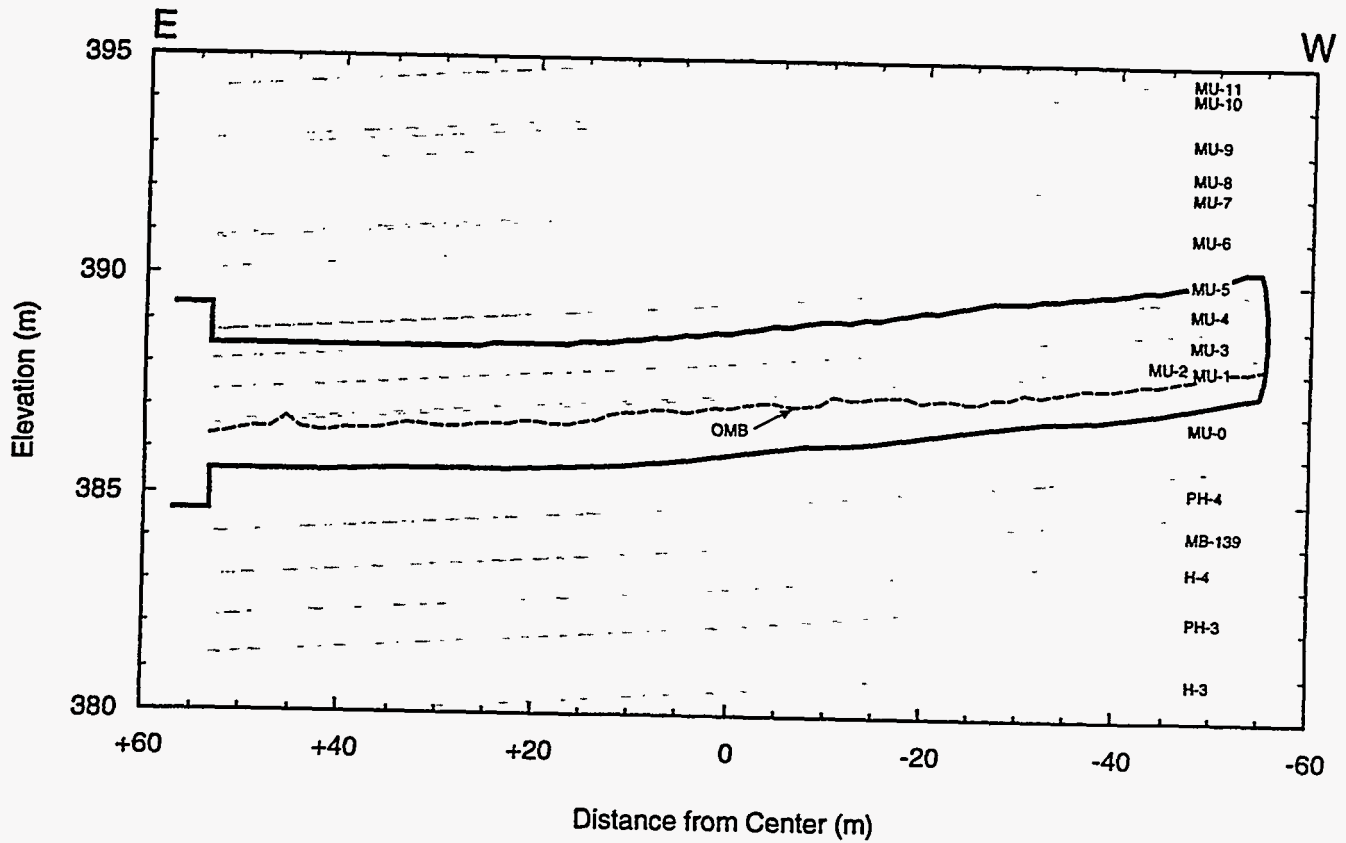
Figure 1-3. As-built profile to Room Q with implied stratigraphy
(vertical exaggeration approximately 4.5:1).

5

local fracturing and possible dilatation within the salt. This deformation is presumed to increase the intrinsic permeability and porosity within the DRZ. Also, elastic and inelastic changes in pore volume, driven by excavation-related stress redistribution, may cause variations in the near-field fluid pressure distribution that are superimposed on fluid-pressure gradients associated with brine flow toward the excavation. Dilatation, drying, and exsolution of dissolved gas that occurs naturally in Salado brines may lead to reduced brine saturations within the DRZ. The DRZ is expected to undergo time-dependent changes in properties, with disturbed halite eventually healing to a final state equivalent to undisturbed halite (Lappin et al., 1989). The circular geometry of Room Q was designed to reduce the excavation-induced rock damage. However, this effect cannot be eliminated completely. Increased permeability and porosity, decreased pore-fluid pressure, and partially saturated conditions all influence fluid flow within the DRZ.

1.2 History of Room Q Development

A detailed description of the development and instrumentation of Room Q is presented in Jensen et al. (1993a) and Jensen et al. (1993b). A chronologic summary is listed in Table 1-1. Room Q was bored in a single pass between July 12, 1989 and August 8, 1989 to a total length of about 109 m. A temporary brattice cloth and aluminum seal was installed in October, 1989 to reduce moisture loss due to evaporation from Room Q. The sealed length of Room Q was 104 m with the temporary single seal in place. In March, 1990 a similar cloth-and-aluminum two-seal system replaced the single seal. The sealed length of the room was 102 m with the double seal in place. In March, 1991, a permanent double-seal system was installed, with a sealed room length of 102 m.

Table 1-1. Chronology of Activities in Room Q

Date	Test Day (from start of excavation)	Activity
July 12, 1989	0	Start boring
August 8, 1989	27	Finish boring (excavated length = 109 m)
October 24, 1989	104	Install temporary single seal
March 13, 1990	244	Install temporary double seal
June 29, 1990*	352*	Access to room limited
March 28, 1991	624	Install permanent double seal
July 6, 1995	2185	Data collection discontinued (seal was deflated in September 1995)

*approximate date

6

Data was periodically collected from Room Q, consisting of both manual and automated measurements. Data includes barometric pressure, temperature, relative humidity, closure, resistivity and accumulated brine mass measurements (see Section 2.0).

1.3 WIPP Fluid Flow Conceptual Models

Two conceptual models for brine movement through the Salado Formation have been proposed, the far-field Darcy flow model and the redistribution model. Under Darcy flow, brine may flow in response to pressure gradients and gravitational forces, with the halite acting as an equivalent porous medium in both the near- and far-field (Bredehoeft, 1988). The redistribution model, proposed by McTigue et al. (1989), suggests that the Salado Formation contains isolated pores of near-lithostatic brine that become interconnected in response to shear deformation and dilatation around an opening. In this model, connected porosity is present only in the near-field. Deal and Roggenthen (1991) present a variation of the redistribution model. They suggest that brine is available only from compaction of undercompacted clay seams that are directly connected to the disposal rooms in response to excavation, and that brine does not flow into the repository from the adjacent halite (or non-clay interbeds) or from the far field.

Room Q experimental results to date make it difficult to distinguish between the two conceptual models. The Salado Formation salt units have very low permeabilities (which implies very little interconnected pore space). Although there is uncertainty as to whether the Darcy flow assumptions are valid at such low permeabilities and flow velocities, far-field Darcy flow models have been successfully applied to predict Salado fluid flow to boreholes (Nowak and McTigue, 1987; Nowak et al., 1988; Beauheim et al., 1991; Beauheim et al., 1993; McTigue, 1993). In some applications, storativity values implied from Darcy flow models have not always been consistent with measured rock compressibilities and porosities (McTigue, 1993). The redistribution model has been used in analysis of brine inflow to small (borehole) scale excavations (Deal et al., 1989; Deal et al., 1991). However, no published detailed quantitative redistribution model exists and the absence of far-field contributions to flow cannot be confirmed.

Room Q was initially designed to identify the conceptual model for brine inflow. Unfortunately, there is considerable uncertainty in the measured brine accumulation data due to inadequate air seals in early-time, possible brine leakage around the seals, and the fact that the experiment was discontinued before the late-time reduction in brine accumulation could be

thoroughly investigated. Numerical simulations (Section 4.0) were performed to evaluate the flow model, however, due to the uncertainty in the measured brine accumulation, a conclusive differentiation between specific flow models cannot be made.

2.0 SUMMARY OF ROOM Q DATA

Data collected from Room Q includes barometric pressure, temperature, relative humidity, closure, resistivity and accumulated brine mass. Measurement locations are shown in Figure 2-1. Evaporation from brine-filled pans located between the seals was also measured. All of the Room Q data and the measurement techniques are described in detail in Jensen et al. (1993b) and Jensen et al. (1996). Unless otherwise stated, these two documents provide the references for the data summaries in the following sections.

2.1 Brine Accumulation Data

Brine accumulation in Room Q was measured by two methods. At early time (prior to installation of the permanent seal at day 624) when brine accumulation was minimal, sponges were used to absorb the brine that had accumulated on the floor. Later measurements were made by vacuuming brine on the floor into collection flasks. The mass of brine collected was converted to a volume using an assumed density of 1230 kg/m^3. A summary of brine collection from Room Q is given in Table 2-1.

Table 2-1. Brine Accumulation Measurements in Room Q

Date	Test Day (from start of excavation)	Cumulative Brine Volume (liters)	Calculated Brine Accumulation Rate (ml/day)
July 12, 1989	0	0.0	0.0
June 19, 1990	342	0.0	0.0
March 11, 1991	607	1.2	4.7
May 28, 1991	685	1.5	3.8
October 1, 1991	811	18.9	137.7
March 10, 1992	972	57.2	237.7
October 7, 1992	1183	106.0	231.4
March 4, 1993	1331	138.2	218.0
November 17, 1993	1589	173.3	135.8
May 9, 1994	1762	202.6	169.7
October 17, 1994	1923	203.1	2.7
April 13, 1995	2101	203.4	1.7
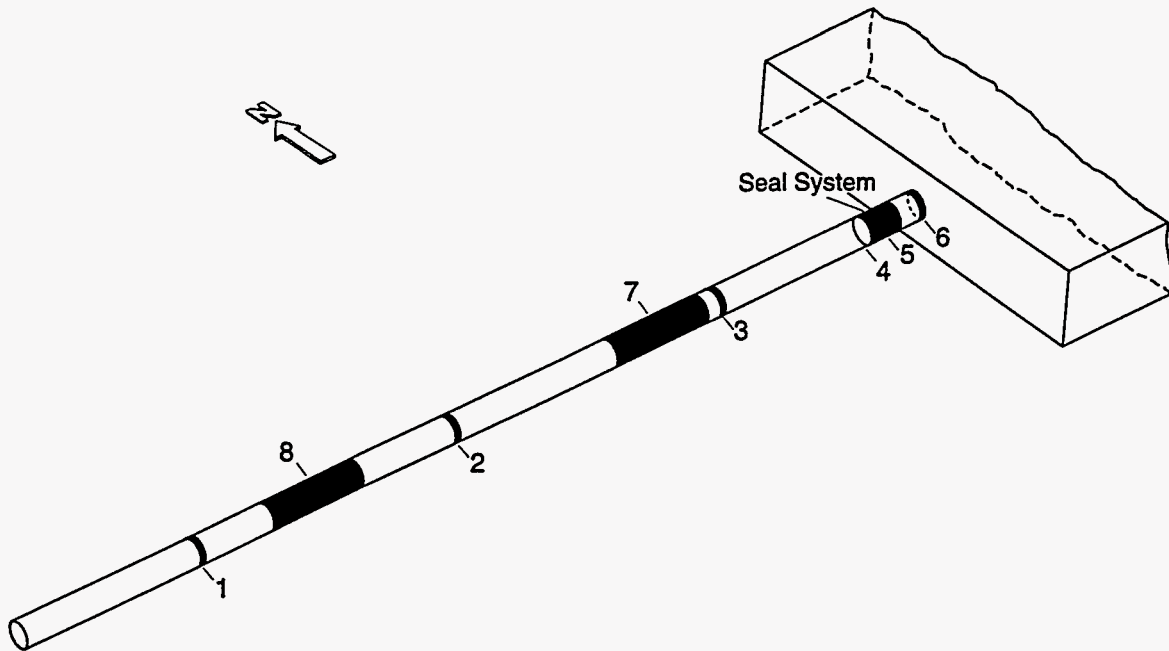
1. Closure, Relative Humidity and Thermal Measurements
2. Closure, Relative Humidity and Thermal Measurements
3. Closure, Relative Humidity and Thermal Measurements
4. Rleative Humidity, Thermal and Pressure Measurements
5. Relative Humidity and Thermal Measurements
6. Closure, Relative Humidity, Thermal and Pressure Measurements
7. Resistivity Array 1
8. Resistivity Array 2

TRI-6119-254-0

Figure 2-1. Primary Room Q measurement stations.

Measured brine accumulation was minimal for about the first two years after excavation. Brine may have been filling up newly-created DRZ porosity during this time or it may have been lost to evaporation in the room, particularly if the temporary seal systems were ineffective. For the next three years (from day 685 to day 1762), brine accumulation rates ranged from 135-237 ml/day (0.05-0.09 m^3/yr). By day 1923, measured brine accumulation had decreased to near-zero. There is some evidence (i.e., brine observed in the airlock outside the seal) that this late-time reduction in brine accumulation was due to brine flowing beneath the room seal through fractures in the floor before it could be measured. Two experiments, a gas tracer test and a brine tracer test, were performed to evaluate the potential for leakage around the seals.

The gas tracer test was performed during the first half of 1995 (starting at approximately day 2000) using sulfur hexafluoride (SF_6) as the tracer. The test is described in Jensen et al. (1996). SF_6 is injected into Room Q to a concentration of about 40 ppb. The concentration of SF_6 in Room Q decreased from an initial value of 40 ppb to about 30 ppb over a 200 day period. This decrease was consistent with diffusion through the DRZ to the airlock, and no conclusions about flow (i.e., DRZ permeability) could be made.

The brine tracer test was performed in April of 1995 and is also described in Jensen et al. (1996). Fluorescein-dyed brine was introduced into a standpipe inside the room near the seal, and a vacuum was applied outside the room in the airlock between the seals. For a 20 day period, a 200 ml/day flow rate was maintained under the vacuum-induced gradient. The dye test confirmed observations that brine could leak out of the room through fractures under the seals. Scoping calculations, which assume gravity-driven drainage due to the dip of the room, predict that about 30 ml/day could leak through the DRZ under the seals (for an assumed DRZ thickness of 0.55m and permeability of 10^{-15} m^2). Depending on assumptions about flow geometry, the leak rate could be as high as 100 ml/day with a gravity-driven gradient and a permeability of 10^{-15} m^2. Higher leak rates would require a larger DRZ permeability, a larger gradient, and/or a different flow mechanism.

Relative humidity measurements were collected outside the room, between the seals, and at various locations within the room. Jensen et al. (1993b) question the validity of some of the relative humidity measurements; however, some general conclusions can be made. Outside the room, the measured relative humidity varied from 20-45%, depending on the temperature. During January (around days 180, 550, etc.), the temperature outside Room Q was about 22°C and the measured relative humidity was about 20%. During August (around days 380, 740, etc.), the temperature

11

outside Room Q was about 30°C and the measured relative humidity was about 45%. Between the seals and inside the room, seasonal temperature fluctuations were smaller, ranging from 26-28°C. Relative humidity measurements between the temporary double seals (which were installed on day 244) began at day 260, roughly coincident with the installation of brine evaporation pans between the seals at day 282 (approximate date). The brine pans were designed to maintain a relative humidity of 75-85% between the seals, equivalent to the relative humidity of air in equilibrium with brine (CRC Press, 1985; p. E-1). The relative humidity between the seals rose from about 25% at day 260 to 70-80% by day 300. During this time the calculated evaporation rate from the brine pans decreased from about 200 ml/day (at day 282) to about 100 ml/day (at approximately day 340). By day 600, the evaporation rate was about 50 ml/day and by day 1600, the evaporation rate was about 20 ml/day. These data suggest that the air between the seals did not become saturated until after the introduction of the brine pans. Relative humidity measurements inside Room Q began at about day 150. The relative humidity inside the room rose from about 60% at day 150 to 70-80% by day 300. These measured values suggest that the room humidity was buffered somewhat by the airlock between the seals.

2.2 Hydrologic Data

Hydrologic data specific to the Salado Formation in the vicinity of Room Q is presented in Domski et al. (1996). Hydraulic testing was performed in 15 boreholes in the Room Q access drift both before and after Room Q mining. Only certain boreholes produced interpretable data. From these tests, interpreted permeabilities ranged from 10^{-23} to 10^{-20} m^2 and specific storage ranged from approximately 10^{-8} to 10^{-6} Pa^{-1}. Pore pressures ranged from 2 MPa near the room to 10 MPa at a distance of 10 m from the room. Interpreted properties were determined for both halite and anhydrite and included both excavation-disturbed and undisturbed salt.

General information regarding the hydrologic properties of the Salado Formation can be found in Sandia WIPP Project (1992), Stoelzel et al. (1995), and Freeze et al. (1995a). Extensive hydraulic testing has been performed to determine the hydrologic properties for the Salado Formation halite and anhydrite under both undisturbed and excavation-disturbed conditions (Beauheim et al., 1991; Beauheim et al., 1993; Domski et al., 1996). Most of the reported values for permeability and rock compressibility are based on interpretations of hydraulic tests. Interpretation methods attempt to determine a combination of hydraulic conductivity (K) and specific storage (S_s) that best reproduces the measured test data. To reproduce pressure response

12

data, independent of flow rate, the ratio of K to S_s (the hydraulic diffusivity) is important. To reproduce flow rate data, independent of pressure response, the product of K and S_s is important. Several non-unique combinations of K and S_s may reproduce the data, so solution techniques typically involve specifying a best-estimate value for S_s and determining K. Uncertainties can be reduced by reproducing both pressure and flow data.

In the Salado Formation, K is strongly dependent on permeability, while S_s is strongly dependent on rock compressibility. Because only flow rate (brine accumulation) data is available for Room Q, the fit of simulation results to observed data will be dependent on the product of K and S_s (or alternatively, the product of permeability and rock compressibility).

In-situ permeability testing indicates a large variability in intrinsic permeability, ranging from less than 10^{-23} m^2 for pure halite to as high as 10^{-18} m^2 for anhydrite interbeds (Beauheim et al., 1991; Howarth et al., 1991; Beauheim et al., 1993). For this study, a baseline halite permeability of 5×10^{-22} m^2 was selected . Sensitivity simulations examined a range from 2.5×10^{-22} m^2, used as a mean value in the most recent performance assessment calculations (Stoelzel et al., 1995), to 1×10^{-21} m^2, used as a baseline value by Freeze et al. (1995a). The porosity of the undisturbed Salado Formation (for both the halite beds and the anhydrite interbeds) is estimated to be 0.01 (Sandia WIPP Project, 1992).

The selected baseline permeability and porosity values are considered representative of undisturbed (i.e., far-field) conditions. The baseline DRZ permeability was selected to be 1×10^{-15} m^2, as specified in Stoelzel et al. (1995). The DRZ porosity was assumed to increase with time, as described in Section 4.3. Extensive sensitivity simulations were performed on the DRZ porosity and permeability.

The baseline halite bulk rock compressibility was 5.4×10^{-12} Pa^{-1}. The corresponding specific storage of 9.3×10^{-8} m^{-1} is approximately the same as the value used for performance assessment (Sandia WIPP Project, 1992). The baseline bulk compressibility for the DRZ was assumed to be one order of magnitude larger than for halite. A sensitivity simulation used a halite compressibility of 5.4×10^{-11} Pa^{-1} (specific storage of 6.6×10^{-7} m^{-1}).

Based on in-situ testing results, the far-field pore pressure was assumed to be 12.5 MPa, which is between hydrostatic (6 MPa) and lithostatic (15 MPa) (Sandia WIPP Project, 1992). Pore

13

pressures are much lower within the first few meters of an excavation due to depressurization resulting from brine flow toward the excavation and/or to dilatation of pores caused by high deviatoric stresses near the excavation (Beauheim et al., 1991).

Baseline model values selected for important flow properties are summarized in Table 2-2. Domski et al. (1996) suggest a permeability of 3×10^{-23} m^2 and a rock compressibility of 3×10^{-11} Pa^{-1} for undisturbed (far-field) Salado halite. These values, which will be a part of the current performance assessment calculations, are both an order of magnitude different from the baseline model values selected in Table 2-2. Simulations presented in Section 4.4 will demonstrate that, because the product of permeability and rock compressibility is similar for both sets of values, brine inflow will be similar under either set of values.

Table 2-2. Baseline Hydrologic Properties For the DRZ and the Intact Salado Formation

Property	DRZ	Intact Salado
Permeability (m^2)	1×10^{-15}	5×10^{-22}
Initial Porosity	$0.01^{(1)}$	0.01
Bulk Compressibility (Pa^{-1})	5.4×10^{-11}	5.4×10^{-12}
Specific Storage (m^{-1})	6.6×10^{-7}	9.3×10^{-8}
Initial Pore Pressure (MPa)	0.1	12.5

[1] The simulated DRZ porosity increases with time.

The Salado brine had a simulated fluid density of 1200 kg/m^3 and a compressibility of 2.5×10^{-10} Pa^{-1}. The 2.5% difference between the simulated fluid density and the measured fluid density is insignificant relative to other uncertainties in the measured data.

2.3 Room Closure Data

Closure of Room Q, due to salt creep and dilation of the DRZ, was measured essentially from the time of excavation. At day 300, measured room closure ranged from 30 mm near the mouth of the room (closest to the instrumentation alcove and access tunnel) to 20 mm near the farthest excavated portion of the room. By day 1400, measured room closure ranged from 60 mm near the mouth to 45 mm near the end. By day 2180, measured closure ranged from 60 to 70 mm over the length of the room.

Munson et al. (1996) modeled room closure and DRZ formation using SPECTROM-32 (Callahan et al., 1989). Model results suggested that between 20 mm and 45 mm of closure occurred before the closure gauges were installed. The total assumed closure of Room Q is summarized in Table 2-3.

Table 2-3. Room Q Closure

Time From Start of Excavation		Closure Diameter (m)	Closure Volume (m³)
(days)	(years)		
10	0.03	0.04	18.5
300	0.8	0.06	27.6
600	1.6	0.07	32.1
1400	3.8	0.09	41.2
2180	6.0	0.10	45.7

Closure volume represents the calculated volume reduction in the room over the 102 m sealed length. The initial volume of Room Q was 673.7 m³. Additional salt deformation results from SPECTROM-32 are discussed in Sections 3.2 and 4.3.

2.4 Resistivity Data

Resistivity measurements are indicative of moisture content within the rock. Low resistivity suggests high moisture content and high resistivity suggests low moisture content. Resistivity data were collected from two arrays (Figure 2-1), starting on March 11, 1990 (day 242). Array 1 (nearest the seals) and Array 2 both had 384 measurement points around the circumference of the room. Resistivity data from both arrays were similar through December 19, 1990 (day 525). Subsequent measurements showed significant differences between the two arrays. These differences suggest that some local-scale behavior is being measured, making it difficult to draw generalized conclusions about the flow regime. Borns (Appendix A1) presents an interpretation of the resistivity data from Array 2, which provides the basis for the following discussion of Room Q.

As evidenced by the room closure measurements, the surface of Room Q moved inward immediately following excavation. SPECTROM-32 simulations (Munson et al., 1996) suggest that the associated deformation causes an expansion in the salt around the room, resulting in a zone of increased porosity. The porosity increase is most rapid in the first 50-100 days after excavation.

15

This early-time porosity increase produces a corresponding decrease in the fluid saturation (moisture content) because the existing fluid cannot fill all of the newly-created porosity. Air drying of the room walls may result in additional moisture loss. The potential for air drying was greatest at early time, prior to the installation of the temporary single seal at day 105. The potential for air drying diminished by day 300, when the relative humidity in the room reached an equilibrium value (Section 2.1).

The first suite of resistivity measurements, at day 242, showed relatively high resistivity values for both Array 1 and Array 2, consistent with a low fluid saturation. The second suite of resistivity values, measured at day 345, were significantly lower than at day 242 for both arrays. This resistivity decrease implies an increased fluid saturation, suggesting that the DRZ started to resaturate with fluid from the far field and/or that air drying decreased. DRZ resaturation may have started before or after day 242, the data only shows that the saturation is higher at day 345 than at day 242. The timing of the resaturation may have been influenced by a reduction in air drying due to installation of temporary single seal (day 105) and the temporary double seal (day 244).

Between day 345 and day 525, several resistivity measurements were made, but there was only a slight increase in resistivity values, indicative of a slight desaturation of the DRZ. This suggests that the resaturation of the DRZ was essentially complete by day 345.

Prior to the next suite of resistivity measurements, at day 685, the permanent seal was installed (day 624). Also, brine accumulation in room, indicative of brine inflow, was observed for the first time at day 607. It is expected that brine inflow and, to a lesser extent, the permanent seal installation would result in increased moisture content (decreased resistivity) in the rock near the walls of room.

The resistivity data presented from day 685 showed significant visual differences between the two arrays. At the location of Array 2, there was renewed resaturation (resistivity decrease) between day 525 and day 792. This is consistent with the observed brine accumulation in the room. As reported in Borns (Appendix A1), there was an unexpected increase in resistivity from day 792 to day 1040, indicative of desaturation, even though large brine inflow rates were being measured at this time. Borns (Appendix A1) suggests that this anomalous behavior is due to dilation of a specific fracture creating additional pore space around Array 2 or around the Array 2 far-field electrode under the room floor.

16

At Array 1, the resistivity measurements were almost the opposite of Array 2 between day 525 and day 792. Because the Array 1 measurements were not consistent with the observed brine accumulation, it is suspected that they were also influenced by a localized fracture. In any case, there is considerable uncertainty associated with the interpretation of the resistivity measurements beyond day 685.

3.0 SUMMARY OF ROOM Q INTERPRETIVE BRINE INFLOW MODELS

3.1 Hydrologic Models

Brine inflow under isothermal conditions has been measured in large-scale (30-36 inch diameter) experimental boreholes (Nowak and McTigue, 1987; Nowak et al., 1988) and in small-scale brine sampling boreholes (Deal and Case, 1987; Deal et al., 1987; Deal et al., 1989; Deal et al., 1991; Deal et al., 1993; Finley et al., 1992). Initial numerical investigations (Bredehoeft, 1988; Nowak et al., 1988; Webb, 1992; McTigue, 1993) suggested that brine inflow to these boreholes could be represented by Darcy flow through a porous medium.

Prior to the construction of Room Q, McTigue (Appendix A3) performed calculations to estimate the quantities of brine inflow. The estimates were based on a radial Darcy flow model with a permeability of 1×10^{-21} m^2, a specific storage of 1×10^{-7} m^{-1}, and a far-field pressure of 15 MPa. Brine inflow estimates were 500 ml/day after 1 year and 400 ml/day after 2 years. These predicted inflows are similar to Darcy flow brine inflow estimates predicted with TOUGH28W (Section 4.4).

McTigue (Appendix A2) performed calculations that assumed brine inflow to Room Q was only from a thin horizontal anhydrite layer intersecting the room. With similar properties to those used by McTigue (Appendix A3), predicted brine inflow was reduced to about 30 ml/day. This reduced brine inflow was more consistent with the low measured rates in the first 2 years following excavation, however, the brine inflow rates predicted by the horizontal flow model are much lower than the measured brine accumulation rates from 2-5 years.

3.2 Mechanical (Snow Plow) Model

This section describes a conceptual model of brine inflow that is based solely upon the extent and level of the damage around an excavated opening. Damage can be envisioned as microfractures that can potentially link discrete brine-filled pores. As damage evolves, progressively more of the salt around the excavated opening is affected by the damage field, releasing brine according to the level of damage achieved. Brine is assumed to drain from the salt instantaneously. Thus the amount of brine released depends upon the amount of damage. This is a mechanical "snow plow" model and is described in detail in Munson et al. (1996). This model is similar to the redistribution model described in Section 1.3.

With the snow plow model, the volume of brine released due to damage is related to the total volume of brine available in a volume of salt. The volume of brine released is dependent on the amount of local damage, ω, which is bounded by an initial and a maximum damage. The initial damage, ω_o, defines the level of damage required to initiate brine release. The maximum damage, ω_{max}, defines the level of damage that links all brine-filled pores, and thus the total volume of available brine may be released. Because of the level of damage decreases with distance away from an excavation, the volume of brine released at a given time is calculated by integration over distance. For discrete radial elements, the integration can be represented by a summation as given by Equation 3-1.

$$V_b(t) = \sum_{i=1}^{n} V_i \, \phi \left(\frac{\omega_i(t) - \omega_o}{\omega_{max} - \omega_o} \right) \tag{3-1}$$

where: $V_b(t)$ = volume of brine released at time t [L^3]

V_i = undeformed volume of salt in element I [L^3]

ϕ = volumetric brine content of salt

$\omega_i(t)$ = level of damage of element I at time t

ω_o = level of damage to initiate brine release

ω_{max} = level of damage to completely drain salt

n = number of radial elements

The snow plow model brine release behavior is distinctive. Both the rate of damage accumulation and brine release diminish with time.

To develop a snow plow model, damage around an excavation must be determined. Munson et al. (1993) and Munson et al. (1996) have predicted salt creep, fracture and damage around WIPP underground excavations using the Multimechanism Deformation Coupled Fracture (MDCF) model (Chan et al., 1992). The MDCF model is an extension of the Modified Multimechanism Deformation (M-D) steady-state creep model with work-hardening/recovery transients proposed by Munson et al. (1989). MDCF predictions of damage are based on maps which relate the mechanisms of creep and fracture as a function of temperature, stress, and pressure conditions at the WIPP repository.

MDCF model predictions of room closure and DRZ formation around Room Q (Munson et al., 1996) were performed using the finite element code SPECTROM-32 (Callahan et al., 1989). The calculation was a two-dimensional, plane strain simulation with the plane normal to the axis of the cylindrical room. The simulated stratigraphy included a clay seam sandwiched between bedded argillaceous halite. The MDCF volumetric strain (damage) results suggest that the DRZ (defined by a volumetric strain greater than or equal to 0.0001) forms almost immediately and extends about 0.5 m from the edge of the room in the horizontal radial direction after one year. For times after one year, the damage levels increase slightly, however the extent of the damage field does not change significantly. The volumetric strain contours around the room after five years are shown in Figure 3-1. The damage field does differ slightly with radial direction around the room, with a notable change in damage at the location of the clay seam that intersects the room near the apex. Volumetric strain is comprised of elastic strain plus the inelastic strain. The inelastic strain is used to predict the increase in DRZ porosity with time (Section 4.3).

The MDCF damage results were used directly with the snow plow model. The parameter values used in the model are given in Table 3-1. The fit of the model to the brine accumulation data from Room Q is shown in Figure 3-2. The brine accumulation data before the permanent seal was emplaced were adjusted by approximately 270 liters to compensate for an assumed loss of brine to evaporation. The agreement between the model results and the data is visually quite good until about five years, at which time observed brine accumulation almost ceases. Loss of brine under the seals is thought to cause the lack of agreement after five years. The maximum damage is a free parameter whose value determines the slope of the predicted brine release (inflow). A value of 0.0004 was determined based upon the fit of the model to the Room Q brine inflow data and is considered a realistic assumption.

Table 3-1. Snow Plow Model Parameter Values

	Parameter	Value
ϕ	volumetric brine content (equivalent to porosity at 100% brine saturation)	0.01
ω_{min}	minimum damage	0.0001
ω_{max}	maximum damage (used as a fitting/ calibration parameter)	0.0004
ω	damage	from MDCF model
r	radius of damage into the salt (m)	from MDCF model
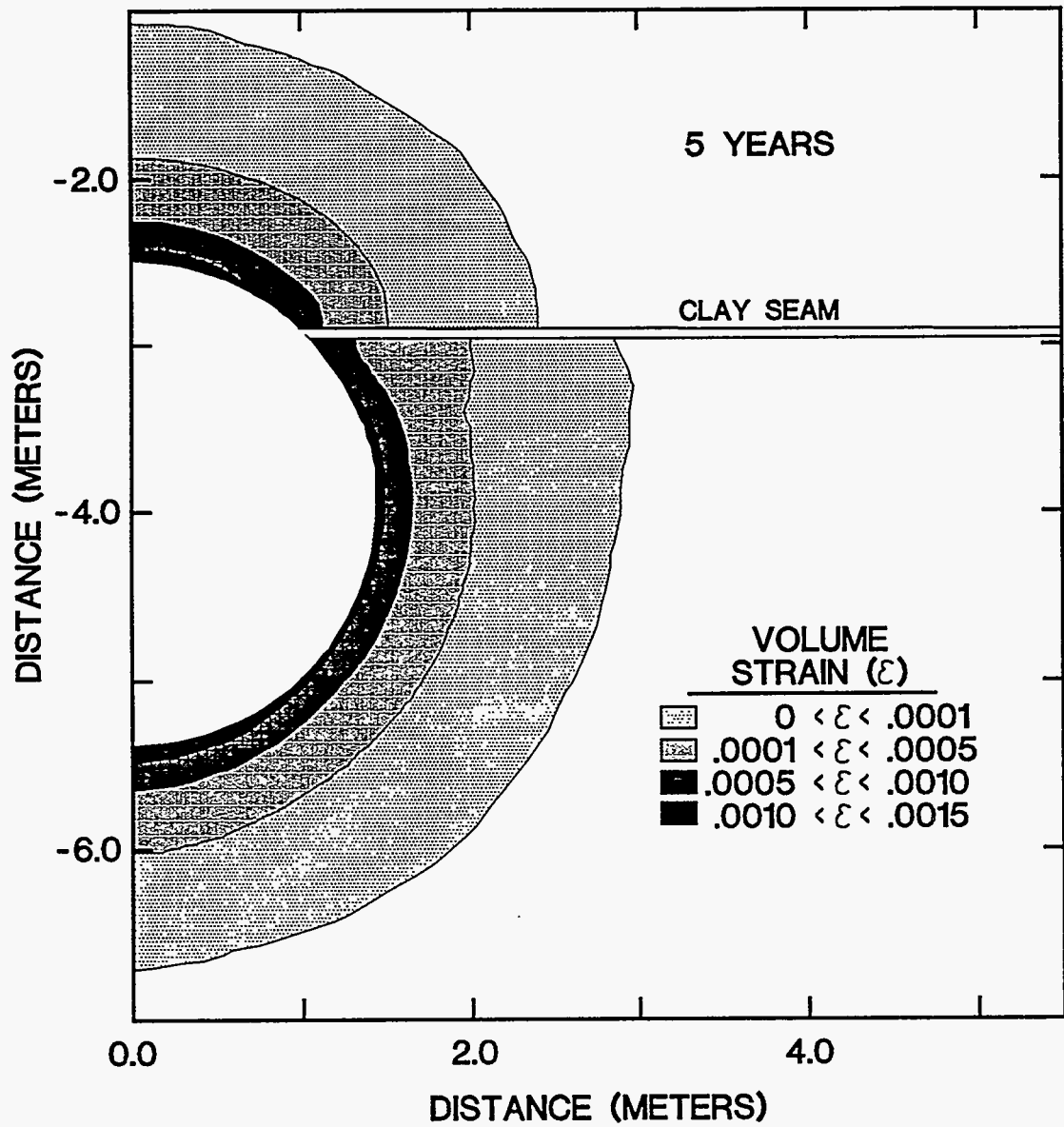
Figure 3-1. Volumetric strain contours around Room Q 10 years after excavation. (from Munson et al., 1996).
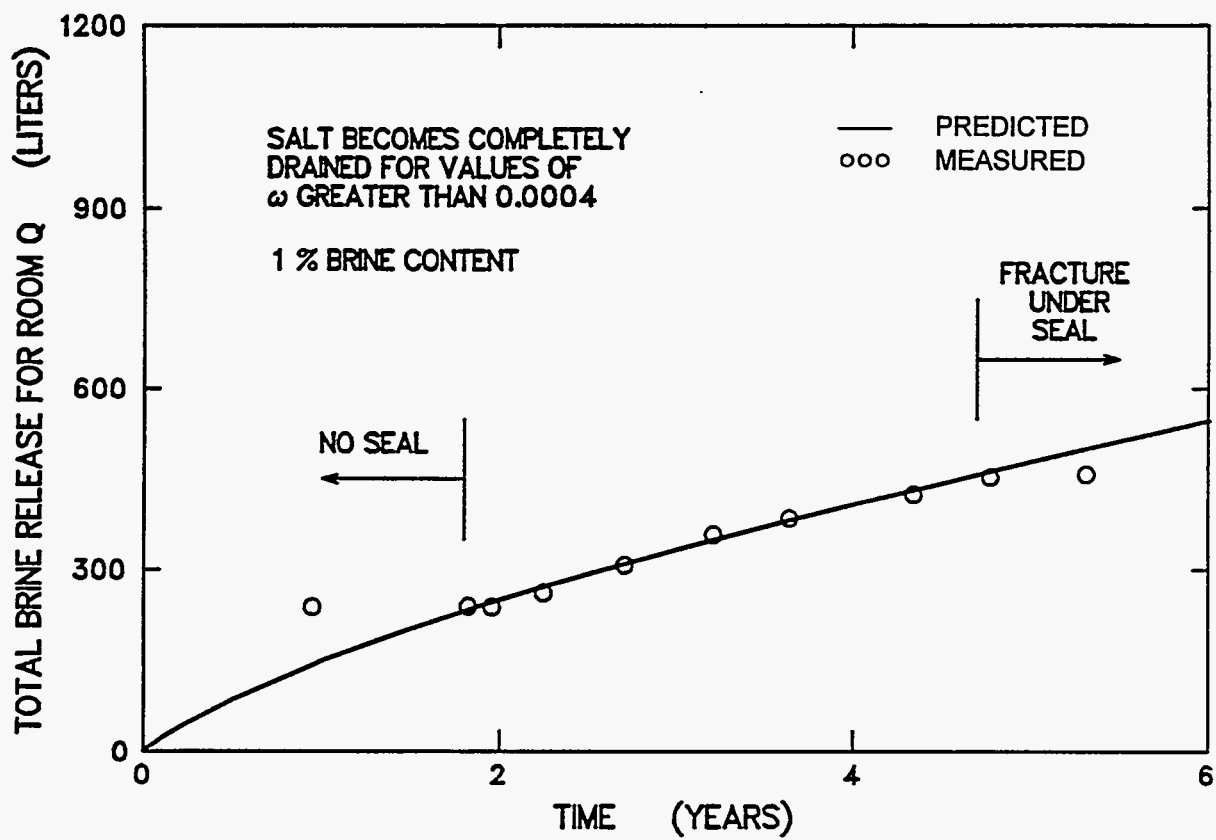
Figure 3-2. Comparison of MDCF predicted and measured brine release for Room Q.
(from Munson et al., 1996).

23

4.0 ROOM Q BRINE INFLOW SIMULATIONS AND RESULTS

4.1 Conceptual Model

Based on general observations from the WIPP underground (Lappin et al., 1989, Sandia WIPP Project, 1992) and specific observations from Room Q, a conceptual model for brine flow into Room Q was developed. Data collected from Room Q (Section 2.0) suggest that brine accumulation in the room is influenced by the time-varying properties of the DRZ. Therefore, the modeled flow regime consists of two regions with different properties: a far-field region of undisturbed halite, and a disturbed region (DRZ) surrounding the room (Figure 4-1). Flow within the Salado is affected by the presence of high permeability anhydrite interbeds (Freeze et al., 1995a). The nearest anhydrite beds to Room Q (anhydrite b above and Marker Bed 139 below) are several meters away. For the short duration of flow examined in this modeling study, the anhydrite interbeds are distant enough to not significantly influence the flow field around Room Q and are not included in the conceptual model. Immediately after excavation, the DRZ porosity starts to increase and there is a significant inward pressure gradient from the Salado Formation (at 12.5 MPa pore pressure) to the room (at atmospheric pressure of 0.1 MPa). Fluid movement is assumed to be radial towards the room. Because Darcy flow models have historically been able to reproduce observed brine inflows at WIPP (Section 3.1), Darcy flow is assumed for this modeling study. Interpretations of hydraulic tests in the permeability testing program support the assumption of far-field Darcy flow (Beauheim et al., 1991; Beauheim et al., 1993).

A general curve for expected Darcy flow behavior is compared to the measured brine accumulation data in Figure 4-2. The expected Darcy flow curve is not a simulation result, it simply illustrates the exponentially-decaying inflow rate that would be observed in Room Q if brine accumulation was only due to far-field Darcy flow. At early time (0-2 years after excavation), significant brine inflow is expected from Darcy flow, whereas no brine accumulation in Room Q was measured during this time. The numerical modeling study described in the remainder of this section examines whether a DRZ pore volume increase, in conjunction with far-field Darcy flow, can cause a reduction in early-time brine inflow to the room. An additional mechanism that could reduce measured brine accumulation is evaporation. Evaporation was examined using simple bounding calculations, but was not included in numerical simulations. The evaporation calculations are described in Section 4.2. The pore volume increase in the DRZ in response to excavation-related
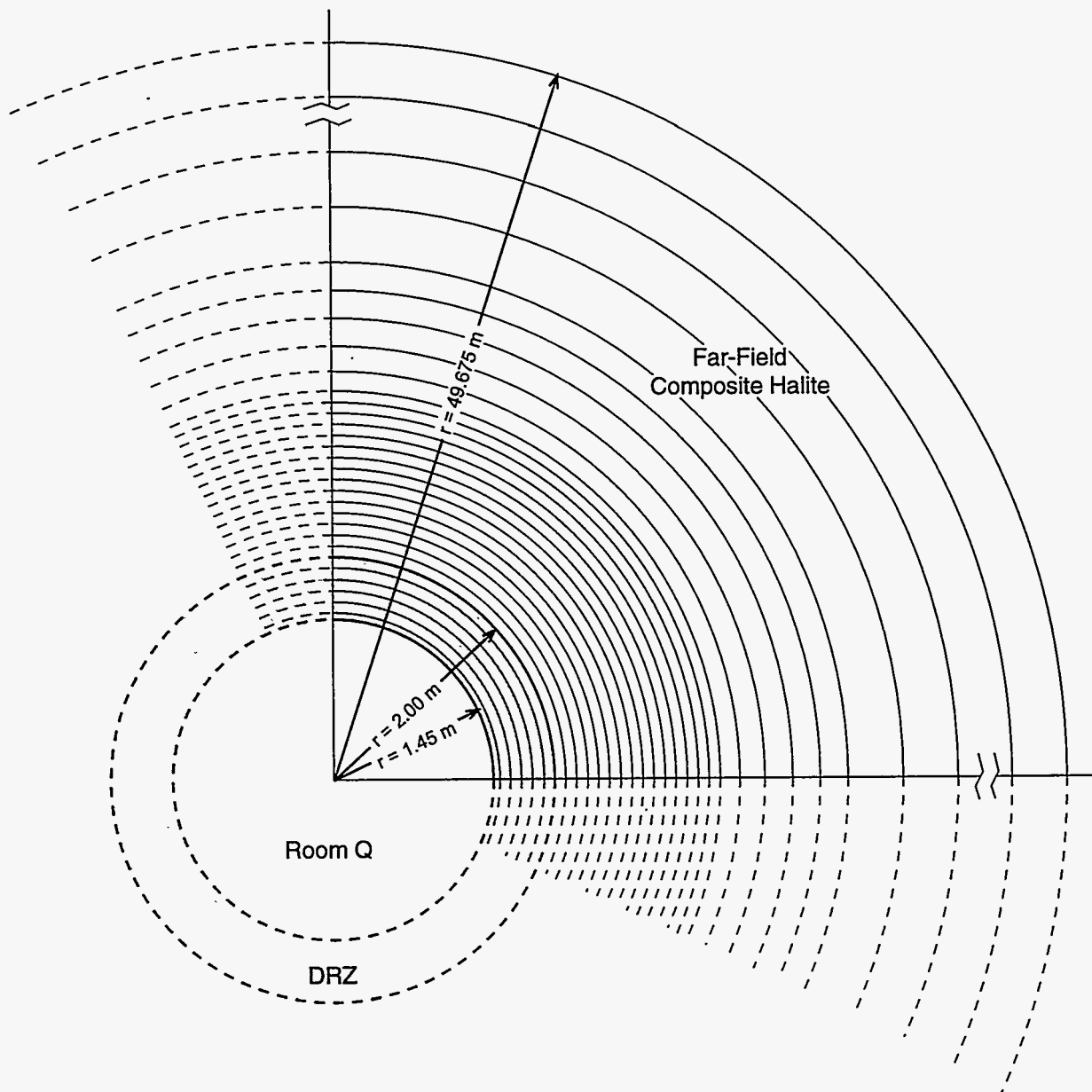
Figure 4-1. Model discretization for brine inflow to Room Q.
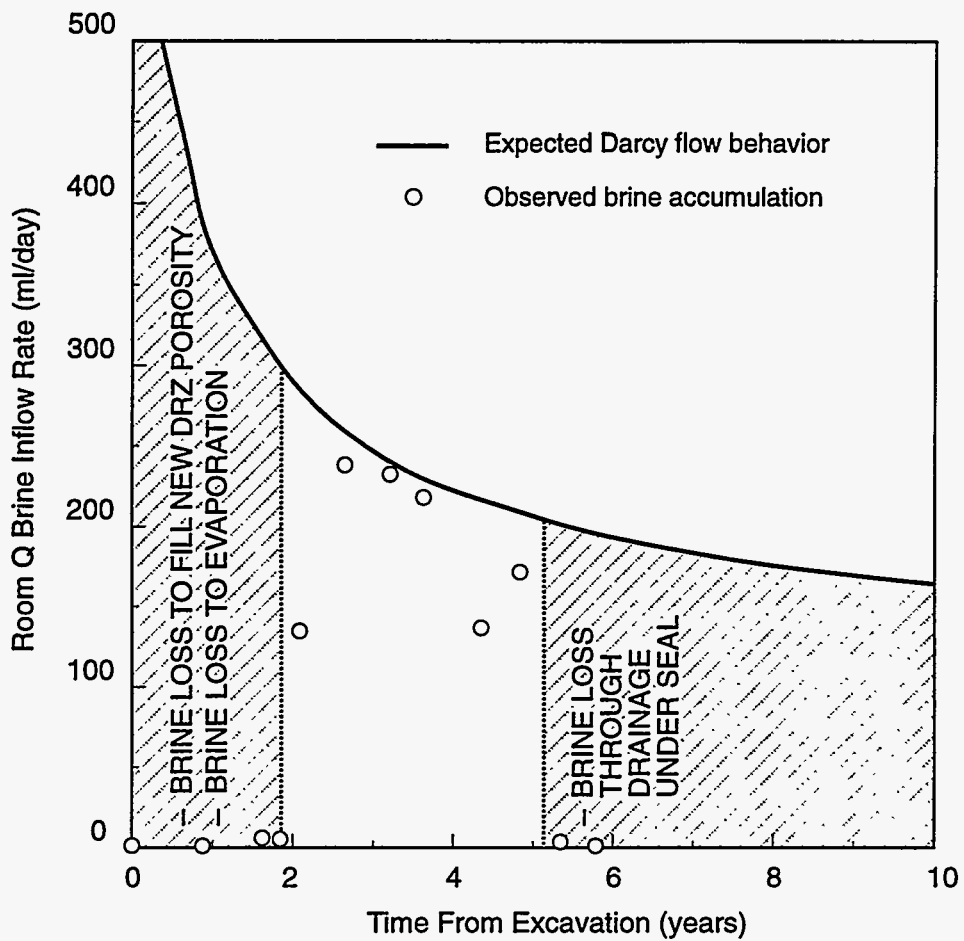
Figure 4-2. A comparison of expected Darcy flow behavior with observed brine accumulation in Room Q to identify possible mechanisms affecting brine accumulation.

27

stress redistribution was calculated using SPECTROM-32. The methodology for implementing this pore volume increase in numerical simulations of brine inflow to Room Q is described in Section 4.3. The simulations are presented in Section 4.4.

Between 2 and 5 years after excavation, measured brine accumulation shows a trend consistent with expected Darcy flow, suggesting that far-field Darcy flow is the dominant process during this time period. At late time (> 5 years after excavation), measured brine accumulation dropped to almost zero. This loss of brine is attributed not to a change in brine flow mechanisms, but rather to leakage of brine out of the room through fractures under the seals before it could be measured. Scoping calculations (Section 2.1) suggest that 100 ml/day could be lost through leakage for an assumed DRZ permeability of 10^{-15} m^2. Leakage was not examined in the numerical simulations.

4.2 Evaporation Calculations

One potential mechanism to explain the absence of brine accumulation in Room Q in the first 2 years after excavation is evaporation. The relative humidity for air in equilibrium with brine is about 80% (CRC Press, 1985; p. E-1). Relative humidity measurements (see Section 2.1) suggest that the room air was undersaturated with water vapor (20-60% relative humidity) up to about day 300. From day 300 onward, the air in Room Q was nearly saturated (80% relative humidity). The increase in relative humidity by day 300 suggests that the installation of the temporary double seal (at day 244) provided significantly more effective sealing of the room. Evaporation rates were measured between the seals from about day 280 onward. Measured rates ranged from 200 ml/day (when the relative humidity was increasing from 25% to 70%) to 20 ml/day (when the relative humidity was about 80%). Based on this evaporation data, a lower bound for the evaporation potential from Room Q is 200 ml/day from day 0 to day 300, when the room air is undersaturated with water vapor, and 20 ml/day from day 300 onward, when the room is at 80% relative humidity. It is important to note two factors controlling the observed evaporation rates. First, the measurements were taken in the 2.4 m long interval between the seals. The evaporation potential for the 102 m long sealed room could be proportionally (42.5 times) larger. Second, the observed rates resulted from an unlimited supply of brine from brine pans that were periodically refilled. In the room, while the evaporation potential is high, the actual evaporation rates are controlled by the limited supply of brine from brine inflow. Stated another way, if the evaporation potential in the

room is about 40 times larger than between the seals, then evaporation rates of 8000 ml/day are possible.

Another approach to examine evaporation potential is to calculate the mass of brine that can vaporize under Room Q conditions (pressure and temperature). The maximum vaporization (highest vapor pressure) occurs at late time when the relative humidity is at 80%. The corresponding vapor pressure is approximately 3.0 kPa. From the ideal gas law (with T=27°C and P=0.1 MPa), this vapor pressure results in 0.0012 moles of water vapor per liter of air. Assuming a brine density of 1230 kg/m³, this corresponds to a maximum of 12.6 liters of brine that can be evaporated per Room Q volume of air. Actual evaporation potential must consider the mass of water vapor present in the repository air. Repository air was measured at anywhere from 20% relative humidity at 22°C (vapor pressure = 0.5 kPa) to 60% relative humidity at 30°C (vapor pressure = 2.5 kPa). Corresponding brine volumes per volume of Room Q air for these two sets of conditions are 2.1 liters and 10.5 liters, respectively. Subtracting these brine volumes from the maximum brine volume (12.6 liters), it is concluded that between 2.1 and 10.5 liters of inflowing brine can be evaporated per Room Q volume of air. To calculate evaporation potential requires knowledge of air exchange rates for Room Q. To achieve 200 ml/day (73 liters/year) evaporation from Room Q would require the exchange of between 7 and 35 Room Q volumes of air per year. As a point of reference, the air flow rate at the air intake shaft, near Room Q, is 316,000 ft³/min (8949 m³/min) (DOE, 1990). The excavated volume of the repository is approximately 196,000 m³ (Lappin et al., 1989), therefore the repository air is exchanged about 66 times per day. Although the airflow at Room Q, which is isolated at the end of a drift, is much lower than at the air intake shaft, these calculations still suggest that there may have been sufficient circulation of air to evaporate significant volumes of brine from Room Q prior to room sealing.

4.3 Structural Data Input

As discussed in Section 3.2, the MDCF constitutive model for salt deformation, implemented in the SPECTROM-32 code, was used to predict room closure and DRZ formation around Room Q (Munson et al., 1996). The SPECTROM-32 simulations calculated damage stress, the damage variable, total volumetric strain, and room closure. The DRZ is delineated by the region of large (greater than 0.0001) volumetric strain (Figure 3-1). Total volumetric strain is comprised of elastic strain plus inelastic strain. The inelastic strain can be related to hydrologic parameters in the form of increased interconnected porosity of the salt and possibly increased permeability. Inelastic strain

as predicted by SPECTROM-32 is representative of the change in porosity. SPECTROM-32 simulation results listing the total volumetric strain and inelastic strain as a function of time and location are included in Appendix B. The inelastic strain data were used to construct DRZ porosity versus time relationships for use in the brine inflow simulations (Section 4.4). Porosity in the vicinity of Room Q, as predicted with SPECTROM-32, is shown in Figures 4-3 and 4-4. Note that in Figure 4-3 and subsequent figures in this section, x denotes radial distance from the center of Room Q. For an assumed initial DRZ porosity of 0.01, the initial DRZ pore volume is 6.08 m^3 (6080 liters). Significant porosity increases (greater than 1% of the initial porosity) occur out to a radius of about 0.55 m from the edge of the room (2.0 m from the room center) (Figure 4-4). Table 4-1 lists the SPECTROM-32 predicted pore volume increase within a 0.55 m DRZ over the 102 m sealed length of the room. Table 4-1 shows that the additional pore volume created is less than 1% of the total closure volume (Table 2-3). The difference is due to the conceptual model (MDCF) used to predict creep in SPECTROM-32. In SPECTROM-32 most of the dislocation (creep) results from boundary subsidence. Physically, this represents separation at bedding plane boundaries rather than increasing interconnected porosity.

Table 4-1. DRZ Pore Volume Increase Predicted by SPECTROM-32

Time From Excavation (years)	Porosity at x=1.45 m (at edge of room)	Porosity at x=1.95 m (near edge of DRZ)	DRZ Pore Volume Increase	
			(m³)	(liters)
1	0.0109	0.01009	0.21	210
2	0.01097	0.01009	0.227	227
3	0.01102	0.0101	0.241	241
5	0.0111	0.01011	0.262	262
8	0.01122	0.01012	0.289	289
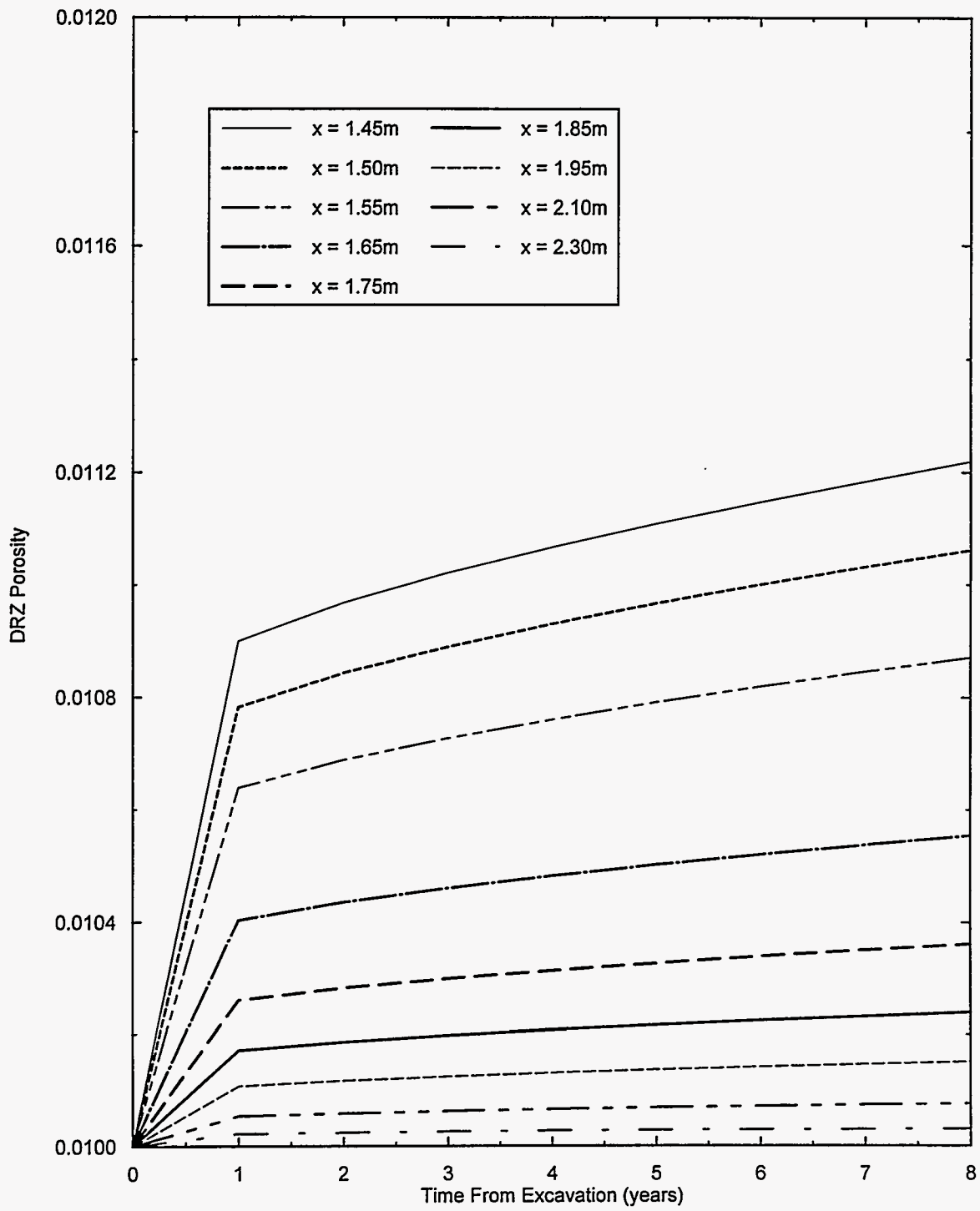
Figure 4-3. Room Q DRZ porosity as a function of time predicted with SPECTROM-32.

31
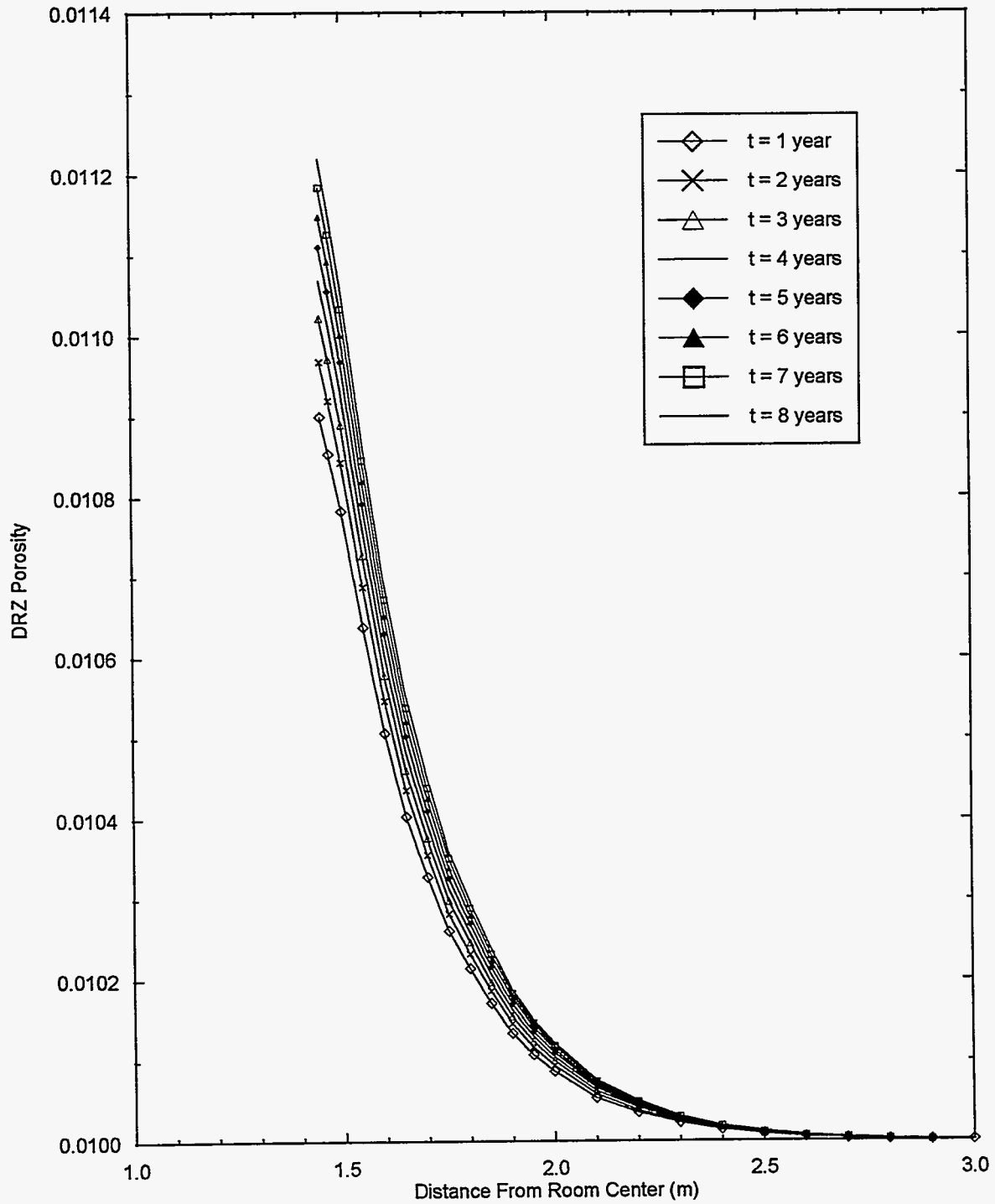
Figure 4-4. Room Q DRZ porosity as a function of distance predicted with SPECTROM-32.

4.4 Numerical Simulation Results

A numerical representation of Darcy flow to Room Q was implemented with the computer code TOUGH28W, which contains only minor modifications from TOUGH2/EOS8 (Freeze et al., 1995b). For Darcy flow, controlling factors include the physical properties (intrinsic permeability, porosity, and rock compressibility), the fluid properties (phase pressures, saturations, and compressibilities), and the two-phase flow relationships (relative permeability and capillary pressure). TOUGH28W was selected because it can simulate changing porosity as a function of time, a capability that was necessary to properly investigate the time-dependent porosity changes in the DRZ. TOUGH28W can also simulate multiphase flow. The multiphase flow capabilities were important because the initial pore volume increase in the DRZ produces unsaturated conditions with certain parameter combinations.

A baseline simulation was performed using best estimates for fluid, DRZ, and halite parameters, as specified in Section 2.2. The baseline model included a 0.55 m radius DRZ with a porosity that increased with time according to predictions from SPECTROM-32 simulations (see Section 4.3). The TOUGH28W DRZ extent of 0.55 m was selected to correspond approximately with the region where porosity changes are greater than 1% of the initial porosity (Figure 4-4).

TOUGH28W has the capability to simulate porosity changes over time by specifying pressure-time-porosity relationships for selected regions. In this case, porosity is only a function of time and is independent of pressure. The DRZ is discretized into six concentric elements, centered at 1.475 m, 1.55 m, 1.65 m, 1.75 m, 1.85 m, and 1.95 m from the edge of the room. Each DRZ element has a specified porosity versus time relationship. Each porosity-time relationship was defined to reproduce the SPECTROM-32 porosity change with time for the corresponding element-center distance from the room edge. A comparison of TOUGH28W DRZ porosities with SPECTROM porosities is included with the baseline simulation results (Figure 4-5).

As discussed previously, the porosity increase in the DRZ has the potential to create two-phase conditions. The baseline simulation assumes a mixed Brooks and Corey relationship for relative permeability and capillary pressure (Webb and Larson, 1996). Relevant parameters are: threshold pressure (p_t) = 0.087 MPa, residual brine saturation (S_{br}) = 0.20, residual gas saturation (S_{gr}) = 0.20, and pore-size distribution index (λ) = 0.7.

Baseline simulation results are compared with the results from a Darcy flow simulation in Figures 4-5a (brine inflow rate) and 4-5b (cumulative brine inflow). The Darcy flow simulation used the same baseline hydrologic properties and DRZ extent, however, the DRZ porosity did not change

33

with time. Additional results from the baseline simulation are presented in Figures 4-5c (DRZ porosity), 4-5d (brine phase saturation), 4-5e (brine phase pressure) and 4-5f (radial pressure profile). The baseline simulation (which had an increasing DRZ porosity) had less brine flow into the room than the Darcy flow simulation. After 1 year, cumulative brine inflow was about 200 liters less and, after 5 years, brine inflow was about 250 liters less. The brine that did not flow into the room instead flowed into the newly created DRZ porosity. The volume of newly created porosity (see Table 4-1) is approximately equivalent to the reduction in brine inflow volume. In addition to the baseline simulation, deterministic sensitivity simulations were performed to examine the sensitivity of brine inflow to various parameters, particularly the DRZ conceptualization.

The baseline simulated brine inflow rate (Figure 4-5a) shows a trend similar to the measured Room Q brine accumulation rates. The only significant differences from the measured rates are the simulated non-zero rates at early time (less than 0.66 years), where evaporation could account for the difference, and at late time (greater than 5 years), where brine leakage under the seals was not simulated. Sensitivity simulations, discussed later in this section, show that simulated early-time brine inflow is also very sensitive to the DRZ porosity changes. Because of the sensitivity of the simulated early-time brine inflow to the DRZ porosity, and because of uncertainties in the measured early-time brine accumulation (brine lost to evaporation, brine not collected during the excavation period), comparison of simulated and measured brine inflow during the first year is not appropriate. Rather, comparisons should focus on inflow rates (Figure 4-5a) and the slope of cumulative inflow (Figure 4-5b) after the first year. The baseline simulation results show a relatively good match to the measured brine accumulation for these two comparisons.

The simulated brine inflow rate can be explained by examining two primary processes, brine inflow from the far-field (Darcy flow into the DRZ) and porosity increase in the DRZ. Both the rate of brine inflow to the DRZ (Figure 4-5a) and the rate of pore volume increase (Figure 4-5c) decrease with time. When the rate of pore volume increase is greater than the rate of brine inflow to the DRZ, the new DRZ pore volume does not completely fill with brine. As a consequence of the new non-brine-filled pore volume, the brine saturation (Figure 4-5d) and the brine phase pressure (Figure 4-5e) in the DRZ decrease, and there is no brine inflow to the room. With time, the DRZ porosity increase slows (Figure 4-5c) and brine inflow from the far-field is sufficient to re-pressurize (and re-saturate) the DRZ. When the DRZ brine phase pressure exceeds the room pressure (0.1 MPa), brine inflow to the room occurs. Only a very small pressure gradient is required for this inflow to occur. Because of the high relative permeability to brine and low capillary pressure that result from the mixed Brooks and Corey relationships, brine inflow is not very sensitive to changes

34

a) Brine Inflow Rate

Legend:
- Measured
- DRZ porosity increasing (Baseline)
- DRZ porosity = 0.01 (Darcy flow)

b) Cumulative Brine Inflow

Legend:
- Measured
- DRZ porosity increasing (Baseline)
- DRZ porosity = 0.01 (Darcy flow)
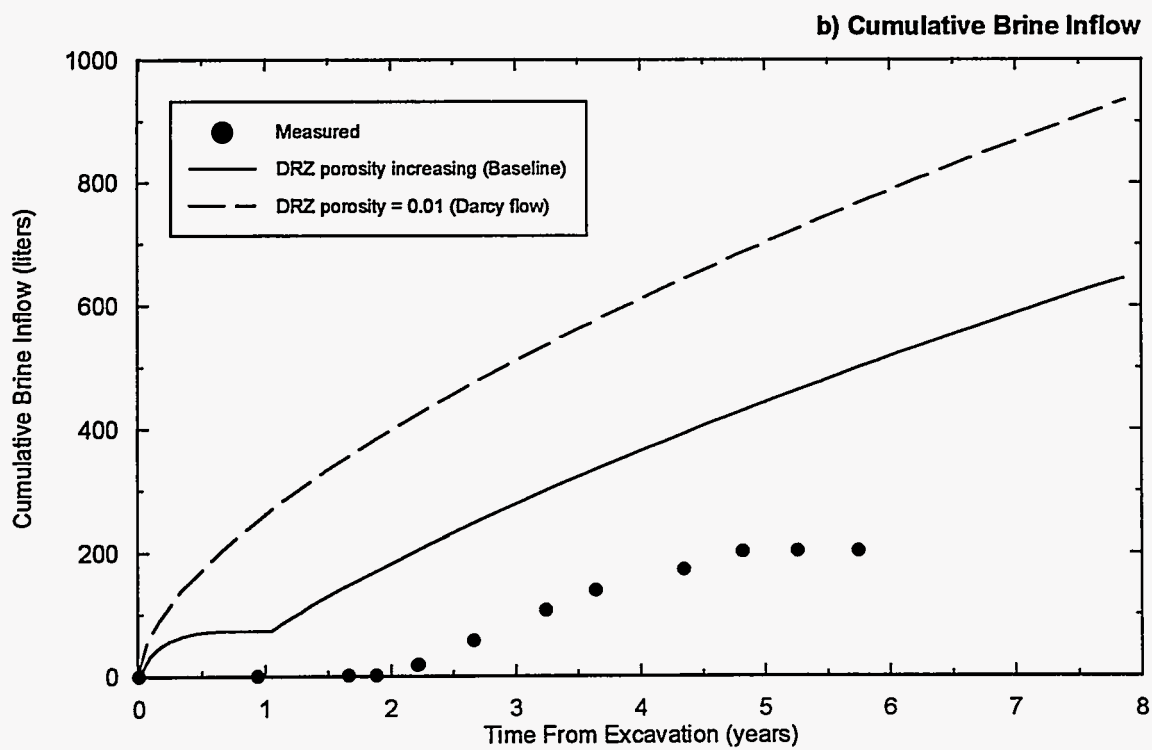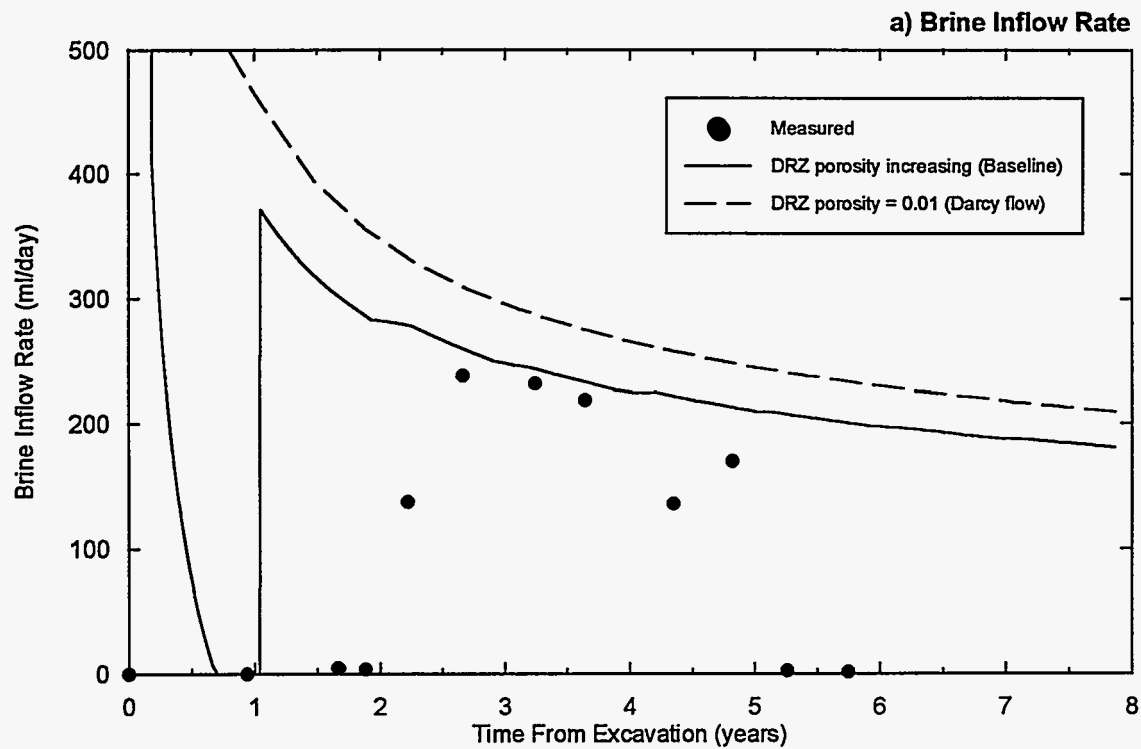
Figure 4-5.   Baseline TOUGH28W simulation (DRZ porosity increasing with time) compared with a Darcy flow simulation (fixed DRZ porosity).

c) DRZ Porosity

d) Brine Phase Saturation
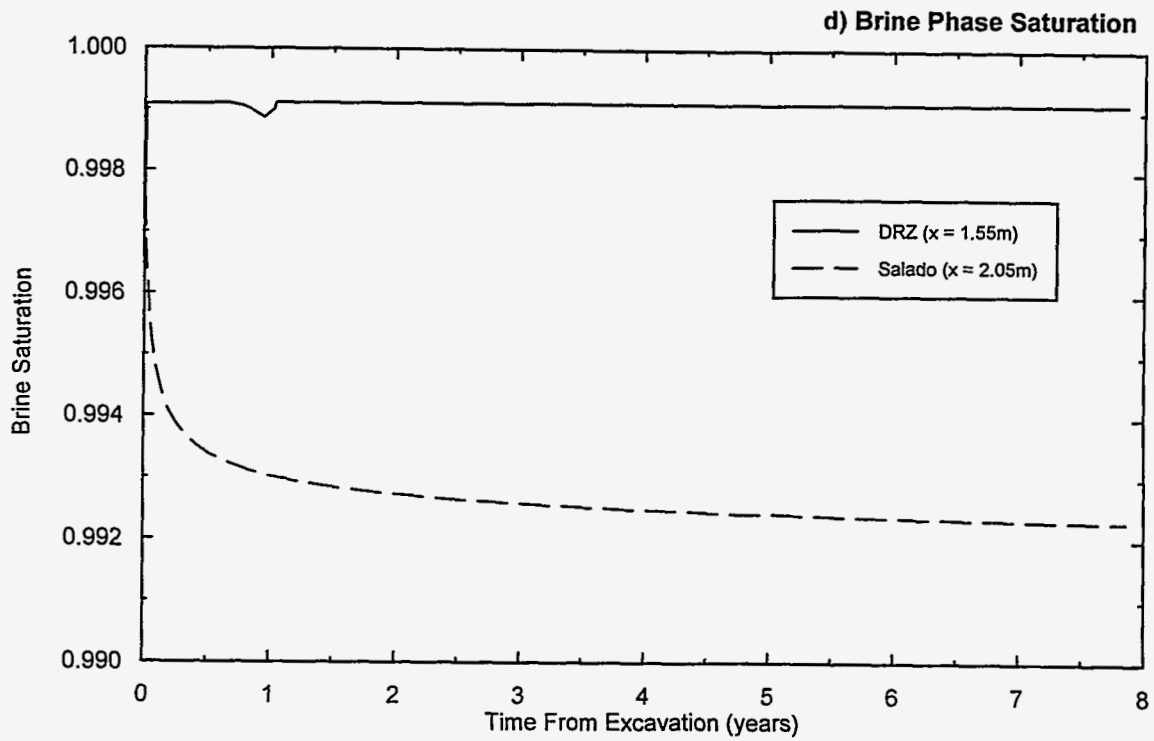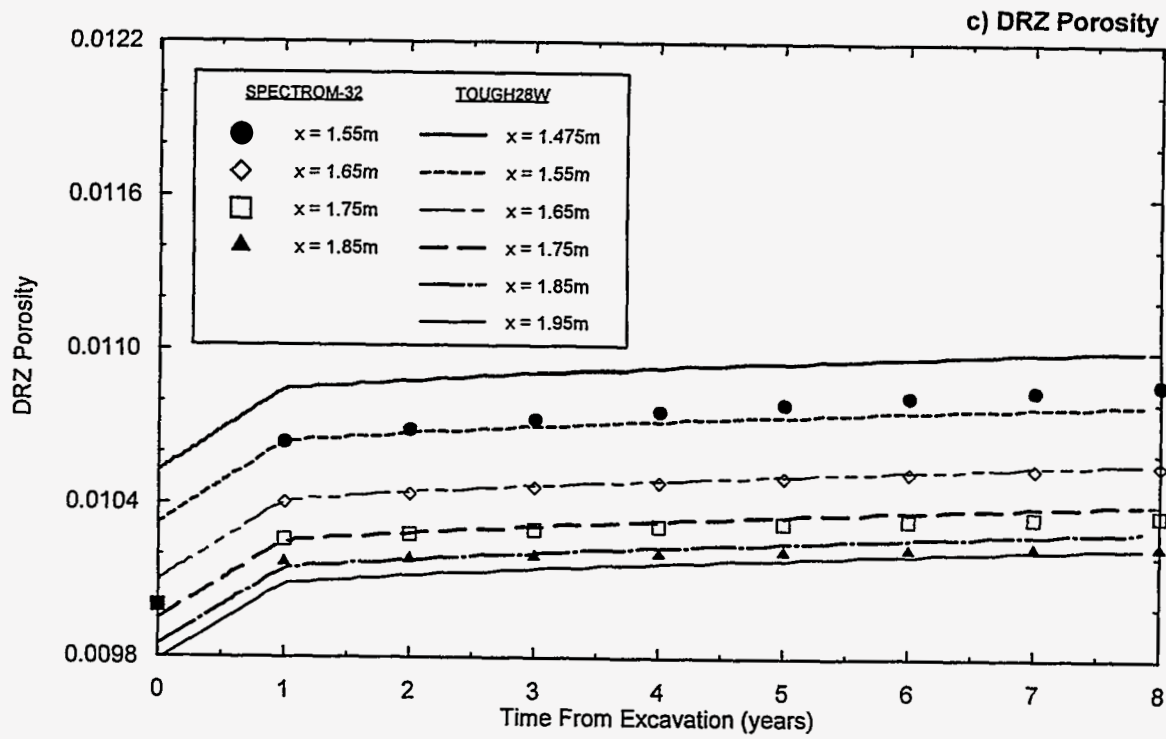
Figure 4-5. (cont.) Baseline TOUGH28W simulation (DRZ porosity increasing with time) compared with a Darcy flow simulation (fixed DRZ porosity).
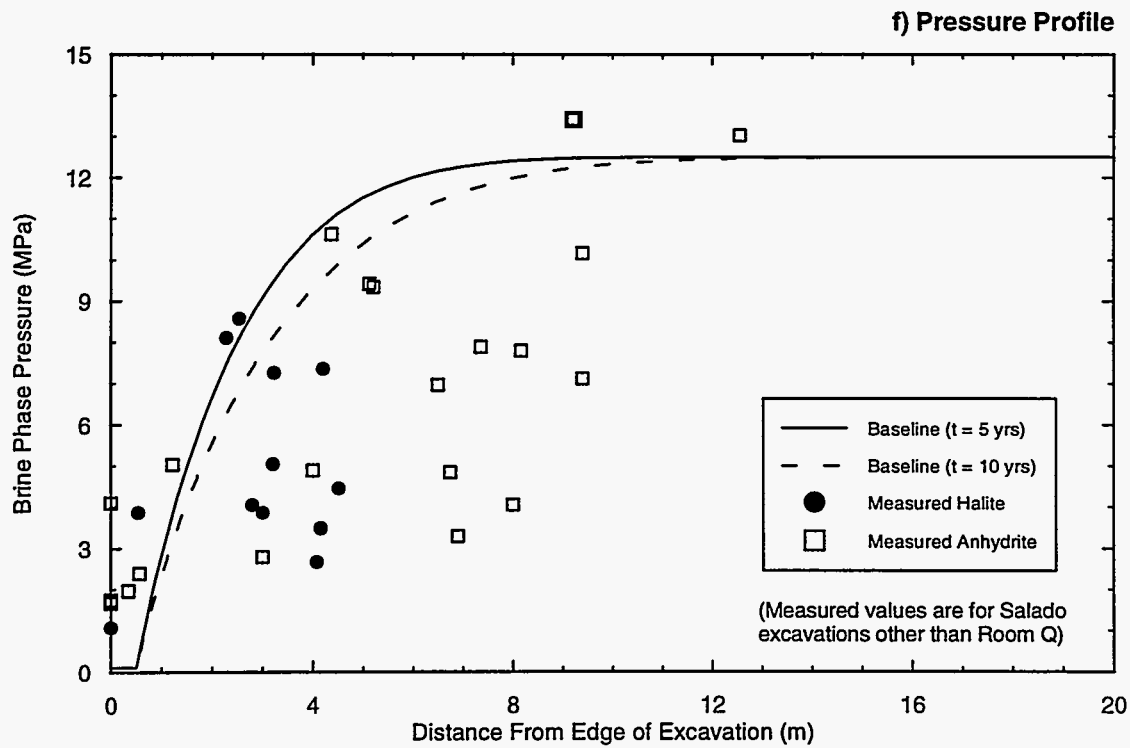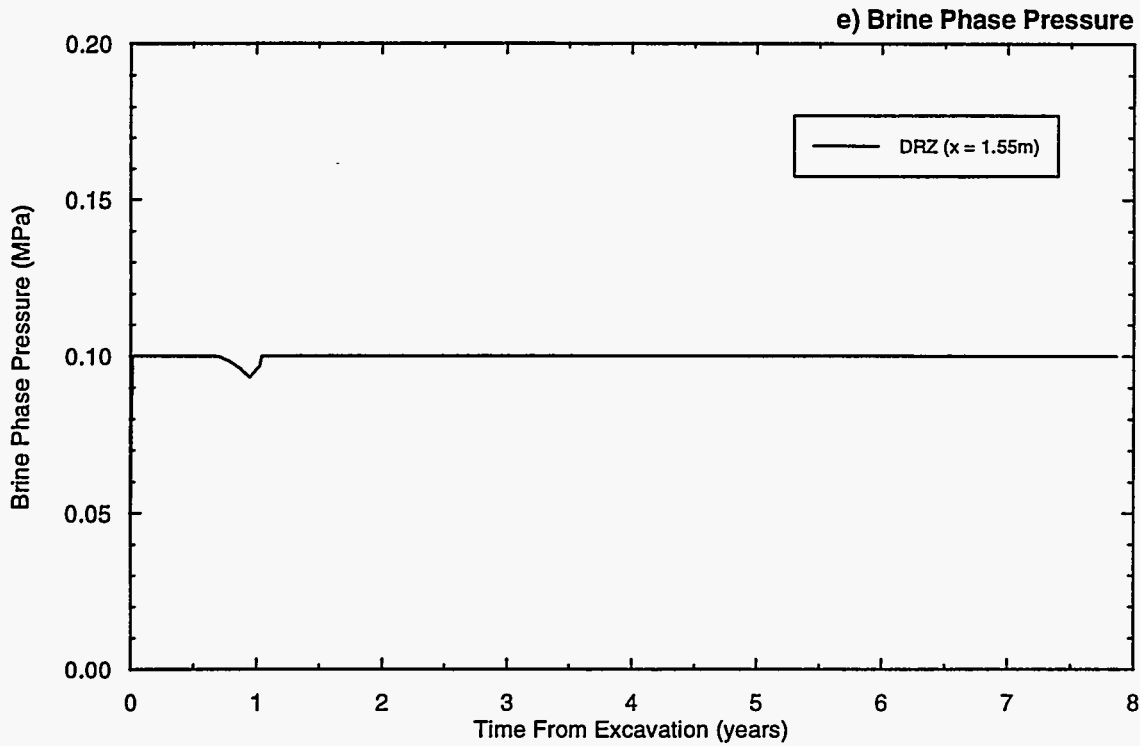
Figure 4-5 (cont.) Baseline TOUGH28W simulation (DRZ porosity increasing with time) compared with a Darcy flow simulation (fixed DRZ porosity)

in brine saturation. In summary, brine inflow to the room occurs when: (1) the rate of brine inflow to the DRZ is greater than the rate of pore volume increase, and (2) the brine phase pressure in the DRZ is greater than the room pressure.

In the baseline simulation, the rate of inflow from the far-field is greater than the rate of porosity increase for the first 0.66 years. During this time, the cumulative brine inflow from the far-field was about 205 liters, the porosity increase was about 135 liters (0.135 m^3), and brine inflow to the room was about 70 liters (Figure 4-5b). At 0.66 years, the rate of brine inflow to the DRZ decreased below the rate of DRZ porosity increase. Brine inflow to the room dropped to zero (Figure 4-5a) and the brine-phase pressure (Figure 4-5e) and saturation (Figure 4-5d) started to decrease. At 1.0 years there was a significant decline in the rate of porosity increase (Figure 4-5c) and it became less than the rate of brine inflow to the DRZ. From 1.0 to 1.04 years, far-field brine re-pressurized and re-saturated the DRZ. By 1.04 years, re-pressurization of the DRZ was sufficient to produce brine inflow to the room again. From 1.04 years to the end of the simulation at 8 years, the rate of brine inflow from the far-field exceeded the rate of porosity increase and brine inflow to the room continued. The volume of brine needed to fill the new DRZ porosity is indicated by the difference between the baseline brine inflow and the Darcy inflow in Figures 4-5a and 4-5b. Note that although specific pressure measurements around Room Q were not available, the baseline simulated brine phase pressure profile out from the room (Figure 4-5f) falls within the bounds of the widely-scattered pressure data collected from other Salado locations.

The baseline DRZ porosity increase (Figure 4-5c) was predicted by the SPECTROM-32 rock deformation code. The DRZ porosity data input to TOUGH28W is limited by the 1 year temporal discretization of the SPECTROM-32 simulation. In the baseline TOUGH28W simulation, the DRZ porosity increase was linear from 0 to 1 year after excavation (Figure 4-5c). In reality, the rate of porosity increase is much greater immediately following excavation than it is 1 year after excavation. Recall that the simulated brine inflow to the room in the first 0.66 years was due to the rate of far-field brine inflow exceeding the rate of porosity increase. A larger rate of porosity increase in the first 0.66 years could possibly shut off early-time brine inflow to the room. Two sensitivity simulations were run to examine the sensitivity of brine inflow to the early-time DRZ porosity change. The baseline porosity relationship produces a porosity increase of 17 liters (0.017 m^3) in the first time step. One sensitivity simulation used a porosity increase of 141 liters in the first time step, the other used a porosity decrease of 106 liters in the first time step. The early-time porosity
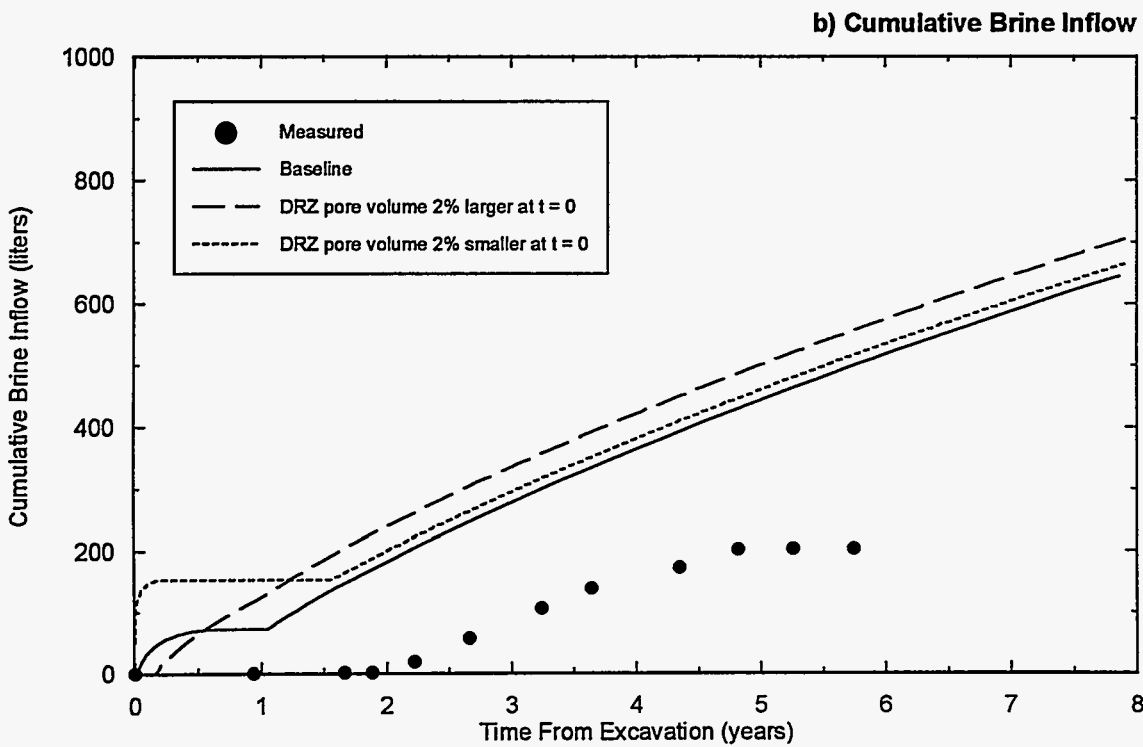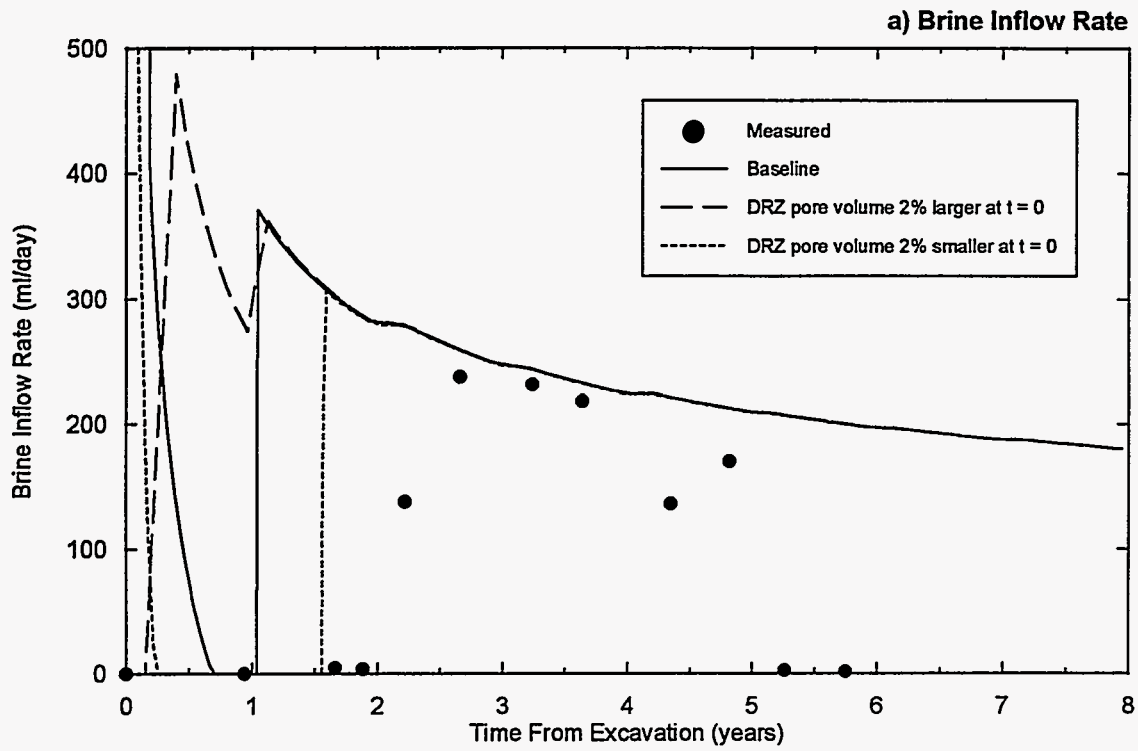
Figure 4-6. TOUGH28W simulations for sensitivity to initial (t = 0) DRZ porosity.

c) DRZ Porosity (x = 1.65 m)

Legend:
- Baseline
- DRZ pore volume 2% larger at t = 0
- DRZ pore volume 2% smaller at t = 0

d) DRZ Brine Phase Pressure (x = 1.55 m)

Legend:
- Baseline
- DRZ pore volume 2% larger at t = 0
- DRZ pore volume 2% smaller at t = 0
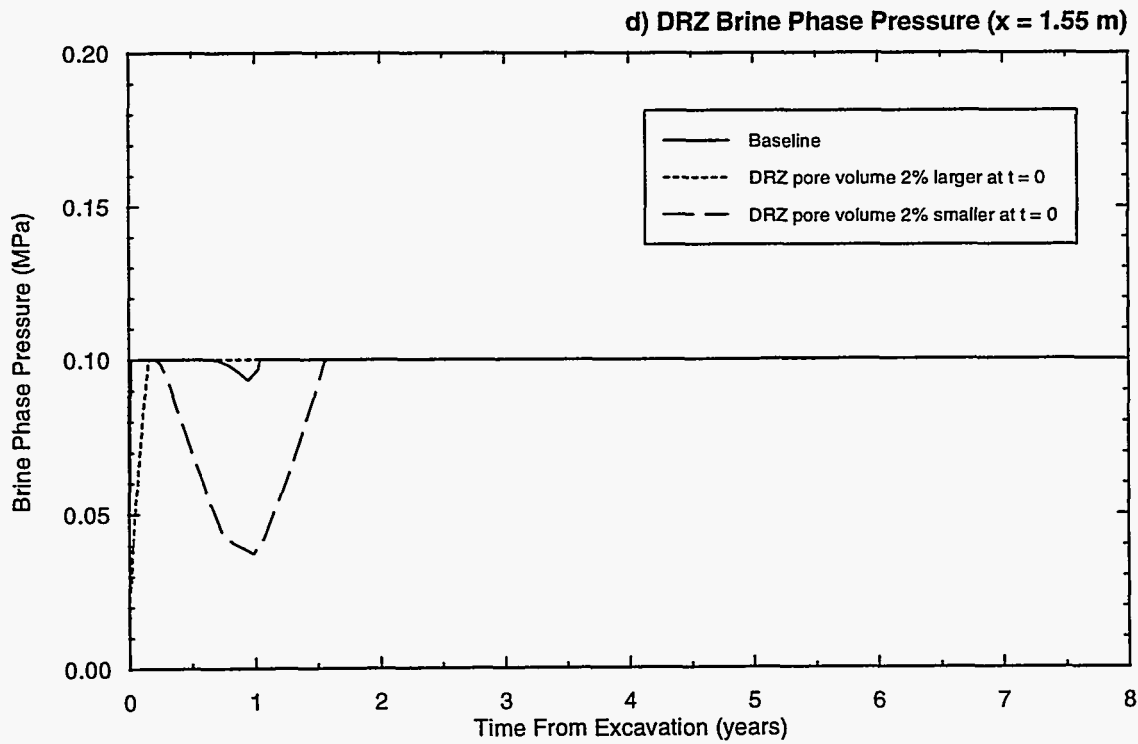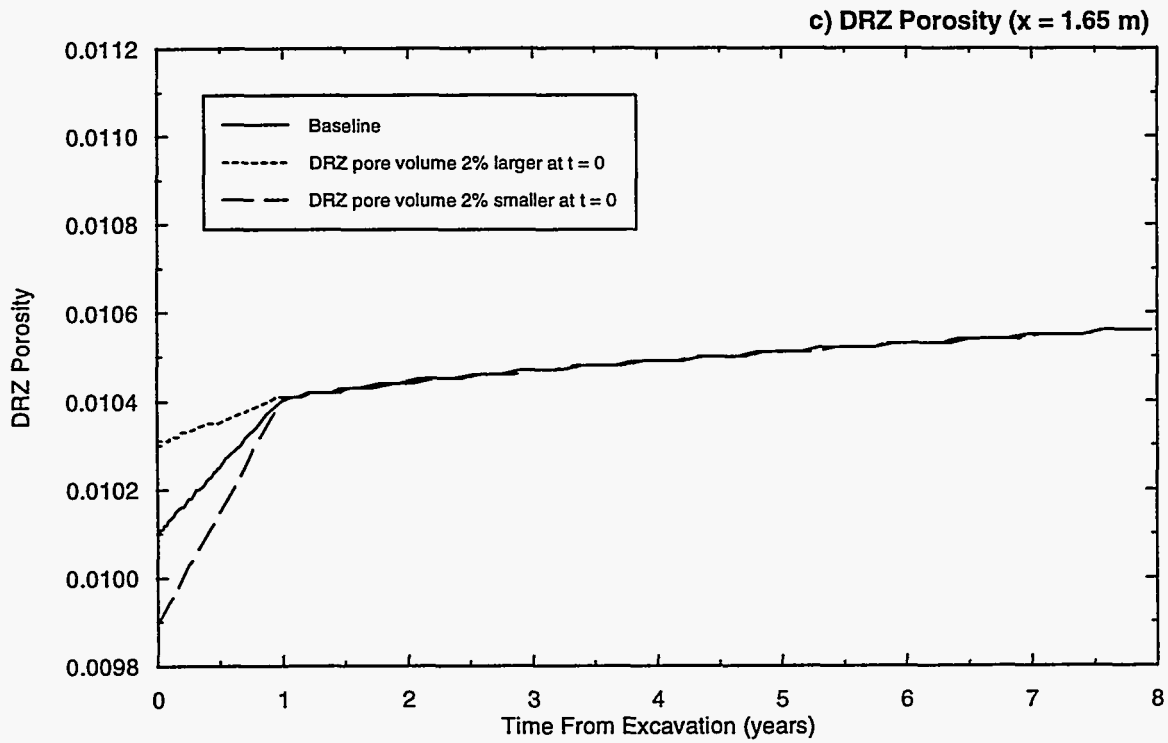
Figure 4-6. (cont.) TOUGH28W simulations for sensitivity to initial (t = 0) DRZ porosity.

was adjusted by changing the specified TOUGH28W porosity at time 0 by only 2% (Figure 4-6c). The 2% change (±0.0002) in the time 0 porosity is small relative to the uncertainty in the SPECTROM-32 model.

The early-time porosity sensitivity simulation results are shown in Figures 4-6a. The early-time brine inflow behavior is shown to be very sensitive to the simulated early-time DRZ porosity increase. Early-time brine inflow to the room can be shut off by a small increase in early-time porosity (Figure 4-6a). Conversely, the period of zero brine inflow can be extended by a small decrease in the early-time porosity. These sensitivity results further suggest that the simulated early-time brine inflow to the room should be ignored when comparisons are made with measured Room Q brine inflow.

Additional sensitivity simulations were performed on the pore volume and extent of the DRZ. The baseline DRZ had an initial pore volume of 6.08 m^3 (6080 liters) and increased by 0.21 m^3 after 1 year, 0.26 m^3 after 5 years, and 0.29 m^3 after 8 years. Sensitivity simulations examined an additional 0.3 m^3 (5%) and 0.6 m^3 (10%) increase in the total DRZ pore volume. The additional increase occurred during the first time step (Figure 4-7c). The rate of increase after the first time step was the same as in the baseline simulation. This is equivalent to an initial DRZ porosity of 0.0105 for a 5% increase and 0.011 for a 10% increase. Sensitivity simulation results are shown in Figure 4-7. Brine inflow to the room (Figure 4-7a) started later than in the baseline simulation because brine first had to re-pressurize (Figure 4-7d) and re-saturate the new DRZ porosity. Note that there is a significant increase in the rate of pressurization (Figure 4-7d) at 1 year, corresponding to time when the rate of DRZ porosity increase is reduced (Figure 4-7c). Note also that the 5% porosity increase simulation provides a better fit to the measured brine inflow than the baseline simulation. An initial DRZ porosity of 0.0105 (rather than 0.01) is well within the uncertainty in DRZ porosity.

The baseline DRZ extends out 0.55 m radially from the edge of the room. A sensitivity simulation was performed with a 0.15 m DRZ. The smaller radius DRZ had approximately the same pore volume and pore volume increase with time as the baseline DRZ. There were small differences in the pore volumes due to averaging in the calculation of the DRZ grid block porosities. Simulation results are shown in Figure 4-8. The brine inflow rates are similar for the two simulations. The small differences in inflow are due to the small differences in the pore volumes. This result suggests that brine inflow is sensitive to the DRZ pore volume, but not to the DRZ extent.
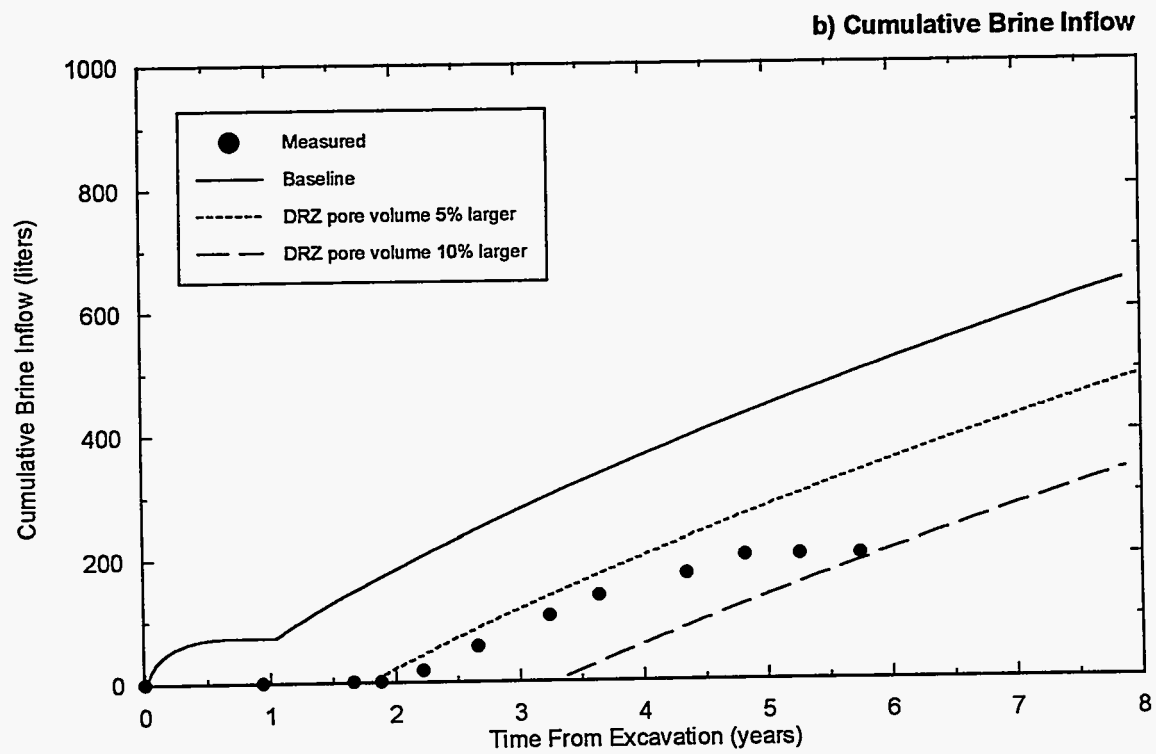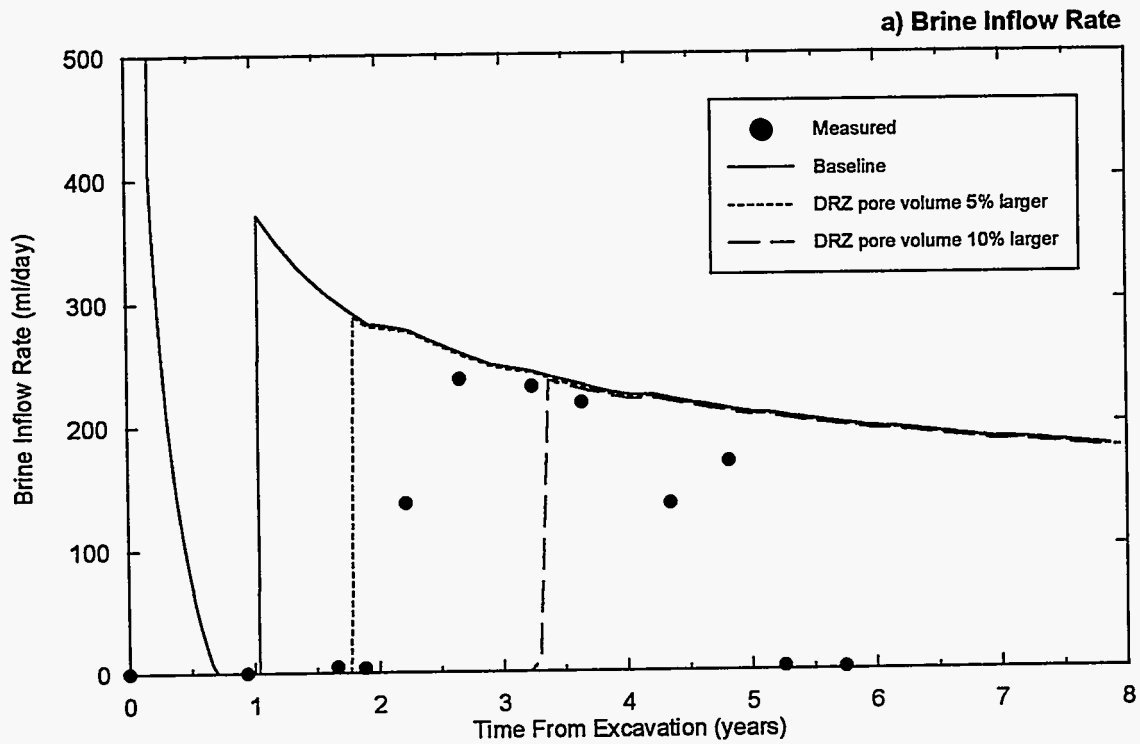
Figure 4-7. TOUGH28W simulations for sensitivity to total DRZ pore volume.

c) DRZ Porosity (x = 1.65 m)

Legend:
- Baseline
- DRZ pore volume 5% larger
- DRZ pore volume 10% larger

DRZ Porosity vs. Time From Excavation (years)

d) DRZ Brine Phase Pressure (x = 1.55 m)

Legend:
- Baseline
- DRZ pore volume 5% larger
- DRZ pore volume 10% larger

Brine Phase Pressure (MPa) vs. Time From Excavation (years)
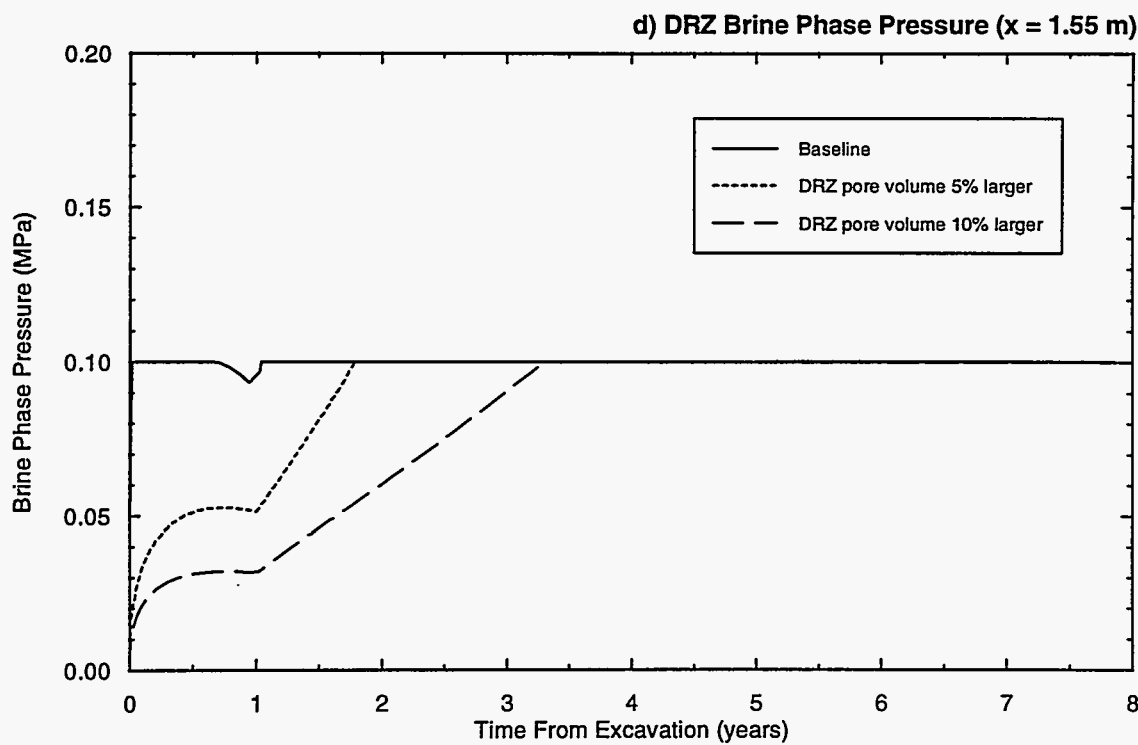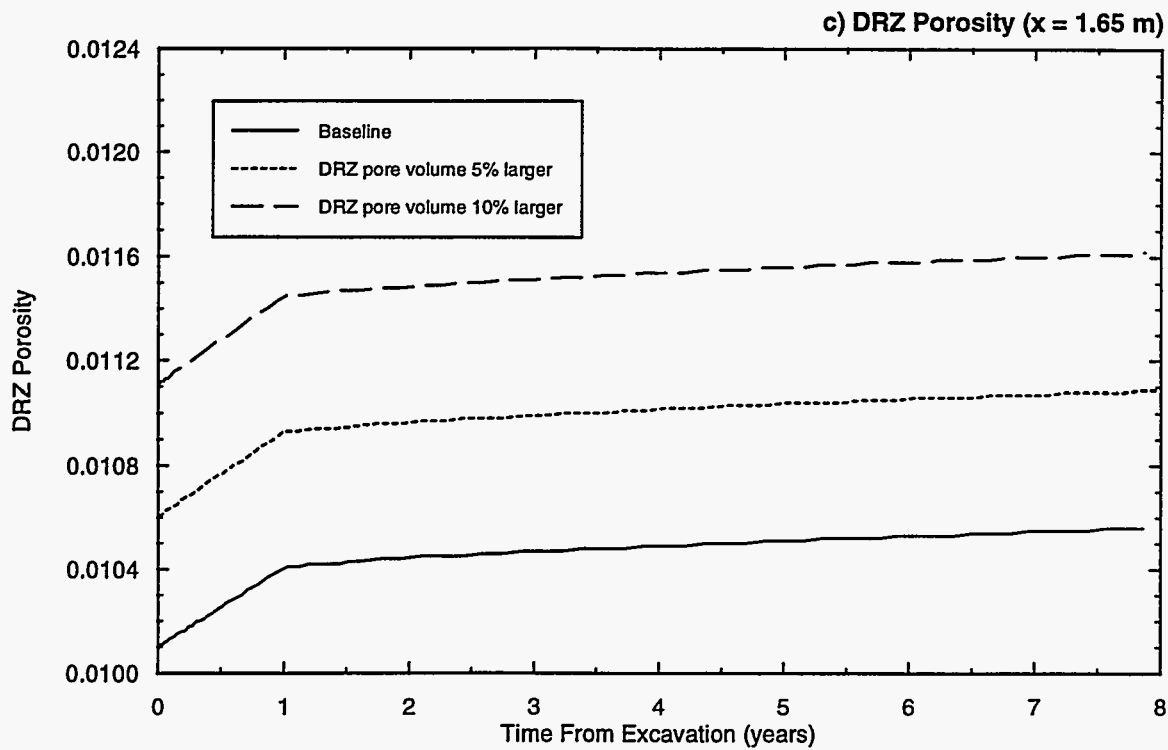
Figure 4-7 (cont.) TOUGH28W simulations for sensitivity to total DRZ pore volume.
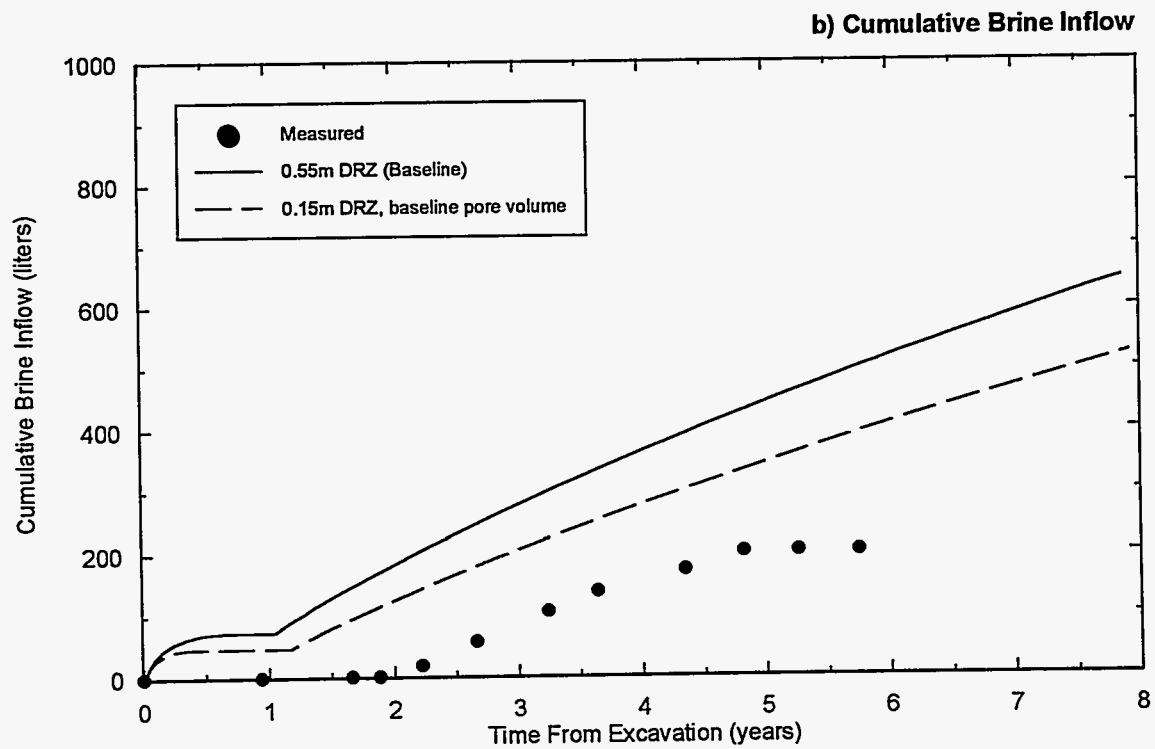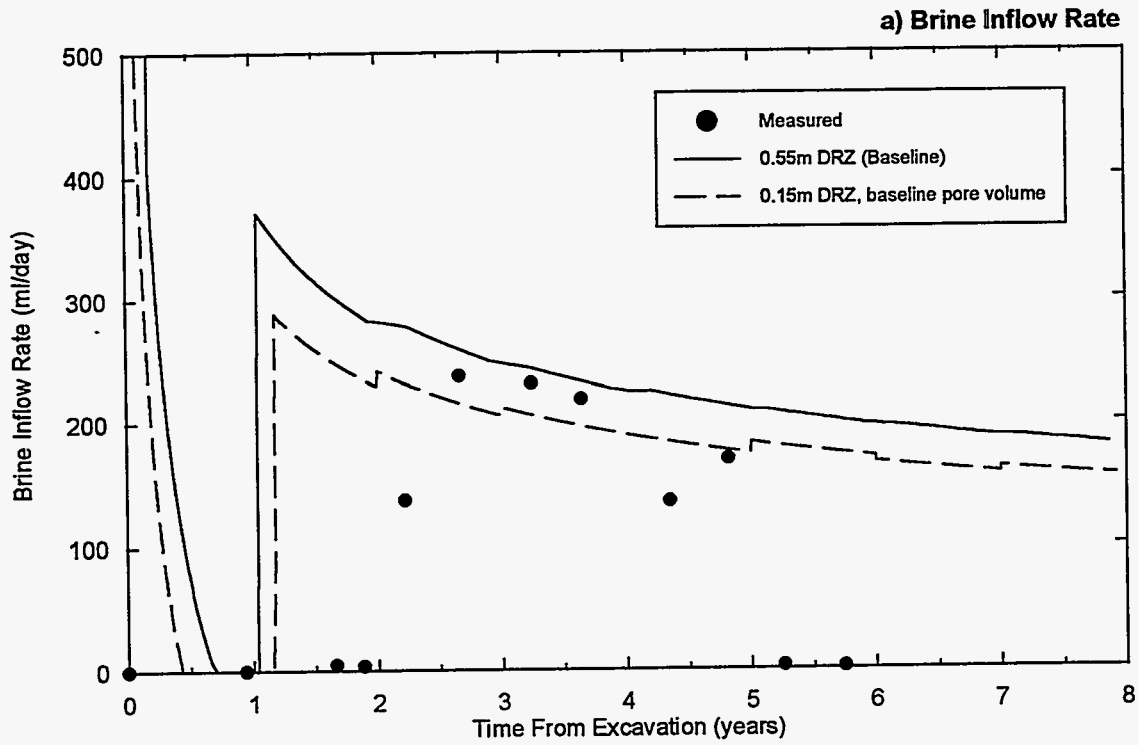
Figure 4-8. TOUGH28W simulations for sensitivity to DRZ extent.

44

A final sensitivity on DRZ properties was performed on intrinsic permeability and on initial pressure. Two DRZ permeabilities, 1×10^{-18} m^2 and 1×10^{-21} m^2, were examined in addition to the baseline value of 1×10^{-15} m^2. There is considerable uncertainty in the DRZ permeability. The six order of magnitude range examined here is representative of the expected range. Simulation results are shown in Figure 4-9. Brine inflow decreased with decreasing permeability. With a permeability of 1×10^{-15} m^2, the DRZ pressure equilibrates very quickly (in the first few time steps) with the 0.1 MPa room pressure. With lower permeabilities, the pressure equilibration is slower, and it takes longer for the DRZ to re-pressurize after the early-time pore volume increase (Figure 4-9c). This time lag in re-pressurization is reflected by a lag in brine inflow (Figure 4-9a) and a reduction in cumulative inflow (Figure 4-9b).

Under certain conditions, the brine inflow is also very sensitive to the initial pressure in the DRZ. The baseline simulation assumed an initial DRZ brine pressure of 0.1 MPa. Sensitivity simulations were run with initial DRZ brine pressures of 12.5 MPa and DRZ permeabilities of 1×10^{-15} m^2 and 1×10^{-21} m^2. Simulation results are shown in Figure 4-10. With a permeability of 1×10^{-15} m^2, brine inflow behavior is very sensitive to the initial DRZ pressure. With an initial pressure of 12.5 MPa, depressurization was accomplished by significant dewatering of the DRZ during the first time step, resulting in a near-instantaneous brine inflow volume of 1550 liters (Figure 4-10b). Subsequent brine inflow from the far-field increased DRZ pressure and saturation, but there was no brine inflow to the room (Figure 4-10a). With a permeability of 1×10^{-21} m^2, pressure equilibration was slower and brine inflow was not very sensitive to initial DRZ pressure. Minor differences in brine inflow were due to minimal dewatering from the 12.5 MPa initial pressure simulation.

The sensitivity simulations discussed thus far examined the DRZ properties. These properties control the early-time brine inflow. The measured brine inflow data from 2-5 years help to define the far-field properties. Sensitivity to far-field permeability is shown in Figure 4-11. Sensitivity to far-field bulk rock compressibility (which is essentially proportional to specific storage) is shown in Figure 4-12. Comparisons are best made to the slope of the measured cumulative brine inflow data. The baseline combination of 5×10^{-22} m^2 and 5.4×10^{-12} Pa^{-1} produces a cumulative brine inflow slope slightly larger than measured (Figure 4-11b). Reducing the permeability by a factor of two slightly underestimates the slope. Increasing the permeability (Figure 4-11b) or the bulk rock compressibility (Figure 4-12b) by an order of magnitude clearly
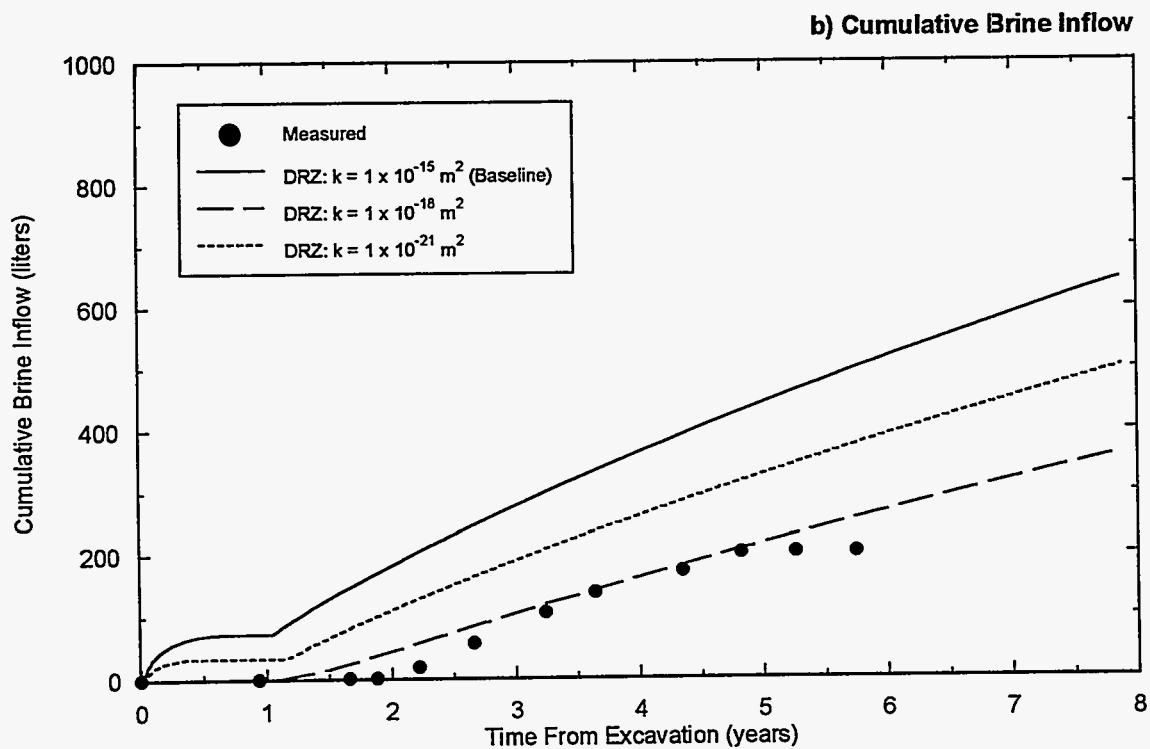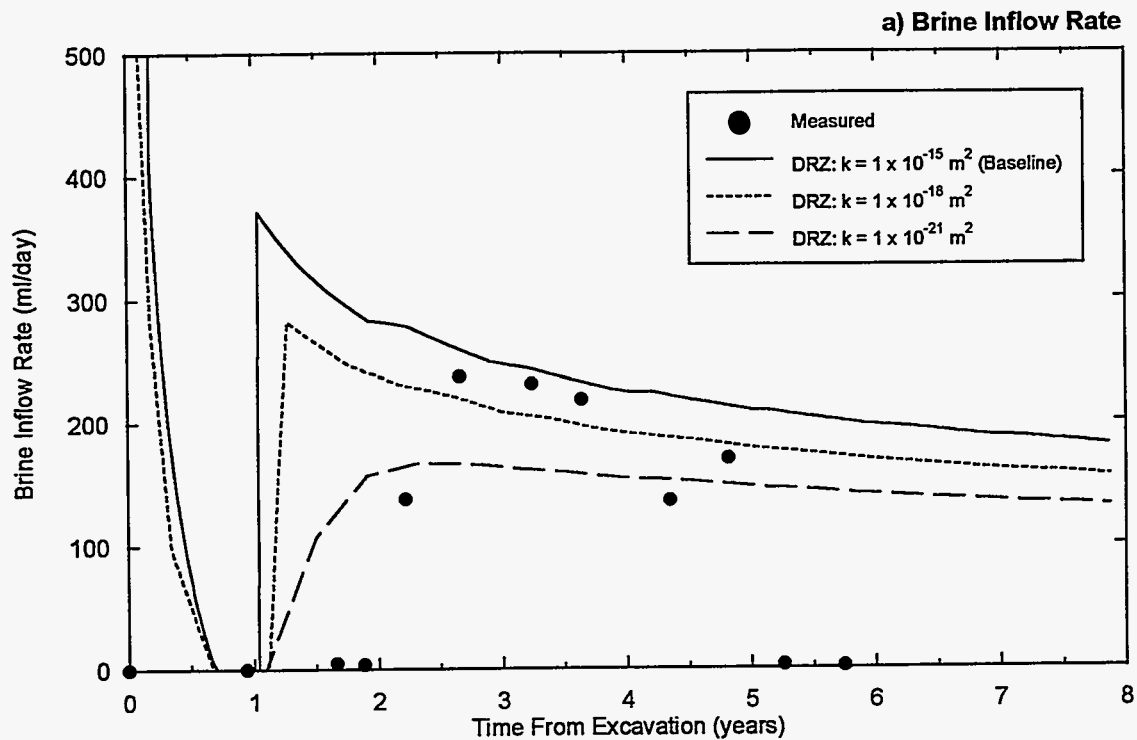
Figure 4-9. TOUGH28W simulations for sensitivity to DRZ permeability.

c) DRZ Brine Phase Pressure (x = 1.55 m)
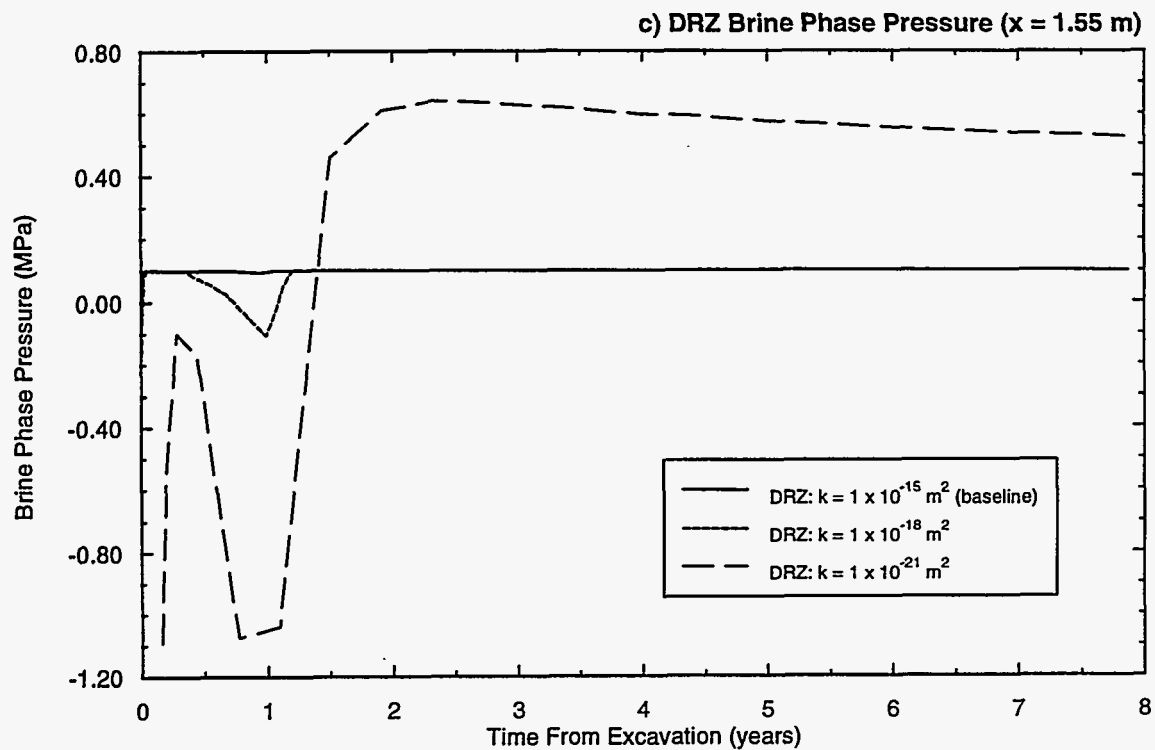
Figure 4-9. (cont.) TOUGH28W simulations for sensitivity to DRZ permeability.
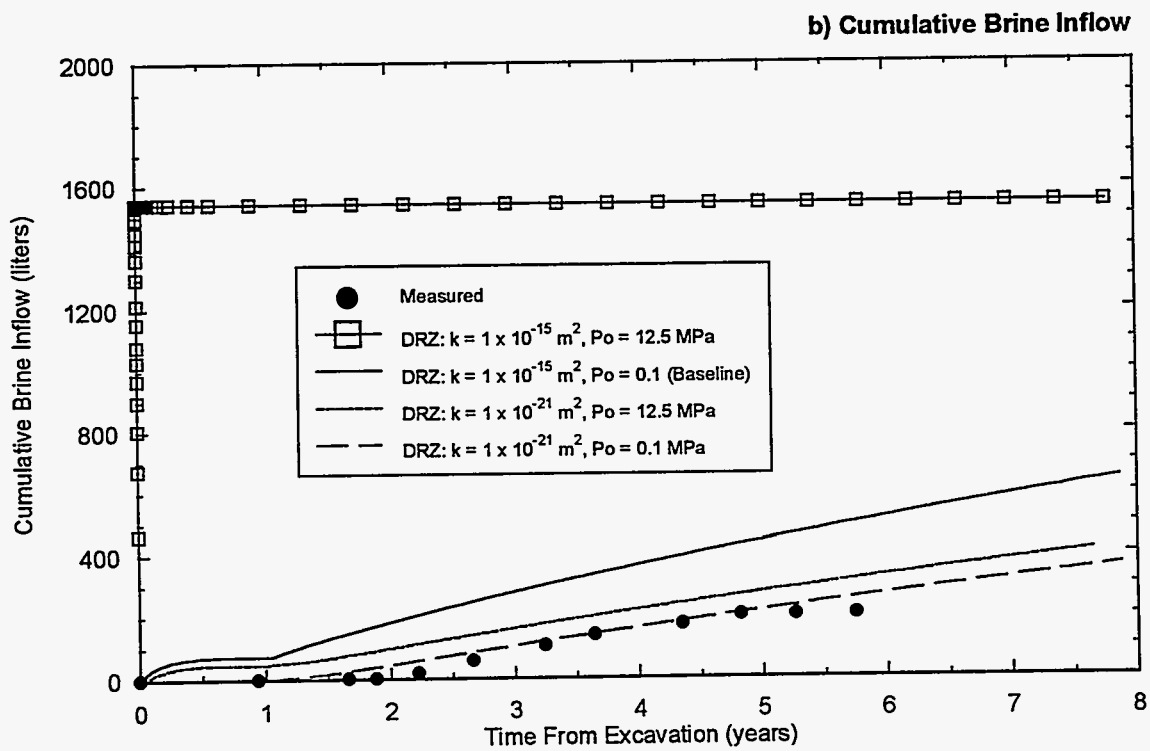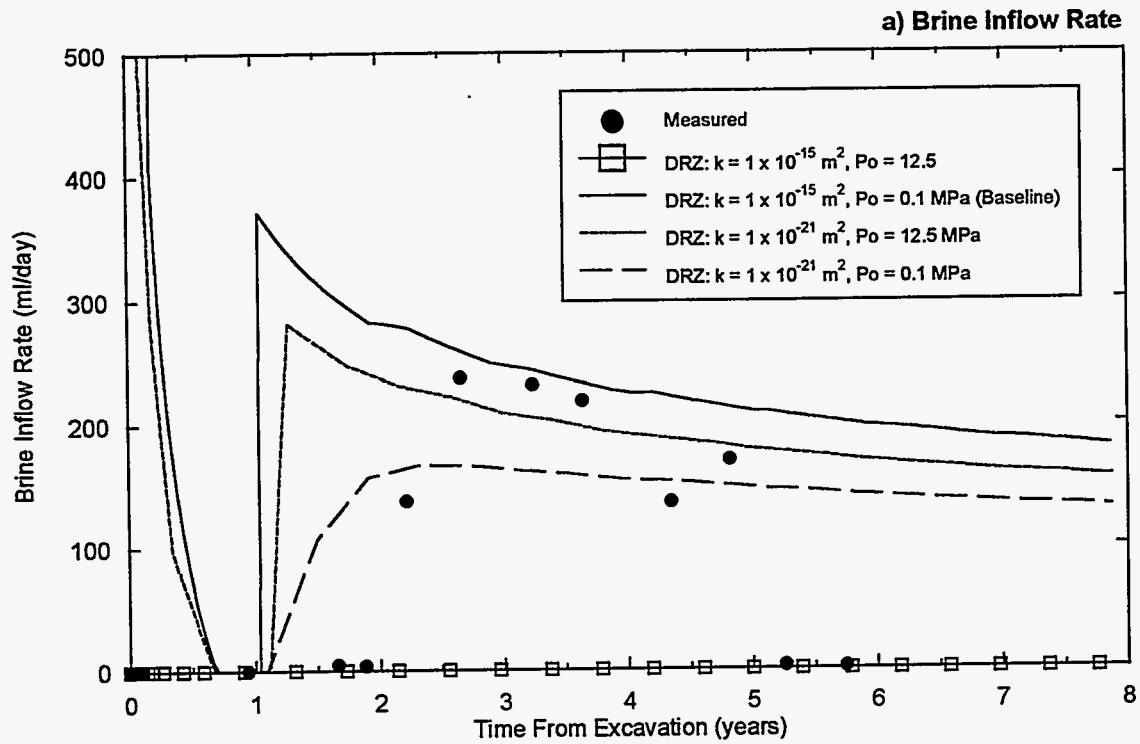
Figure 4-10. TOUGH28W simulations for sensitivity to DRZ initial brine pressure.

a) Brine Inflow Rate

Brine Inflow Rate (ml/day)

800
700
600
500
400
300
200
100
0

- ● Measured
- —— $k = 1.0 \times 10^{-21}$ m^2
- —— $k = 5.0 \times 10^{-22}$ m^2 (Baseline)
- – – $k = 2.5 \times 10^{-22}$ m^2
- —□— $k = 1.0 \times 10^{-25}$ m^2

Time From Excavation (years)

0 1 2 3 4 5 6 7 8

b) Cumulative Brine Inflow

Cumulative Brine Inflow (liters)

1200
1000
800
600
400
200
0

- ● Measured
- —— $k = 1.0 \times 10^{-21}$ m^2
- —— $k = 5.0 \times 10^{-22}$ m^2 (Baseline)
- – – $k = 2.5 \times 10^{-22}$ m^2
- —□— $k = 1.0 \times 10^{-25}$ m^2

Time From Excavation (years)

0 1 2 3 4 5 6 7 8
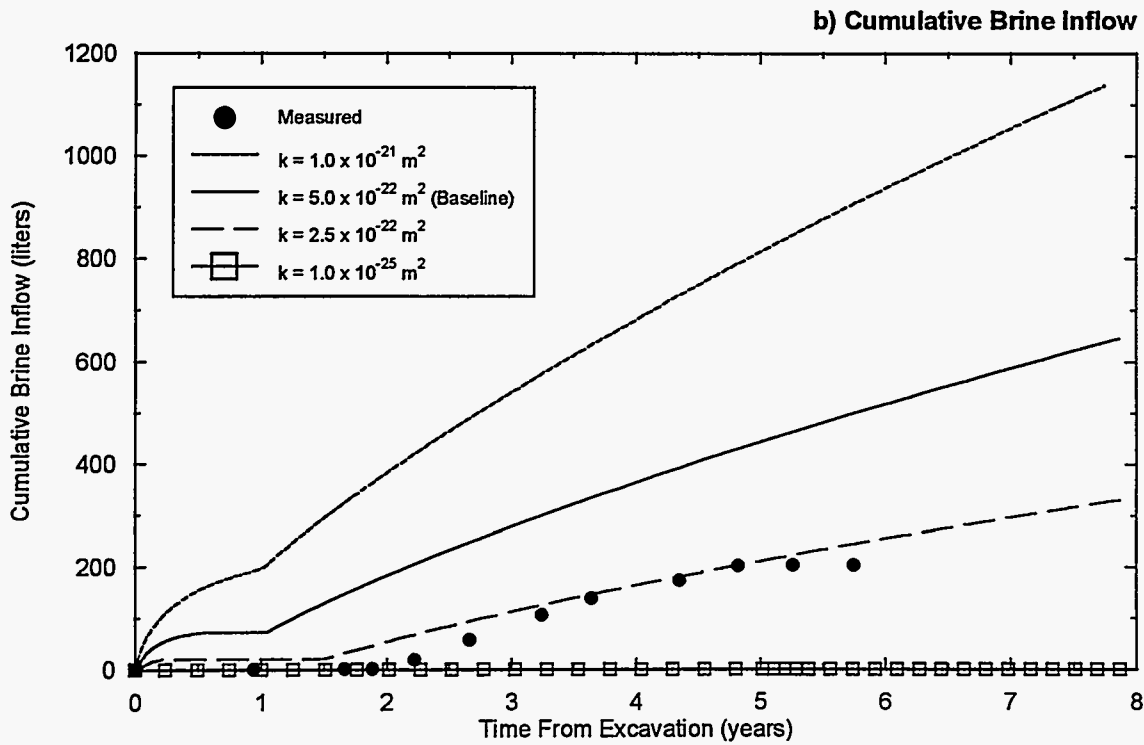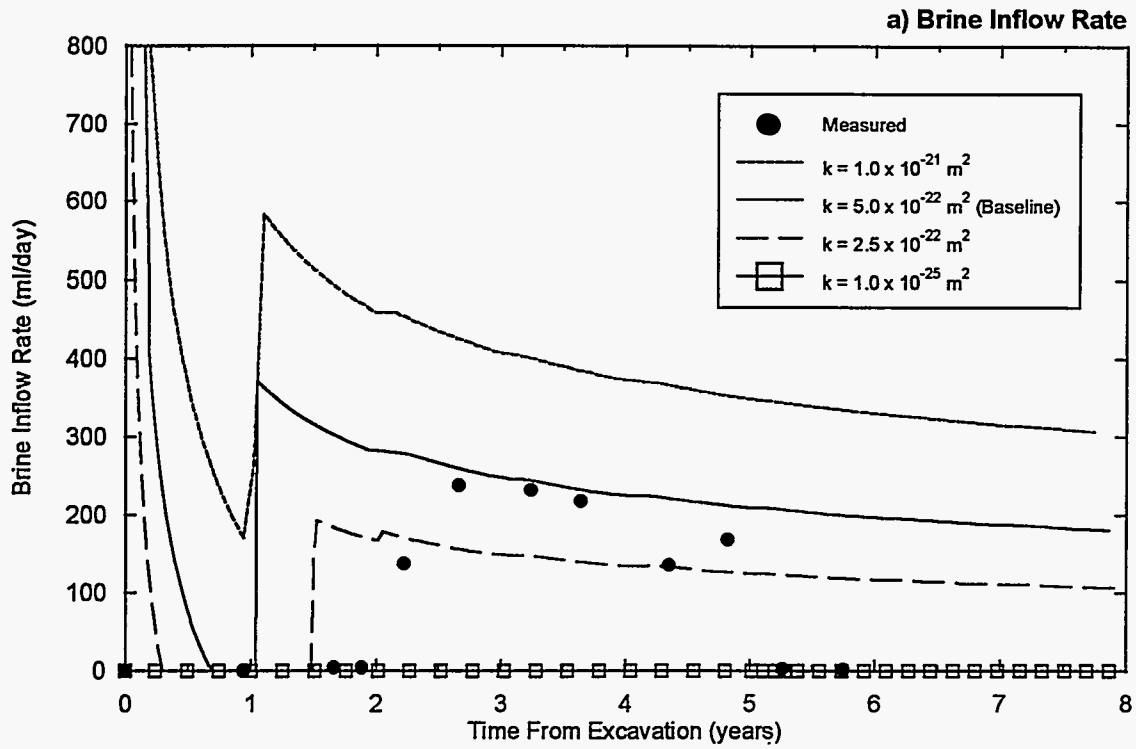
Figure 4-11. TOUGH28W simulations for sensitivity to far-field halite permeability.
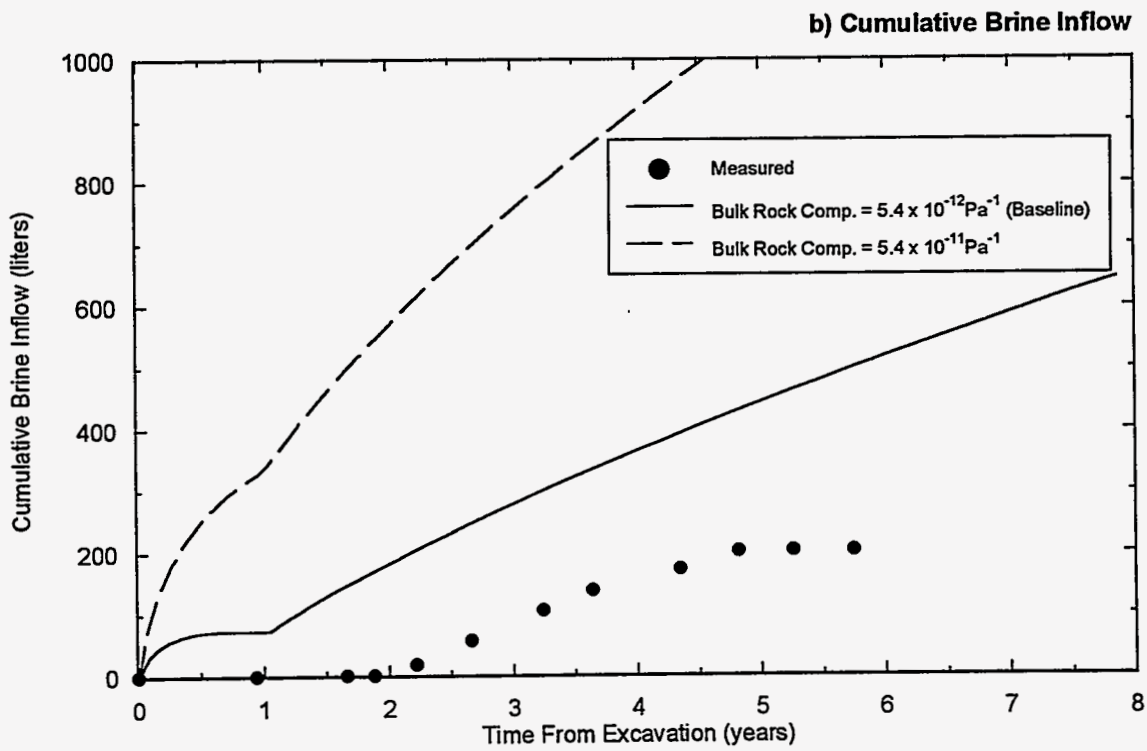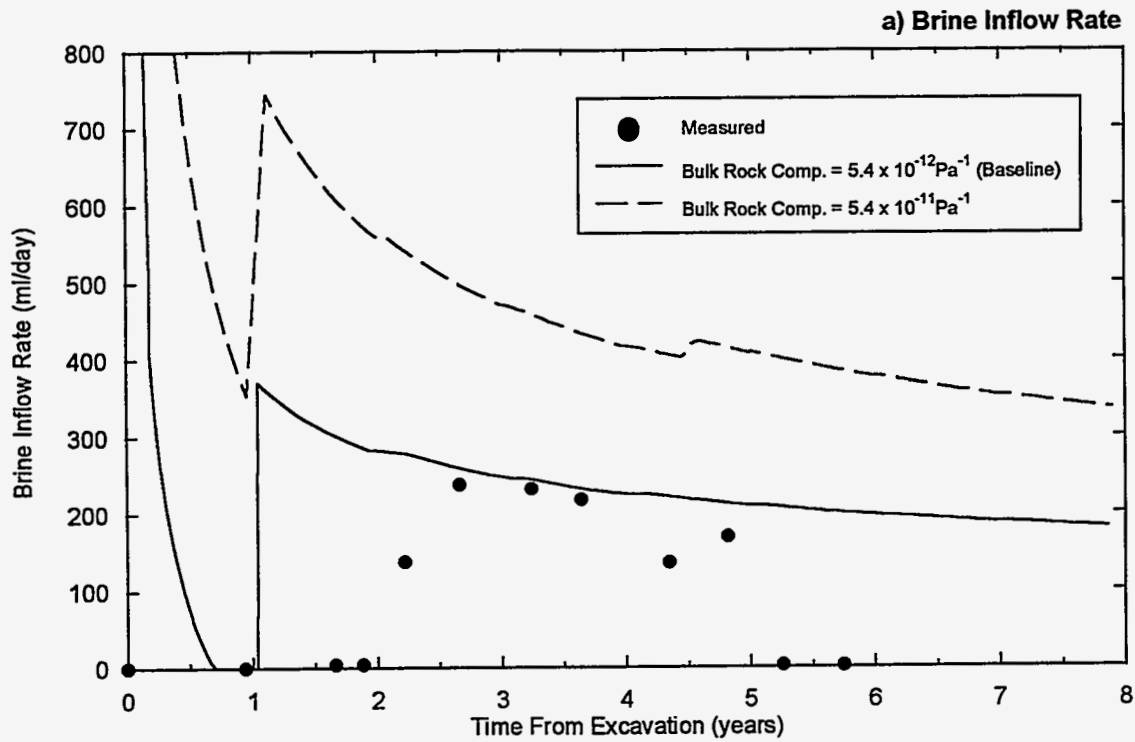
Figure 4-12. TOUGH28W simulations for sensitivity to far-field halite bulk rock compressibility.

overestimates the brine inflow. These simulation results suggest that the baseline combination of far-field permeability and compressibility is reasonable. Changing either parameter by more than a factor of two would require a commensurate change in the other parameter to maintain the proper slope in cumulative brine inflow. As discussed in Section 2.2, the simulated brine inflow is dependent on the product of permeability and rock compressibility. The baseline combination has a similar product to the current performance assessment parameters suggested by Domski et al. (1996). Note that a near-zero (1×10^{-25} m^2) far-field permeability (i.e., no far-field flow as is consistent with the redistribution model) results in zero brine inflow immediately after excavation and does not produce any brine inflow from 2-5 years. Sensitivity simulations were also run for DRZ bulk compressibility. Increasing the DRZ bulk compressibility did not have any impact on the simulated brine inflow rates.

Sensitivity simulations were performed for the two-phase properties. Changing the two-phase Brooks and Corey parameters (residual phase saturations, threshold pressure) had little effect on brine inflow. Similarly, using the van Genuchten and Parker relationships did not significantly alter brine inflow. This insensitivity to two-phase parameters is due to the fact that brine saturations remained high and brine relative permeabilities were therefore near 1.0. If conditions within the DRZ produced lower brine saturations, it is possible that the two-phase properties would be more important.

4.5 Implications For Performance Assessment

The baseline and sensitivity simulations described in Section 4.4 suggest that early-time brine inflow to Room Q can be reduced by 300 liters or more (Figure 4-5b) with an increasing DRZ porosity. A similar reduction in early-time brine inflow (relative to Darcy flow) to a waste disposal room could result in a significant reduction in brine-dependent corrosion and gas-generation rates. For the short duration (<10 years) Room Q simulations, the DRZ porosity was continually increasing. For the 10,000-year WIPP Performance Assessment (PA) calculations, the process of DRZ healing (decreasing DRZ porosity with time) should also be considered. In long-term simulations that include healing, the 300 liters of brine might flow into the room at a later time, if healing is sufficient to "squeeze" it back out of the DRZ. Even if healing is significant, the time offset in brine inflow due to an early-time DRZ porosity increase could still have important implications to repository performance.

51

The method for increasing DRZ porosity with time as used in the TOUGH28W simulations is too computationally intensive for use in WIPP PA calculations. Instead, an alternative DRZ conceptualization is proposed for use in PA. The suggested PA DRZ conceptualization assumes a fixed porosity that is equivalent to a time-averaged DRZ pore volume. The baseline simulation can be represented by a PA conceptualization with a fixed DRZ porosity of 0.0104 and an initial brine phase saturation of 0.96. The PA conceptualization does not utilize the porosity versus time relationships in the DRZ. The PA conceptualization is hereafter referred to as the PA model. Both models, baseline and PA, have an initial brine volume of approximately 6070 liters and an initial DRZ brine pressure of 0.1 MPa. The baseline model creates 210 liters of new DRZ porosity by the end of 1 year and 289 liters by the end of 8 years. During the first year, the rapid creation of pore volume produces a depressurization of the DRZ, which shuts off brine inflow to the room. In contrast, the PA model has an extra 250 liters of DRZ porosity that is initially air-filled. However, because the extra DRZ pore volume is an initial condition, there is no mechanism to depressurize the DRZ and therefore, the mechanism that shuts off early-time brine inflow in the baseline simulation is not available in the PA model conceptualization. In the PA model, the lack of an underpressured DRZ allows brine that flows into the DRZ from the far-field to flow directly into the room (i.e., Darcy flow) rather than re-pressurizing and re-saturating the DRZ. Simulation results for the 250-extra-liter PA model DRZ are shown in Figure 4-13. The PA model approximately matches Darcy flow (Figure 4-5).

Fortunately, the PA model DRZ can be depressurized through a different mechanism. When the air phase in the DRZ is mobile (gas saturation greater than the residual saturation of 0.20), some pressure equilibration occurs through gas flow from the DRZ to the room. Because of capillary effects in the DRZ, equilibration of air phase pressures between the room and the DRZ results in DRZ brine phase pressures of less than 0.1 MPa. To test this hypothesis, a second PA model was constructed, with different parameters. The second PA model had the same initial brine volume of approximately 6070 liters and initial DRZ brine pressure of 0.1 MPa as the first PA model. However, the initial air volume was the sum of: (1) the volume of air required to establish residual gas saturation (0.20) throughout the DRZ (1520 liters), and (2) an extra volume of 250 liters, representative of newly created air-filled porosity. These brine and air volumes were represented by a second PA model DRZ with a fixed porosity of 0.0129 and an initial brine phase saturation of 0.775.

a) Brine Inflow Rate

Legend:
- ● Measured
- —— Baseline (changing DRZ porosity)
- —— PA (fixed DRZ porosity = 0.0104)
- – – PA (fixed DRZ porosity = 0.0129)

b) Cumulative Brine Inflow

Legend:
- ● Measured
- —— Baseline (changing DRZ porosity)
- —— PA (fixed DRZ porosity = 0.0104)
- – – PA (fixed DRZ porosity = 0.0129)
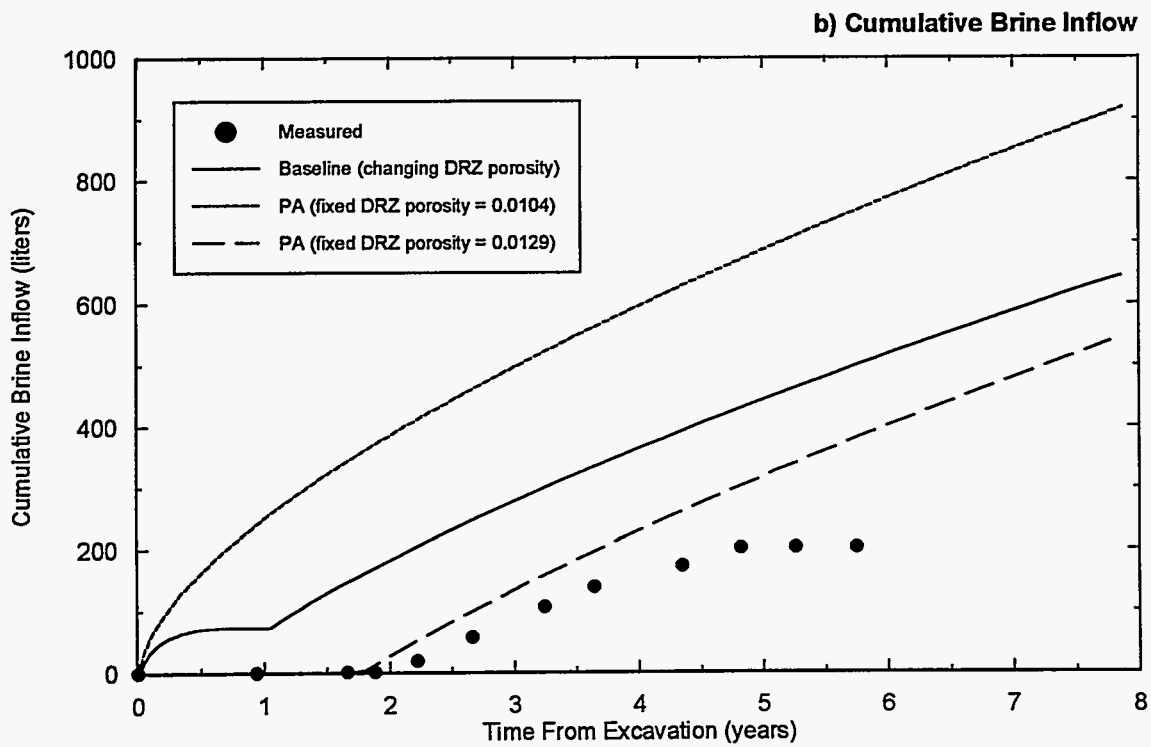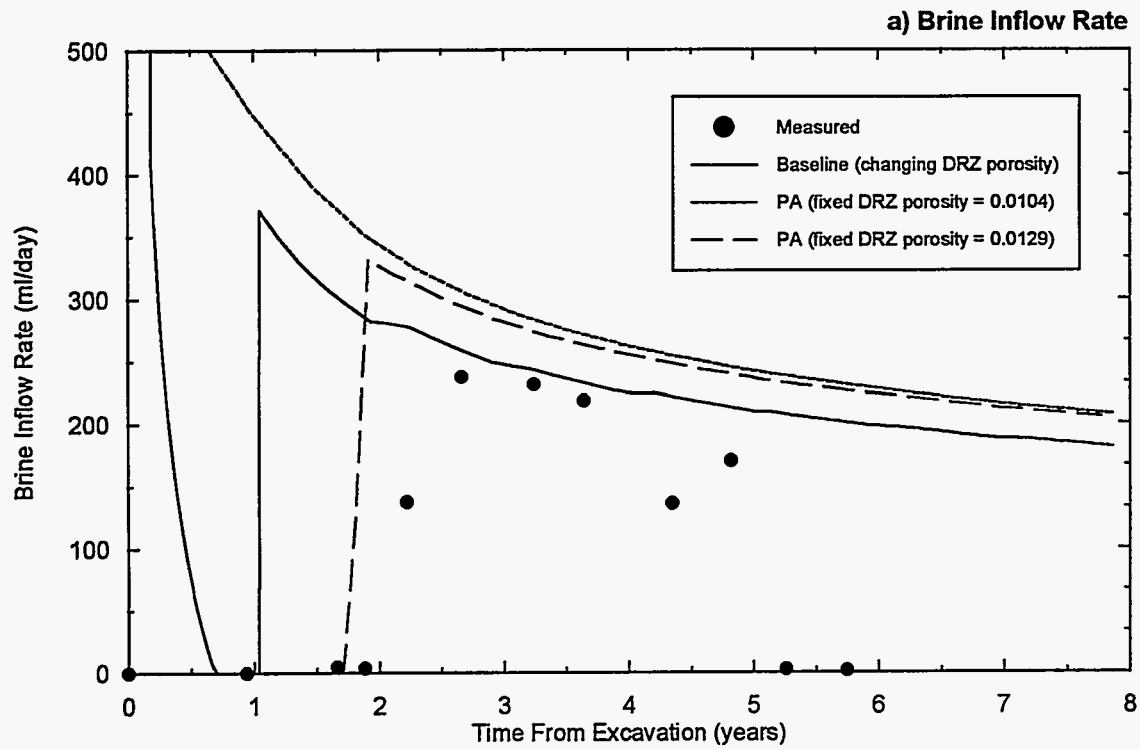
Figure 4-13. Simulations using the suggested Performance Assessment
conceptualization of the DRZ.

53

c) DRZ Brine Phase Pressure (x = 1.55m)
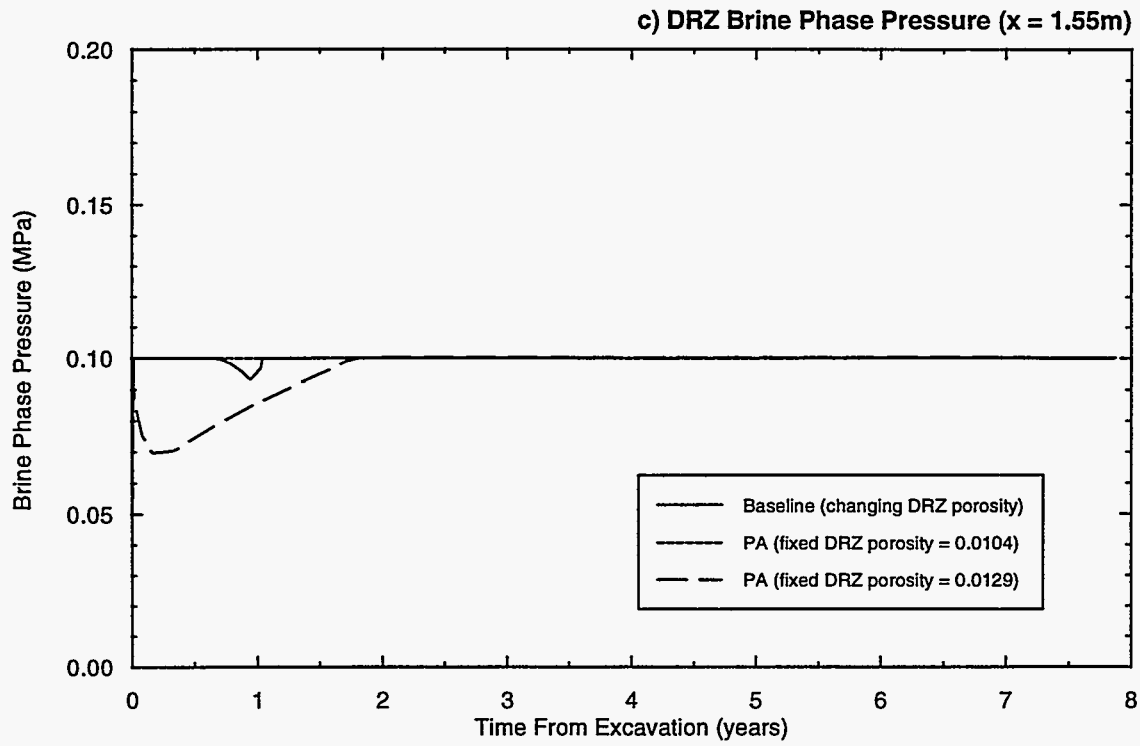
Figure 4-13. (cont.)   Simulations using the suggested Performance
Assessment conceptualization of the DRZ.

Simulation results for the second PA model are compared with the first PA model and with the baseline simulation in Figure 4-13. The second PA model produces similar brine inflow (Figures 4-13a and 4-13b) to the TOUGH28W baseline and in fact provides a slightly better fit to the measured inflows. Note that the PA model does not produce the early-time brine inflow "spike" characteristic of the changing porosity conceptualization. In the first 0.2 years, the DRZ brine pressure in the second (0.0129 porosity) PA model decreases to 0.07 MPa (Figure 4-13c) as a result of air flow from the DRZ to the room. From 0.25 to 1.8 years, brine inflow from the far-field re-pressurized the DRZ, and there was no brine (or gas) inflow to the room. From about 2 years onward, the DRZ was slightly above 0.1 MPa and there was brine inflow to the room. The PA model brine inflow rates (Figure 4-13a) are higher than the baseline inflow rates from 2 years onward, because some of the brine in the baseline model flows into DRZ porosity that is continually being created rather than into the room.

The suggested PA implementation uses early-time gas flow from the DRZ to the room to depressurize the DRZ, whereas the changing porosity implementation uses rapidly increasing pore volumes to depressurize the DRZ. Despite this difference, the two methods give similar results and both methods shut off early-time brine inflow to the room, consistent with the measured brine accumulation.

5.0 CONCLUSIONS AND RECOMMENDATIONS

A modeling study was performed to gain insight into the flow mechanisms around Room Q. A conceptual model for brine inflow to Room Q, which assumes far-field Darcy flow, is summarized in Figure 4-2. The lack of measured brine accumulation in the room for the first two years following excavation is attributed to (1) far-field brine flowing into newly created DRZ porosity, and (2) evaporation of brine from the walls of the room. Measured brine accumulation in the room from 2-5 years following excavation is attributed to Darcy flow from the far-field. The lack of measured brine accumulation after 5.5 years is attributed to brine leaking out of the room through fractures under the room seals before it can be measured.

Numerical simulations were performed with TOUGH28W to examine far-field Darcy flow combined with an increasing DRZ pore volume. Measured data was available from the 6-year period following excavation, however, there is considerable uncertainty associated with much of the data. The primary measured data used for evaluation were brine accumulation volumes and rates. Data predicting the DRZ porosity increase with time was taken from SPECTROM-32 rock deformation simulations. Evaporation and brine leakage under the seals were not simulated, however, bounding calculations were made to estimate their potential impact on measured brine accumulation.

Simulation results show that early-time brine inflow to the room can be reduced to zero if an increasing DRZ porosity with time is simulated. The early-time brine inflow to the room is very sensitive to the DRZ pore volume. Small changes in pore volume can produce large changes in cumulative brine inflow in the first 2 years. Reasonable assumptions about the DRZ pore volume result in simulated early-time brine inflow volumes ranging from 0-300 liters. Even in the case where 300 liters of brine inflow is predicted in the first year, the potential for evaporation (which may be anywhere from 200-8000 ml/day in the first 300 days) is enough to remove 300 liters from the room in 1 year. Because there is considerable uncertainty in the measured brine inflow rates and the DRZ pore volume, it is not possible to draw specific conclusions regarding the volume of brine that fills newly created DRZ porosity relative to the volume of brine that is lost to evaporation. However, reasonable assumptions about the DRZ pore volume can produce enough new DRZ porosity in the first 2 years to completely shut off brine inflow to the room. Also, if no new DRZ porosity were being created, predicted brine inflow rates are on the order of 3000-6000 ml/day in the first week after excavation. Since the tunnel boring personnel did not document any inflow rates of this magnitude, and there were no salt encrustations on the room walls to suggest evaporation

57

rates of this magnitude, it is likely that there was at least some brine flow into the newly created DRZ porosity. This brine may become available at a later time if DRZ healing is sufficient to "squeeze" brine out of the pore space.

The measured brine inflow data from 2-5 years was used to define the far-field properties because it is less sensitive than early-time inflow to the DRZ effects. The baseline combination of 5×10^{-22} m^2 permeability and 5.4×10^{-12} Pa^{-1} bulk rock compressibility produces a cumulative brine inflow that closely matches the measured values. Changing either parameter by more than a factor of 2 would require a commensurate change in the other parameter to maintain the proper slope in cumulative brine inflow.

The reduction in brine accumulation after 5.5 years was not reproduced in simulations. A near-zero far-field permeability results in zero brine inflow immediately after excavation. The only possible mechanisms to shut off brine inflow after 5.5 years in the current conceptual model would be a sudden reduction in far-field permeability or a sudden increase in DRZ pore volume. Neither of these mechanisms is very likely. Scoping calculations indicate that, for an assumed DRZ permeability of 10^{-15} m^2, 100 ml/day of brine could leak out of the room under the seals prior to being measured. Greater leakage is possible if the DRZ permeability is larger. Leakage under the seals is the most plausible explanation for the absence of late-time brine accumulation. Alternatively, evaporation was measured at 20 ml/day from a small sealed region. This extrapolates to as much as 800 ml/day over the entire length of the sealed room.

In summary, the proposed model, which uses far-field Darcy flow and a changing DRZ porosity, reproduces the measured Room Q brine accumulation data. Early-time brine inflow to Room Q can be reduced to zero if the DRZ porosity increases with time in a manner consistent with room closure/rock mechanics calculations. This phenomena can be implemented in Performance Assessment calculations through the use of a fixed porosity DRZ region with a reduced initial brine saturation.

6.0 REFERENCES

Beauheim, R.L., G.J. Saulnier, Jr., and J.D. Avis. 1991. *Interpretation of Brine-Permeability Tests of the Salado Formation at the Waste Isolation Pilot Plant Site: First Interim Report.* SAND90-0083. Albuquerque, NM: Sandia National Laboratories.

Beauheim, R.L., R.M. Roberts, T.F. Dale, M.D. Fort, and W.A. Stensrud. 1993. *Hydraulic Testing of Salado Formation Evaporites at the Waste Isolation Pilot Plant Site: Second Interpretive Report.* SAND92-0533. Albuquerque, NM: Sandia National Laboratories.

Borns, D.J., and J.C. Stormont. 1988. *An Interim Report on Excavation Effect Studies at the Waste Isolation Pilot Plant: The Delineation of the Disturbed Rock Zone.* SAND87-1375. Albuquerque, NM: Sandia National Laboratories.

Borns, D.J., and J.C. Stormont. 1989. "The Delineation of the Disturbed Rock Zone Surrounding Excavations in Salt," *Rock Mechanics as a Guide for Efficient Utilization of Natural Resources: Proceedings of the 30th U.S. Symposium, West Virginia University, Morgantown, WV, June 19-22, 1989.* Ed. A.W. Khair. SAND88-2230C. Brookfield, VT: A.A. Balkema. 353-360.

Bredehoeft, J.D. 1988. "Will Salt Repositories Be Dry?," *EOS Transactions, American Geophysical Union.* Vol. 69, no. 9, pp. 121, 131.

Callahan, G.D., A.F. Fossum, and D.K. Svalstad. 1989. *Documentation of SPECTROM-32: A Finite Element Thermomechanical Stress Analysis Program.* DOE/CH/10378-2; RSI-0269. Argonne, IL: U.S. Department of Energy, Chicago Operations Office; Rapid City, SD: RE/SPEC Inc.

Chan, K.S., S.R. Bodner, A.F. Fossum, and D.E. Munson. 1992. "A Constitutive Model for Inelastic Flow and Damage Evolution in Solids Under Triaxial Compression," *Mechanics of Materials.* SAND92-0546J. Vol. 14, no. 1, 1-14.

CRC Press. 1985. *Handbook of Chemistry and Physics.* Ed. R.C. Weast. 66th ed. Boca Raton, FL: CRC Press. pp. E-1.

Deal, D.E., and J.B. Case. 1987. *Brine Sampling and Evaluation Program, Phase I Report.* DOE-WIPP 87-008. Carlsbad, NM: Westinghouse Electric Corporation.

Deal, D.E., and R.M. Roggenthen. 1991. "Evolution of Hydrologic Systems and Brine Geochemistry in a Deforming Salt Medium: Data from WIPP Brine Seeps," *Waste Management '91, Waste Processing, Transportation, Storage and Disposal, Technical Programs and Public Education, Tucson, AZ, February 24-28, 1991.* Ed. R.G. Post. DOE/WIPP-90-040C. Tucson, AZ: University of Arizona. Vol. II, 507-516.

Deal, D.E., J.B. Case, R.M. Deshler, P.E. Drez, J. Myers, and J.R. Tyburski. 1987. *Brine Sampling and Evaluation Program Phase II Report*. DOE-WIPP-87-010. Carlsbad, NM: Westinghouse Electric Corporation.

Deal, D.E., R.J. Abitz, D.S. Belski, J.B. Case, M.E. Crawley, R.M. Deshler, P.E. Drez, C.A. Givens, R.B. King, B.A. Lauctes, J. Myers, S. Niou, J.M. Pietz, W.M. Roggenthen, J.R. Tyburski, and M.G. Wallace. 1989. *Brine Sampling and Evaluation Program, 1988 Report*. DOE-WIPP-89-015. Carlsbad, NM: Westinghouse Electric Corporation.

Deal, D.E., R.J. Abitz, J. Myers, J.B. Case, D.S. Belski, M.L. Martin, and W.M. Roggenthen. 1991. *Brine Sampling and Evaluation Program, 1990 Report*. DOE-WIPP 91-036. Prepared for U.S. Department of Energy by IT Corporation and Westinghouse Electric Corporation. Carlsbad, NM: Westinghouse Electric Corporation, Waste Isolation Division.

Deal, D.E., R.J. Abitz, J. Myers, D.S. Belski, M.L. Martin, D.J. Milligan, R.W. Sobocinski, and P.P.J. Lipponer. 1993. *Brine Sampling and Evaluation Program, 1991 Report*. DOE-WIPP 93-026. Prepared for U.S. Department of Energy by IT Corporation and Westinghouse Electric Corporation. Carlsbad, NM: Westinghouse Electric Corporation, Waste Isolation Division.

DOE (U.S. Department of Energy). 1990. "Underground Mine Ventilation System." Drawing No. 54-W-001-W. Carlsbad, NM: Westinghouse Waste Isolation Division, Waste Isolation Pilot Plant. (Copy on file in the Sandia WIPP Central Files, Sandia National Laboratories, Albuquerque, NM as WPO#30937.)

Domski, P.A., D.T. Upton, and R.L. Beauheim. 1996. *Hydraulic Testing Around Room Q: Evaluation of the Effects of Mining on the Hydraulic Properties of Salado Evaporites*. SAND96-0435. Albuquerque, NM: Sandia National Laboratories.

Finley, S.J., D.J. Hanson, and R. Parsons. 1992. *Small-Scale Brine Inflow Experiments - Data Report Through 6/6/91*. SAND91-1956. Albuquerque, NM: Sandia National Laboratories.

Freeze, G.A., K.W. Larson, and P.B. Davies. 1995a. *Coupled Multiphase Flow and Closure Analysis of Repository Response to Waste-Generated Gas at the Waste Isolation Pilot Plant (WIPP)*. SAND93-1986. Albuquerque, NM: Sandia National Laboratories.

Freeze, G.A., K.W. Larson, and P.B. Davis. 1995b. *A Summary of Methods for Approximating Salt Creep and Disposal Room Closure in Numerical Models of Multiphase Flow*. SAND94-0251. Albuquerque, NM: Sandia National Laboratories.

Howarth, S.M., E.W. Peterson, P.L. Lagus, K.H. Lie, S.J. Finley, and E.J. Nowak. 1991. "Interpretation of In-Situ Pressure and Flow Measurements of the Salado Formation at the Waste Isolation Pilot Plant," *Rocky Mountain Regional Meeting and Low-Permeability Reservoirs Symposium, Denver, CO, April 15-17, 1991*. SAND90-2334C; SPE 21840. Richardson, TX: Society of Petroleum Engineers. 355-369.

Jensen, A.L., C.L. Howard, R.L. Jones, and T.P. Peterson. 1993a. *Room Q Data Report: Test Borehole Data From April 1989 Through November 1991.* SAND92-1172. Albuquerque, NM: Sandia National Laboratories.

Jensen, A.L., R.L. Jones, E.N. Lorusso, and C.L. Howard. 1993b. *Large-Scale Brine Inflow Data Report for Room Q Prior to November 25, 1991.* SAND92-1173. Albuquerque, NM: Sandia National Laboratories.

Jensen, A.L., C.L. Howard, C. Chester, and R.F. Bower. 1996. *Large-Scale Brine Inflow Data Report for Room Q: November 25, 1991 through July 6, 1995.* SAND94-1393. Albuquerque, NM: Sandia National Laboratories. (Copy of 5/14/96 draft on file in the Sandia WIPP Central Files, Sandia National Laboratories, Albuquerque, NM as WPO#37958.)

Lappin, A.R., R.L. Hunter, D.P. Garber, and P.B. Davies, eds. 1989. *Systems Analysis, Long-Term Radionuclide Transport, and Dose Assessments, Waste Isolation Pilot Plant (WIPP), Southeastern New Mexico; March 1989.* SAND89-0462. Albuquerque, NM: Sandia National Laboratories.

McTigue, D.F. 1993. *Permeability and Hydraulic Diffusivity of Waste Isolation Pilot Plant Repository Salt Inferred from Small-Scale Brine Inflow Experiments.* SAND92-1911. Albuquerque, NM: Sandia National Laboratories.

McTigue, D.F., S.J. Finley, and E.J. Nowak. 1989. "Brine Transport in Polycrystalline Salt: Field Measurements and Model Considerations," *EOS Transactions, American Geophysical Union.* SAND87-1274A. Vol. 70, no. 43, 1111.

Munson, D.E., A.F. Fossum, and P.E. Senseny. 1989. "Approach to First Principles Model Prediction of Measured WIPP In Situ Room Closure in Salt," *Rock Mechanics as a Guide for Efficient Utilization of Natural Resources: Proceedings of the 30th U.S. Symposium on Rock Mechanics, West Virginia University, Morgantown, WV, June 19-22,* 1989. Ed. A.W. Khair. SAND88-2535C. Brookfield, VT: A.A. Balkema. 673-680.

Munson, D.E., J.R. Weatherby, and K.L. DeVries. 1993. "Two- and Three-Dimensional Calculations of Scaled In Situ Tests Using the M-D Model of Salt Creep," *International Journal of Rock Mechanics and Mining Sciences & Geomechanics Abstracts.* SAND92-2063C. Vol. 30, no. 7, 1345-1350.

Munson, D.E., A.L. Jensen, S.W. Webb, and K.L. DeVries. 1996. "Brine Release Based on Structural Calculations of Damage Around an Excavation at the Waste Isolation Pilot Plant (WIPP)," *2nd North American Rock Mechanics Conference, Montreal, Canada, June 17-19, 1996.* SAND95-1704C. Albuquerque, NM: Sandia National Laboratories.

Nowak, E.J. 1990. "Test Plan: Brine Inflow and Related Tests in the Brine Inflow Room (Room Q) of the Waste Isolation Pilot Plant (WIPP)." DOE/DP/00789-T286. Albuquerque, NM: Sandia National Laboratories.

Nowak, E.J., and D.F. McTigue. 1987. *Interim Results of Brine Transport Studies in the Waste Isolation Pilot Plant (WIPP)*. SAND87-0880. Albuquerque, NM: Sandia National Laboratories.

Nowak, E.J., D.F. McTigue, and R. Beraun. 1988. *Brine Inflow to WIPP Disposal Rooms: Data, Modeling, and Assessment*. SAND88-0112. Albuquerque, NM: Sandia National Laboratories.

Sandia WIPP Project. 1992. *Preliminary Performance Assessment for the Waste Isolation Pilot Plant, December 1992. Volume 3: Model Parameters*. SAND92-0700/3. Albuquerque, NM: Sandia National Laboratories.

Stoelzel, D., P. Vaughn, J. Bean, and J. Schreiber. 1995. "Summary of 1993-94 WIPP Preliminary Undisturbed Repository Calculations," *Coupled Multiphase Flow and Closure Analysis of Repository Response to Waste-Generated Gas at the Waste Isolation Pilot Plant (WIPP)*. G.A. Freeze, K.W. Larson, and P.B. Davies. SAND93-1986. Albuquerque, NM: Sandia National Laboratories. C-25 through C-47.

Stormont, J.C., E.W. Peterson, and P.L. Lagus. 1987. *Summary of and Observations About WIPP Facility Horizon Flow Measurements Through 1986*. SAND87-0176. Albuquerque, NM: Sandia National Laboratories.

Webb, S.W. 1992. "Sensitivity Studies for Gas Release from the Waste Isolation Pilot Plant (WIPP)," *Gas Generation and Release from Radioactive Waste Repositories, 3rd Organisation for Economic Co-Operation and Development/Nuclear Energy Agency (OECD/NEA) Gas Workshop, Aix-en Provence, France, September 23-26, 1991*. SAND91-1872C. Paris, France: Organisation for Economic Co-Operation and Development. 309-326.

Webb, S.W., and K.W. Larson. 1996. *The Effect of Stratigraphic Dip on Brine Inflow and Gas Migration at the Waste Isolation Pilot Plant*. SAND94-0932. Albuquerque, NM: Sandia National Laboratories.

APPENDIX A

REFERENCED MEMORANDA

Appendix A: Referenced Memoranda

date: October 3, 1994

to: Paul Davis, Org. 6307/MS-1345

from: David J. Borns, Org. 6116/MS-0750

subject: Implications of Geophysical Surveys in the WIPP Underground on the
Interpretation of the Relative Roles of the Three Proposed Conceptual
Models for Salado Fluid Flow

Introduction

The Technical Baseline Document for Salado Fluid Flow proposes three conceptual models
for the observed brine inflow at the repository level. The three models are *1. Far-field
Flow, 2. Redistribution of brine with the pore structure of the Disturbed Rock Zone, and 3.
Clay consolidation within the Disturbed Rock Zone.* As we witnessed at the stakeholder's
meeting in Carlsbad on 29 October, the relative roles and importance of these models for
fluid flow appear unclear. The strategy to test these models remains uncertain..

However, observations based on geophysical surveys, predominantly electrical, suggest that
Far-Field Flow is the dominant mechanism. In summary, these observations are:
  1. The Disturbed Rock Zone (DRZ) is observed to resaturate in a sealed room, Room Q.
     This observation suggests that there is a source of brine external to the DRZ that
     with time is able to resaturate the porosity of the DRZ.
  2. The Salado halites and interbeds can support electrical current flow, which suggests
     that even in low permeability units there exists an interconnected pore structure to
     support ionic flow. Measured resistivities in the Salado halites and interbeds have
     successfully predicted permeabilities.
  3. Distinct electrical self potentials within the individual map units of the facility
     horizon suggest that far field flow is ongoing around the excavation.

In the remainder of this memo, I will elaborate on these points in detail.

Electrical Methods

The flow of electrical current in rocks takes place through ionic conduction in the pore
space or conduction through conducting minerals. In rocks of the upper crust including
evaporites, ionic conduction in the pore space dominates as a mechanism. For the units of
the Salado, clays possibly act as a conducting mineral, which facilitates electrical flow in
addition to ionic flow. To support current flow as a mineral conductor, the clays must link
as a continuous phase in the rock matrix or along a pore channel pore. Since clays comprise
less that 5% of Salado halites and anhydrite, where a modal distribution of greater than 30%
is generally required to form a continuous phase in the matrix, mineral conductance in the
matrix probably is limited to the clay interbeds. Clays lining pore networks, such as

diagenetic dewatering conduits, or fractures may support mineral conductance rather than ionic flow. The time dependent variations in resistivity are, however, more consistent with ionic flow in pore network of the Salado units since the clay distribution in the matrix and pores does vary significantly with time. The measured resistivities of the Salado units range from hundred to a thousand ohm-m. In comparison, the measured resistivities of domal salts range from tens of thousands to hundred of thousand ohm-m. Therefore, our assumption is that the electrical current flow that we induce or observe is supported by an interconnected partially (probably greater than 70%) to completely brine saturated pore network. Based on this assumption, we can relate the resistivity to the porosity, pore saturation and the tortuosity of the pore network and chemistry of the pore fluid. Brace (1977) utilized resistivity methods to determine permeabilities of tight crystalline rocks undergoing deformation in a laboratory.

At WIPP, we have used Poiseuille's equation as developed by Brace to estimate variations in permeability along the length of a borehole for the Salado Two-Phase Flow Laboratory Program: anhydrite core damage assessment and properties restoration (Howarth, 1993). In Figure 1, resistivity measurements where made in and between two vertical boreholes (E25 and E26) that penetrate Marker Bed 139. From these measurements, we calculated permeabilities for the halite and anhydrite intercepted by the boreholes (Borns and others, 1994). The calculated permeabilities duplicate the range for anhydrite and halite determined in laboratory and field experiments (Howarth, 1993). *This suggests that the interconnected pore network model represents the electrical current flow in the Salado.*
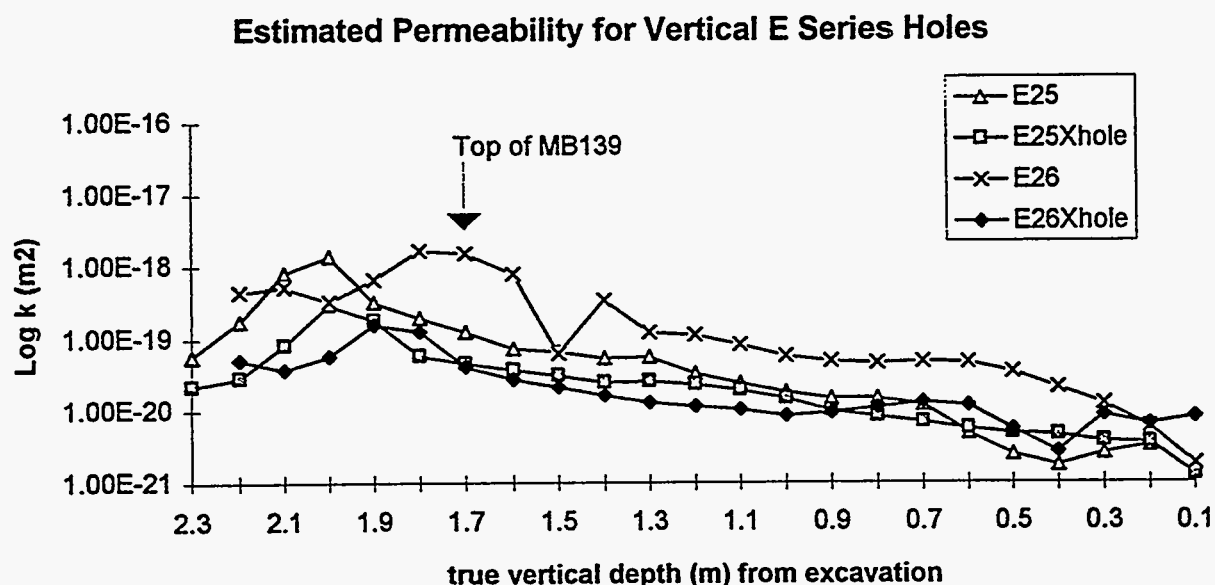
Figure 1: Calculated Permeabilities from Resistivity Surveys
in Halite and Anhydrite beneath the Repository Floor

Room Q Arrays

We emplaced two electrical arrays in Room Q in the autumn of 1989 and have monitored the electrical response (changes are resistance and self potential) around Room Q through August 1993 (Pfeifer and others, 1989; Jensen and others 1992; Truskowski, 1994).These are sensitive to changes in electrical properties in a region four meters radially outward from the excavation. Figures 3 a, b, and c show the change in resistance along a series of lines parallel to the length of Room Q *along the centerline of the array, Ring 13 (Fig. 3a), on the floor (Fig. 3b), the rib (Fig. 3c), and the roof (Fig. 3d)*. Along the x-axis is time sine 1/1/90 to 8/20/93 (0 to 2.63 fractional years). From these plots, apparently the resistance increased (blue and yellow contours) in the first six months after we had access to the room (12/89). This increase is interpreted to mirror desaturation of the DRZ based on forward modeling (Pfeifer and others, 1989). After this increase, the resistance decreases (toward red contours) for two years. Based on forward modeling, this decrease in resistance is interpreted to represent *resaturation* of the DRZ. At 2 years, a rapid rise in resistance especially in the floor occurs followed by a decrease in resistance. Again based on modeling, this behavior is interpreted as a fracture opening between the floor and the far field electrode. In turn this fracture resaturated resulting in the decrease in resistance.

Another way to view the changes around Room Q with time is a series of graphs showing the percentage change in resistance between an index measurement (6/20/90 in most analyses) and the date of a following measurement. Figure 4 displays the cylindrical surface of Room Q projected onto a plane with the floor at Row 13, the rib at Row 9, and the roof at Row 3. These figures show the change in resistance for the periods **a) 3/11/90 to 6/22/90** (the period within a year of excavation and before an effective seal was installed), **b) 6/22/90 to 8/14/90** (the period for which access was beginning to be limited and partially seals were in place); **c) 6/22/90 to 8/12/91** (a period covering over a year of operation); and **d) 6/22/90 to 8/20/93** (a period covering the last documented measurement of the array in Room Q). These figures covering almost three years of the room's history show the initial increase in resistance with the opening of the DRZ and its desaturation (Figure 4a) and the subsequent reduction in resistance with resaturation of the DRZ (Figures 4b, c, and d). *In conclusion, we observe that the field data suggests that the DRZ can resaturate over a 2.6 year period.*

Figure 3a: Resistance change with time for all electrodes along Ring 13 (centerline of array) in Room Q

Room Q Resitance: Row 13
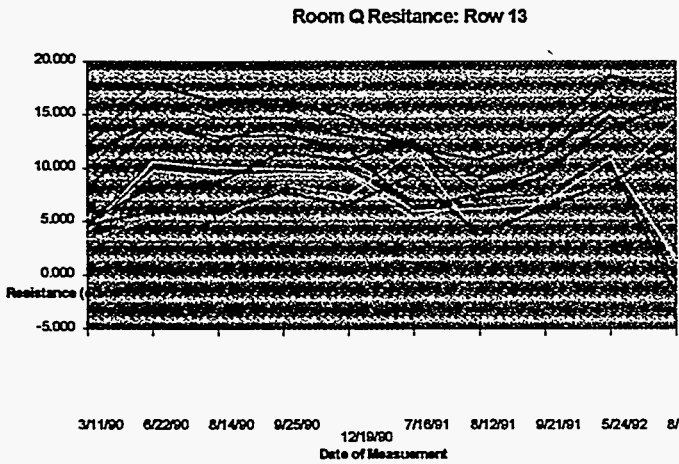
Figure 3b: Change in resistance with time along Room Q floor

ROW 11 (Floor) Room Q Array
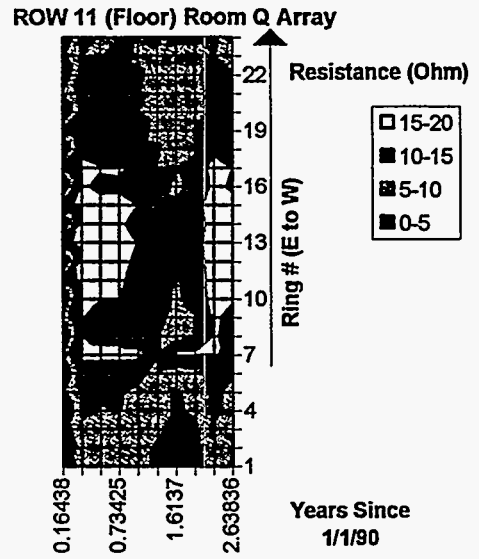
Figure 3c: Change in resistance with time along Room Q rib

ROW 8 (Rib) Room D Array
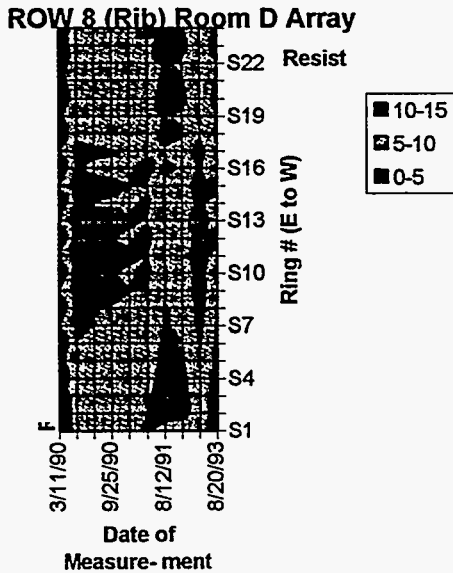
Figure 3d: Change in resistance with time along Room Q roof

ROW 5 (Roof): Room Q Array
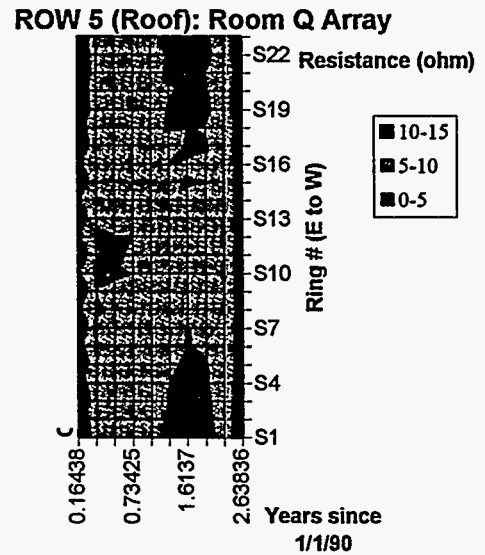
Figure 4a: Change in resistance (resistance increasing with development and desaturation of DRZ)

%Change in Resistance 3/11/90 to 6/22/90

■20000-25000
▣15000-20000
■10000-15000
□5000-10000
■0-5000
▣-5000-0
■-10000--5000
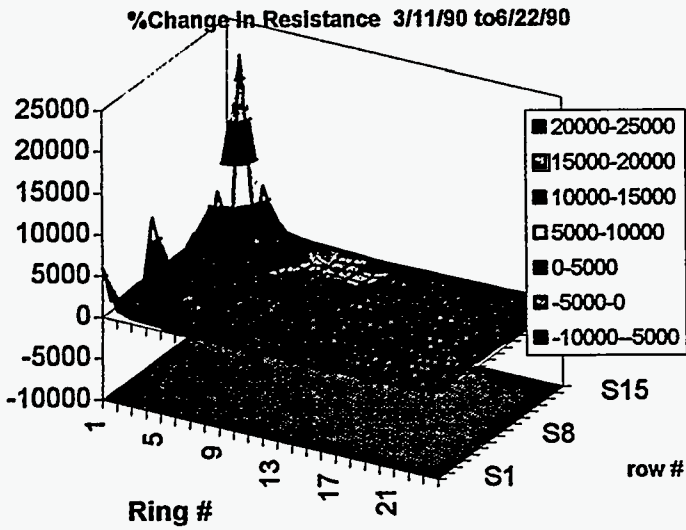
Figure 4b: Change in resistance (resistance decreasing with resaturation of DRZ)

%Change in Resistance 6/22/90 to 8/14/90

▣50-100
■0-50
□-50-0
■-100--50
▣-150--100
■-200--150
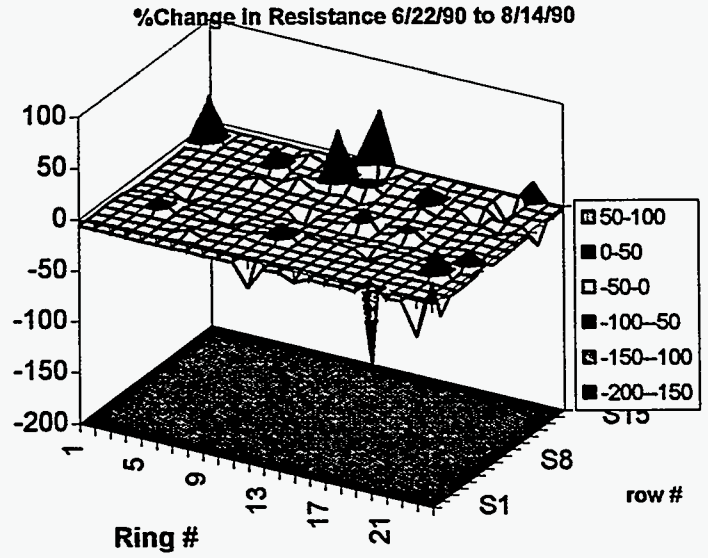
Figure 4c: Change in resistance (resistance decreasing with resaturation of DRZ)

%Change in Resistance 6/22/90 to 8/12/91

■200-300
▣100-200
■0-100
□-100-0
■-200--100
▣-300--200
■-400--300
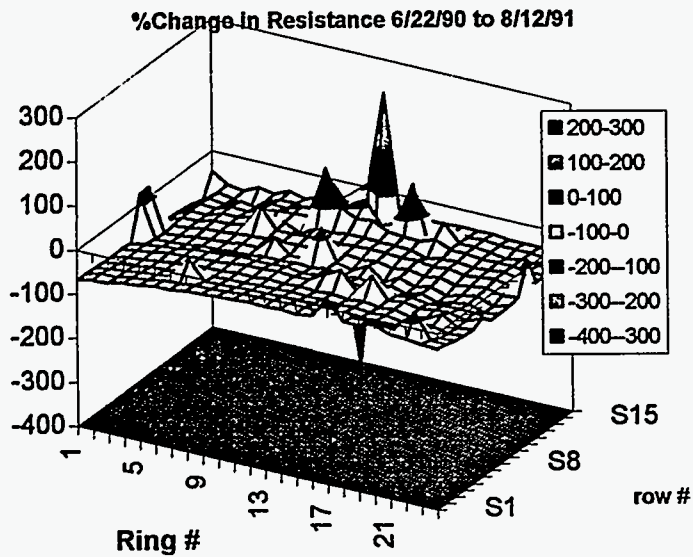
Figure 4d: Change in resistance (resistance decreasing with resaturation of DRZ; zone of higher resistance may reflect the opening of a secondary fracture[s] in the floor)

%Change in Resistance 6/22/90 to 8/20/93

■600-800
■400-600
□200-400
■0-200
□-200-0
■-400--200
▣-600--400
■-800--600
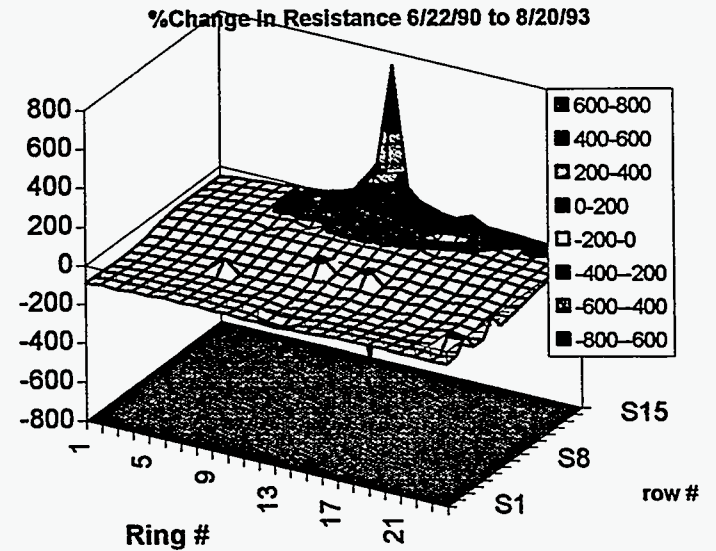
Self Potential Surveys in Room Q

We measure electrical self potential regularly as a background check for electrical surveys in Room Q and elsewhere in the underground. The self potential measures the background current flow when our induced sources are turned-off. This self potential is commonly induced by ionic flow accompanying fluid flow in rocks. As such, the self potential is used to detect zones of fluid flow (e.g., leaks in man made structures). In the WIPP underground, the self potential may not be totally natural and may reflect perturbations in the electrical field due to the shafts and underground mine operations. However, the observed self potentials show that the ionic flow occurs in the pore network of the Salado. Figure 3 shows the self potentials measured in the electrical arrays of Room Q.
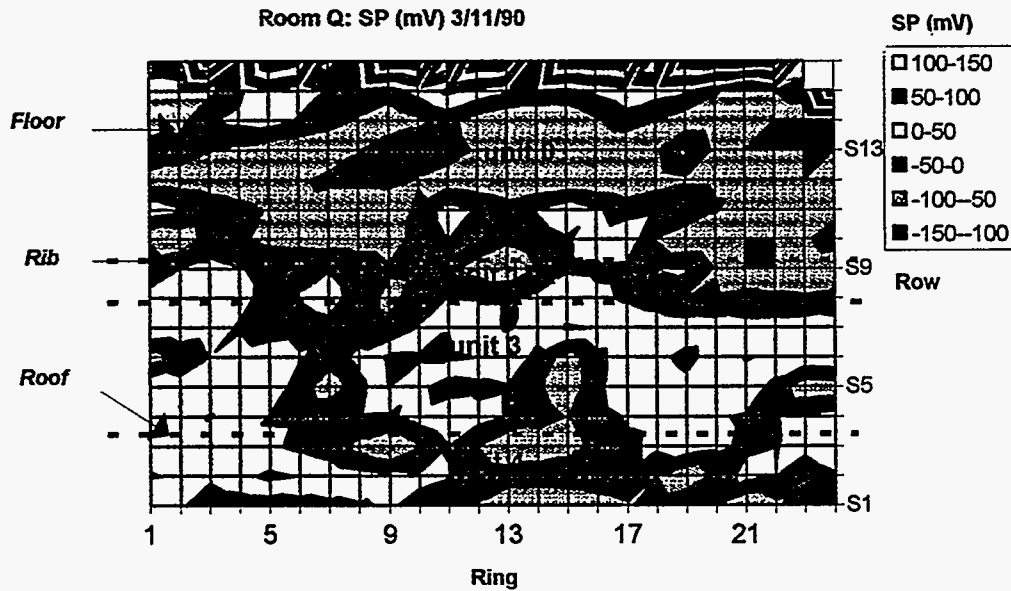
Figure 4: Self Potential (SP) measured in Room Q on 3/11/90. Figure represents the cylindrical surface of room projected onto a planar surface. The intersection of the excavation with the map units is marked by the dotted lines. The relative positions of the floor, rib and roof are marked by arrows.

observed in Room Q related to the map units. These map units represent the sedimentary layering of the Salado as marked by variations in texture and clay content. **Map Unit 0** has a distinct self potential, which is 100 mV greater than **Map Unit 3**. The boundary between these two units is horizontal and corresponds to the relatively thinner **Map Units 1 and 2**. *The distribution of self potentials suggests that layer stratified ionic flow is occurring around the Room Q excavation.*

References:

Borns, D. J., H. T. Andersen, and D. I. Neuman, 1994, Electrical Resistance Measurements of Boreholes: E3X23, E3X24, E3X25, E3X26, E3X27, and E3X28 in Alcove E300N90:Field Test Portion of the Core Damage Assessment Study for the Salado Two-Phase Flow Laboratory Program, Sandia Report, SAND94-1200, Sandia National Laboratories, Albuqerque, New Mexico

Brace, W. F., 1977, Permeability and Resistance and Pore Shape, Journal of Geophysical Research, 82, 3343-3349

Howarth, S., 1993, Conceptual Plan: Two Phase Flow Laboratory Program for the Waste Isolation Pilot Plant, Sandia Report, SAND93-1197, Sandia National Laboratories, Albuquerque, New Mexico

Jensen, A. L., R. L. Jones, E. N. Lorusso, and C. L. Howard, 1991, Large-scale brine inflow data report for Room Q prior to November 25, 1991, Sandia Report, SAND92-1173, Sandia National Laboratories, Albuqerque, New Mexico

Pfeifer, M. C., D. J. Bornsm C. K. Skokan, H. T. Andersen, and J. Starrett, 1989, Geophysical methods to monitor development of the disturbed rock zone around underground excavation in bedded salt, Procedding of the Symposium on the Application of Geophysics to Engineering and Environmental Problems (SAGEEP), Golden, CO, March 1989, SAND89-7055A

Truskowski, M. G., 1994, Detecting material proerty changes and fluid flow using a stationary DC resistance grid, M.S. Thesis, Colorado School of Mines, Golden, CO.

Distribution	Org.	MS
Rick Beauheim	6115	1324
Susan Howarth	6115	1324
Kurt Larson	6115	1324
Al Lappin	6115	1324
Marianne Walck	6115	1324
Dwight Deal	WID	

date: June 24, 1991

to: Distribution

from: D. F. McTigue, 1511

subject: Horizontal Darcy Flow to Room Q

Introduction

This memo reports order-of-magnitude estimates of brine seepage to Room Q assuming horizontal, Darcy flow confined to argillaceous halite. The calculation is in response to questions raised by the National Academy of Sciences (NAS) WIPP Panel at meetings held in Albuquerque on June 2 and June 4.

Susan Howarth (6344) reported at the NAS meeting that approximately 1.8 liters of brine were collected in Room Q in March 1991, representing the measurable accumulation since December 1990. With improved seals, approximately 3 to 7 liters of brine accumulated in the room from March to May 1991. She noted that even the latter volume is one to two orders of magnitude less than the quantities predicted by early calculations [1] based on radial Darcy flow to the room. The calculations referred to considered a range of properties and initial conditions. Permeabilities of 10^{-21} m^2 and 10^{-20} m^2 were assumed; the hydraulic diffusivity was computed based on the known elastic properties of the brine and salt, and fell in the corresponding range of about 10^{-7} m^2/s to 10^{-6} m^2/s. Initial pressures of 6 MPa and 15 MPa were assumed. These calculations predicted that, 21 months after mining (the approximate age of Room Q in April 1991), the flux to the room would be in the range 2–24 ml per day per meter length, or about 0.22 to 2.6 liters per day for the 109 m long room. The average inflow rate observed for the period March to May 1991 was of the order of 0.03 to 0.08 liters per day. The higher estimate for the observed accumulation rate (0.08 ℓ/d) is about one third of the lowest predicted rate (0.22 ℓ/d), while the lower estimate for the observed rate (0.03 ℓ/d) is only about 1% of the high prediction (2.6 ℓ/d).

Several other presentations to the NAS Panel showed evidence that brine seepage in the salt may be confined to certain lithologies, most notably anhydrite interbeds (*e.g.*, Marker Bed 139) and argillaceous halite. In this case, the effective permeability of the salt might be regarded as highly anisotropic, with flow predominantly in horizontal planes. The radial flow calculations performed previously would then be inappropriate. NAS Panel members asked how calculations based on the assumption of horizontal flow only compare

to the radial-flow calculations, and whether this might bring the predictions into better agreement with the observations.

Horizontal Flow

Horizontal flow has been addressed previously [2, 3], and those results are simply applied here to the conditions of Room Q. In particular, the previous work showed that one-dimensional, rectilinear flow to an open face yields:

$$|q| = \frac{kp_0}{\mu\sqrt{\pi ct}} , \qquad (1)$$

where $|q|$ is the magnitude of the flux (volume flow rate per unit area), k is permeability, p_0 is the initial formation pressure, μ is brine viscosity, and c is hydraulic diffusivity. Note that the diffusivity, c, is related to the permeability and capacitance, C, by

$$c = \frac{k}{\mu C} . \qquad (2)$$

Note that the flux due to horizontal flow (1) drops off like $t^{-1/2}$ for all time. In contrast, the flux due to *radial* flow drops of like $(\ln t)^{-1}$ at late time. Thus, the flow rate due to horizontal flow falls off much more quickly after sufficiently long time. Also, horizontal flow in a semi-infinite layer (1) involves no intrinsic length scale; *i.e.*, the flux is independent of the dimensions of the excavation.

Because there are still some unresolved questions concerning the appropriate values of hydraulic properties for the salt, two cases are considered here (see Table 1). It is emphasized that these calculations are intended to be order-of-magnitude estimates only. For Case 1, it is assumed that the capacitance is $C = 10^{-11}$ Pa^{-1}; this value is consistent with the value used in the previous calculations discussed above [1], and is based on known elastic compressibilities for the salt and brine. It is also consistent with values used by Beauheim, *et al.* [4] in evaluating *in situ* permeability tests. For permeability $k = 10^{-21}$ m^2 and viscosity $\mu = 1.6 \times 10^{-3}$ Pa·s, this yields, from eq. (2), a diffusivity $c = 6.2 \times 10^{-8}$ m^2/s. Measured formation pressures in the vicinity of Room Q are about 10 MPa. The age of the room in April 1991 was about 21 months, or 5.5×10^7 s. These values yield, from eq. (1), a flux of about 1.9×10^{-12} m/s.

It is further assumed that the flow to Room Q is confined to the argillaceous halite intersecting the sides in bands approximately 1 m thick. Thus, the total area of argillaceous halite cut by the room is about $A = 218$ m^2 (bands one meter thick and 109 m long on each side of the room). The total volume flow rate corresponding to the above flux, then, is about 4.1×10^{-10} m^3/s. For comparison, assume 5 ℓ of brine accumulated over the three month period from March to May 1991. This yields an average volume flow rate of about 6.3×10^{-10} m^3/s, in very close agreement with the calculated value developed immediately above.

Table 1. Sample Calculations of Horizontal Brine Flow.

Quantity	Symbol	Units	Case 1	Case 2
Permeability	k	m^2	1.0×10^{-21}	1.0×10^{-22}
Capacitance	C	Pa^{-1}	1.0×10^{-11}	6.2×10^{-10}
Diffusivity	c	$m^2\,s^{-1}$	6.2×10^{-8}	1.0×10^{-10}
Initial pressure	p_0	Pa	1.0×10^7	1.0×10^7
Viscosity	μ	Pa·s	1.6×10^{-3}	1.6×10^{-3}
Volume flux*	$|q|A$	$m^3\,s^{-1}$	4.1×10^{-10}	10.2×10^{-10}

*Compare to observed: $\sim 6.3 \times 10^{-10}$ m^3/s

Case 2 considers a much larger capacitance, as suggested by recent analysis of data for seepage to open boreholes (*i.e.*, at atmospheric pressure), as presented to the NAS Panel by Sharon Finley (6344). Typical values for the diffusivity found in that study are of the order of $c \sim 10^{-10}$ m^2/s, and the inferred permeabilities tend toward relatively low values of order $k \sim 10^{-22}$ m^2, implying a large capacitance ($C \sim 6.2 \times 10^{-10}$ Pa^{-1}). These values are shown in Table 1 as Case 2. The effects of smaller permeability and smaller diffusivity are offsetting to some extent, particularly since the effect of a large change in diffusivity is weakened by the square-root dependence. Thus, the predicted flux for Case 2 is only 2.5 times greater than that in Case 1, and is still in order-of-magnitude agreement with the observed value.

It is emphasized that the two cases considered here were chosen to be representative of properties assumed or inferred for the salt in various aspects of the WIPP program. Other properties or combinations of properties that also appear to be reasonable do not yield the same agreement of predicted and observed brine flux. For example, consider a permeability of order 10^{-20} m^2 and diffusivity of order 10^{-9} m^2/s, which are not exceptional estimates from recent fits to data for seepage to boreholes [5]. These properties yield, with (1), a volume flow rate of about 3.3×10^{-8} m^3/s, a factor of 50 times greater than the rate accounted for by the brine collected.

Conclusions

In response to a question asked by the NAS WIPP Panel, simple calculations for horizontal brine flow to Room Q have been carried out. For reasonable choices of material properties, rough agreement is obtained with the observed flow rate estimated from the

brine volume collected between March and May 1991. However, estimates based on higher permeabilities and lower diffusivities (but still within the range of parameters inferred from data for seepage to boreholes) can be one to two orders of magnitude greater than the observed rate.[1]

References

1. McTigue, D. F., Brine flow to a mined room, memo to Distribution, October 12, 1987.

2. Nowak, E. J., D. F. McTigue, and R. Beraun, Brine Inflow to WIPP Disposal Rooms: Data, Modeling, and Assessment, **SAND88-0112**, Sandia National Laboratories, Albuquerque, NM, September, 1988.

3. McTigue, D. F., Calculations of brine flux and cumulative brine volume for Room Q, based on a Darcy flow model, memo to Distribution, April 3, 1989.

4. Beauheim, R. L., G. J. Saulnier, Jr., and J. D. Avis, Interpretation of Brine-Permeability Tests of the Salado Formation at the Waste Isolation Pilot Plant Site: First Interim Report, **SAND90-0083**, Sandia National Laboratories, Albuquerque, NM, in review, 1991.

5. Finley, S. J., and D. F. McTigue, D. F., Parameter estimates from the small-scale brine inflow experiments, memo to Distribution, June 17, 1991.

DFM:1511

Key Words: **0395.180, radioactive waste, hydrology, porous media**

---

[1]Note, however, that the brine collected represents a *minimum*, because of unknown losses due to storage in dilated salt around the room and/or leaks to external air.

Copy to:

1510 J. C. Cummings
1510 QA File
1511 J. S. Rottler
1511 D. F. McTigue (day file)
1514 H. S. Morgan
1514 C. M. Stone
1540 J. R. Asay
1550 C. W. Peterson, Jr.
6340 W. D. Weart
6340 S. Y. Pickering
6340 A. R. Lappin
6341 R. C. Lincoln
6342 D. R. Anderson
6342 R. P. Rechard
6344 E. D. Gorham
6344 D. B. Barber
6344 R. L. Beauheim
6344 P. B. Davies
6344 S. J. Finley
6344 F. Gelbard
6344 S. M. Howarth
6344 S. W. Webb
6345 B. M. Butcher
6345 F. T. Mendenhall
6346 J. R. Tillerson
6346 E. J. Nowak
DOE/WPO J. Carr
DOE/WPO R. Becker

date: April 3, 1989

to: Distribution

from: D. F. McTigue, 1511

subject: Calculations of Brine Flux and Cumulative Brine Volume For Room Q, Based on a Darcy-Flow Model

1 Introduction

Room Q is to be mined at the WIPP in order to perform a carefully controlled brine-inflow test at large scale. It is to have a circular cross section, 1.524 m (5 ft) in radius. An attempt will be made to collect all brine that arrives at the tunnel wall over a period of approximately two years, providing data for cumulative brine volume and average brine flux at the wall. The test-room configuration does not purport to represent a waste-storage room.

This memo summarizes calculations of the expected brine inflow to Room Q based on a classical Darcy flow model. The model simply states that the circular tunnel introduces a face at zero (atmospheric) pressure into a region of pore water at some initial pressure p_0. The initial pressure is expected to be between hydrostatic and lithostatic for the repository depth. Flow is driven toward the tunnel wall by the diffusion-like process of Darcy flow. Because the diffusivity is small, and the ratio of tunnel radius to length is small, it is reasonable to approximate the flow as one-dimensional (radial). Although this model is highly idealized, it has been shown previously [1] to reproduce observed brine fluxes in the WIPP to the correct order of magnitude.

2 The Classical Darcy Flow Model

It has been shown previously [2] that the magnitude of the Darcy flux to a circular tunnel or borehole is given by

$$|q|(t) = \frac{kp_0}{\mu a} \frac{4}{\pi^2} \int_0^\infty \frac{\exp(-cu^2 t/a^2)}{J_0^2(u) + Y_0^2(u)} \frac{du}{u}, \qquad (1)$$

where k is the permeability, p_0 is the initial brine pressure, μ is the brine viscosity, a is the radius of the hole, and c is the brine diffusivity. One can avoid having to integrate over

the singularity in (1) by using the approximation:[1]

$$|q|(t) \simeq \frac{kp_0}{\mu a} \left[\frac{\exp(-c\epsilon^2 t/a^2)}{-\ln(C\epsilon/2)} + \frac{4}{\pi^2} \int_\epsilon^\infty \frac{\exp(-cu^2 t/a^2)}{J_0^2(u) + Y_0^2(u)} \frac{du}{u} \right], \tag{2}$$

where ϵ is an arbitrarily small number.

The cumulative volume per unit area of wall, v (*e.g.*, in m^3/m^2), is obtained by integration of (1) with respect to time:

$$v(t) = \frac{kp_0 a}{\mu c} \frac{4}{\pi^2} \int_0^\infty \frac{1 - \exp(-cu^2 t/a^2)}{J_0^2(u) + Y_0^2(u)} \frac{du}{u^3}. \tag{3}$$

It is again convenient when evaluating (3) to use the approximation:

$$v(t) \simeq \frac{kp_0 a}{\mu c} \left[\frac{ct/a^2}{-\ln(C\epsilon/2)} + \frac{4}{\pi^2} \int_\epsilon^\infty \frac{1 - \exp(-cu^2 t/a^2)}{J_0^2(u) + Y_0^2(u)} \frac{du}{u^3} \right]. \tag{4}$$

3 Material Properties, Geometry, and Initial Conditions

The Darcy model requires estimates of the brine diffusivity, c. A well-known model (summarized in [2]) for a porous, elastic material gives:

$$c = \frac{k}{\mu} \frac{2G(1 - \nu)}{1 - 2\nu} \left[\frac{B^2(1 + \nu_u)^2(1 - 2\nu)}{9(1 - \nu_u)(\nu_u - \nu)} \right], \tag{5}$$

where

$$\frac{1}{B} = 1 + \phi_0 \frac{K}{K_f} \frac{1 - K_f/K_s}{1 - K/K_s}, \tag{6}$$

$$\nu_u = \frac{3\nu + B(1 - 2\nu)(1 - K/K_s)}{3 - B(1 - 2\nu)(1 - K/K_s)}, \tag{7}$$

G is the shear modulus, ν is Poisson's ratio, ν_u is the undrained Poisson's ratio, ϕ_0 is the reference (connected) porosity, K_f is the fluid bulk modulus, and K_s is the mineral bulk modulus. Estimated values for these parameters representative of WIPP salt are given in Table 1.

The values chosen for two parameters listed in Table 1 differ from values used in earlier calculations [1, 2]. First, the fluid bulk modulus, K_f, is here increased to 3.7 GPa from the value 2.1 GPa used previously. The newer value is based on data [5, p. 609, Table 40] for the compressibility of sodium chloride solutions, and is believed to be more accurate. Second, the porosity chosen here is 0.01 (1%), while previous calculations used a value of 0.001 (0.1%). One percent brine by volume appears to be typical of WIPP halite [*e.g.*, 6]; the value appropriate to the present model is the *interconnected* porosity, which is not known. Thus, the assumption $\phi_0 = 0.001$ implies that only a small fraction of the

---

[1]Details of the derivation of this approximation will appear in a separate document.

total brine in a typical sample is in interconnected pores. There is at present no strong argument for one choice over another, and, in any case, the influence on the calculations is not large. In particular, the two changes discussed here tend to be offsetting; the greater incompressibility of the brine tends to decrease the calculated capacitance, while the increased porosity increases the capacitance. For $k = 1.0 \times 10^{-21}$ m², the previous estimates yield a diffusivity of $c = 1.1 \times 10^{-7}$ m²/s, while the properties in Table 1 yield $c = 0.8 \times 10^{-7}$ m²/s. Other things being equal, an order-of-magnitude increase in ϕ_0 results in a 30% decrease in the diffusivity, while the 80% increase in K_f results in a 30% increase in the diffusivity. These changes do not affect the scale of the brine flux; they affect only the time scale over which the flux falls off. Thus, their overall effect on the present estimates of brine inflow is relatively small.

The radius used in the calculations is $a = 1.524$ m. Initial pressures were set to 6.0 MPa (approximately hydrostatic) and 15.0 MPa (approximately lithostatic) for the cases calculated, and permeabilities were set to 10^{-21} m² and 10^{-20} m². The four cases treated are summarized in Table 2.

Table 1. Estimated Material Properties for WIPP Salt.

Property	Symbol	Value	Units	Source
Drained Blk. Mod.	K	20.7	GPa	[3]
Shear Modulus	G	12.4	GPa	[3]
Poisson's Ratio	ν	0.25	—	[3]
Solid Blk. Mod.	K_s	23.5	GPa	[4]
Fluid Blk. Mod.	K_f	3.7	GPa	[5]
Viscosity	μ	1.6×10^{-3}	Pa·s	[5]
Porosity	ϕ_0	0.01	—	[6]
Permeability	k	$(1.0\text{--}10.0) \times 10^{-21}$	m²	[7]
Undrained Bulk Mod.	K_u	22.6	GPa	
Undrained Poiss. Rat.	ν_u	0.268	—	
Skempton Coeff.	B	0.719	—	
Diffusivity	c	$(0.8\text{--}8.0) \times 10^{-7}$	m²/s	

Table 2. Conditions for Calculations.

	Permeability, k (m^2)	Initial Pressure, p_0 (MPa)
Case 1	10^{-21}	6.0
Case 2	10^{-21}	15.0
Case 3	10^{-20}	6.0
Case 4	10^{-20}	15.0

4   Results

Results from the calculations are summarized in Figures 1 and 2 and Tables 3 and 4. The calculated fluxes (Figure 1, Table 3) are in the range of a few to a few tens of milliliters per day per meter length of tunnel. The calculated cumulative volumes (Figure 2, Table 4) are in the range of a few to a few tens of liters of brine per meter length of tunnel after two years.

5   Summary

This memo provides calculated estimates of brine inflow to Room Q based on a Darcy-flow model. For permeabilities in the range 10^{-21} m^2 to 10^{-20} m^2 and initial pressures in the range 6.0 MPa to 15.0 MPa, the model predicts:

- flow rates of the order of 1–50 milliliters per day per meter length of tunnel, and

- cumulative volumes of the order of 2–20 liters per meter length of tunnel after two years.

It is reiterated that these estimates are for Room Q only, and do not purport to represent brine inflow to a waste-storage room.

References

1. McTigue, D. F., and E. J., Nowak, Brine Transport in the Bedded Salt of the Waste Isolation Pilot Plant (WIPP): Field Measurements and a Darcy Flow Model, *Scientific Basis for Nuclear Waste Management XI*, M. J. Apted and R. E. Westerman, eds., Materials Research Society Symposium Proceedings, **112**, 1988, 209–218.

2. Nowak, E. J., and D. F. McTigue, Interim Results of Brine Transport Studies in the Waste Isolation Pilot Plant (WIPP), **SAND87–0880**, Sandia National Laboratories, Albuquerque, NM, May 1987.

3. Krieg, R. D., Reference Stratigraphy and Rock Properties for the Waste Isolation Pilot Plant (WIPP) Project, **SAND83–1908**, Sandia National Laboratories, Albuquerque, NM, January 1984.

4. Sumino, Y., and O. L. Anderson, Elastic Constants of Minerals, *CRC Handbook of Physical Properties of Rocks*, **III**, R. S. Carmichael, ed., CRC Press, Boca Raton, FL, 1984, 39–138.

5. Kaufman, D. W., ed., *Sodium Chloride; The Production and Properties of Salt and Brine*, ACS Monograph **145**, American Chemical Society, Washington, D. C., 1960, 609.

6. Black, S. R., R. S. Newton, and D.•K. Shukla, eds., Results of the Site Validation Experiments, Vol./ II, Supporting Document 10, Brine Content of Facility Interval Strata, U. S. Department of Energy, Waste Isolation Pilot Plant, 1983.

7. Peterson, E. W., P. L. Lagus, and K. Lie, WIPP Horizon Free Field Fluid Transport Characteristics, **SAND87–7164**, Sandia National Laboratories, Albuquerque, NM, December 1987.

DFM:1511

Table 3. Calculated Flux.

Time (months)	Flux ((ml/d)/m)			
	Case 1	Case 2	Case 3	Case 4
1	4.763	11.907	20.654	51.635
2	3.624	9.060	16.761	41.903
3	3.114	7.786	14.971	37.428
4	2.808	7.020	13.873	34.683
5	2.597	6.493	13.106	32.766
6	2.441	6.101	12.529	31.322
7	2.318	5.795	12.072	30.180
8	2.219	5.546	11.698	29.244
9	2.136	5.339	11.383	28.458
10	2.065	5.164	11.114	27.784
11	2.004	5.011	10.879	27.197
12	1.951	4.878	10.671	26.678
13	1.904	4.760	10.486	26.216
14	1.862	4.654	10.320	25.800
15	1.823	4.559	10.169	25.423
16	1.789	4.472	10.031	25.078
17	1.757	4.393	9.905	24.762
18	1.728	4.320	9.788	24.470
19	1.701	4.253	9.679	24.199
20	1.676	4.190	9.579	23.947
21	1.653	4.132	9.484	23.711
22	1.631	4.078	9.396	23.490
23	1.611	4.027	9.313	23.282
24	1.592	3.979	9.234	23.085

Table 4. Calculated Cumulative Volume.

Time (months)	Cumulative Volume (liters/m)			
	Case 1	Case 2	Case 3	Case 4
1	0.218	0.545	0.965	2.412
2	0.343	0.857	1.524	3.811
3	0.445	1.112	2.005	5.012
4	0.534	1.336	2.443	6.106
5	0.617	1.541	2.853	7.131
6	0.693	1.733	3.242	8.106
7	0.765	1.914	3.616	9.041
8	0.834	2.086	3.978	9.945
9	0.901	2.252	4.329	10.823
10	0.965	2.412	4.672	11.679
11	1.026	2.566	5.006	12.516
12	1.087	2.717	5.334	13.335
13	1.145	2.864	5.656	14.140
14	1.203	3.007	5.973	14.932
15	1.259	3.147	6.285	15.711
16	1.314	3.284	6.592	16.480
17	1.368	3.419	6.895	17.238
18	1.421	3.552	7.195	17.988
19	1.473	3.682	7.491	18.728
20	1.524	3.811	7.784	19.461
21	1.575	3.937	8.075	20.186
22	1.625	4.062	8.362	20.905
23	1.674	4.186	8.647	21.617
24	1.723	4.308	8.929	22.322
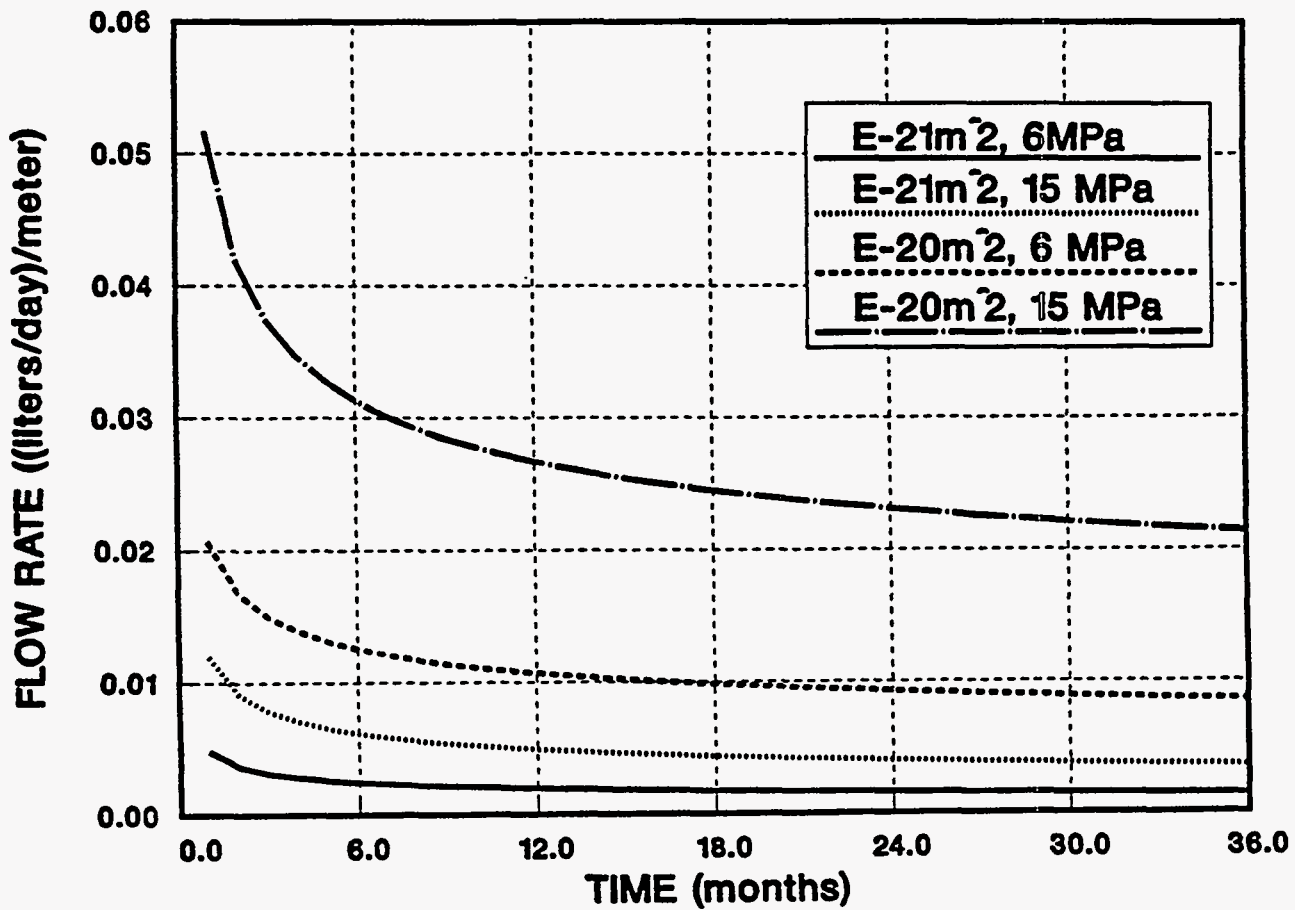
Figure 1. Calculated brine flux to a circular tunnel of radius 1.524 m (5 ft); flow rate is given in liters per day per meter length of the tunnel; four cases correspond to permeabilities $k = 10^{-21}$ and 10^{-20} m^2 and initial pressures $p_0 = 6.0$ and 15.0 MPa.
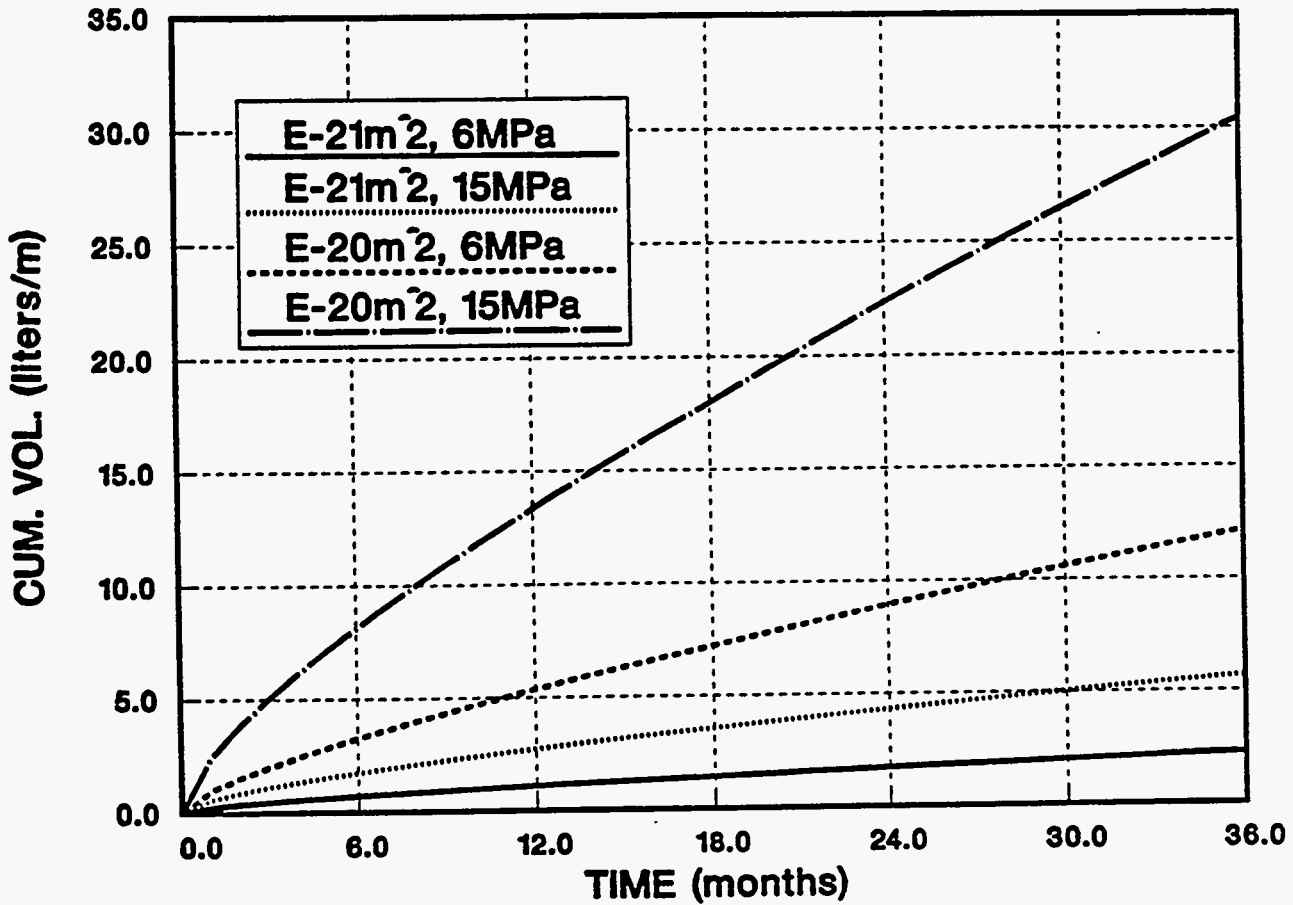
Figure 2. Calculated cumulative brine volume for a circular tunnel of radius 1.524 m (5 ft); volume is given in liters per meter length of the tunnel; four cases correspond to permeabilities $k = 10^{-21}$ and 10^{-20} m^2 and initial pressures $p_0 = 6.0$ and 15.0 MPa.

Copy to:
1510 J. W. Nunziato
1511 D. K. Gartling
1511 D. F. McTigue (day file)
1512 J. C. Cummings
1513 D. W. Larson
1520 L. W. Davison
1530 D. B. Hayes
1550 C. W. Peterson
6330 W. D. Weart
6331 A. R. Lappin
6331 R. L. Beauheim
6331 P. B. Davies
6332 L. D. Tyler
6332 R. Beraun
6332 B. M. Butcher
6332 S. J. Finley
6332 E. J. Nowak
6334 D. R. Anderson
6334 L. H. Brush

APPENDIX B

DATA FROM SPECTROM-32 SIMULATIONS

APPENDIX B: DATA FROM SPECTROM-32 SIMULATIONS

The following Room Q simulation data was provided by Kerry L. DeVries, RE/SPEC Inc. SPECTROM-32 Room Q simulation data was post-processed using a variable interpolation program, INTERPOLATE (Version 1.02, released October 1995). The following information is relevant to the SPECTROM-32 and INTERPOLATE datasets.

FILENAME: DMVOL-Q.TRP (Room Q Damage 10/20/95)
ENGINEERING REFERENCE PROBTYPE = 3 (10:52:30 10/30/95)
DATA POINT LOCATION INPUT FILE: DAMVOL-HOR.INT
PLOTTING DATABASE INPUT FILE: ROOMQ-V0407.PDB
VARIABLE INTERPOLATED OUTPUT FILE: DAMVOL-HOR.TRP

Time	X co-ord.	Y co-ord.	Damage	Inelastic Strain	Volumetric Strain
(years)	(m)	(m)	(DMAGE)	(DMVOL)	(VOLUM)
0.1000E+01	0.1450E+01	-0.3940E+01	0.1260E-03	0.8999E-03	0.1331E-02
0.1000E+01	0.1470E+01	-0.3940E+01	0.1241E-03	0.8544E-03	0.1283E-02
0.1000E+01	0.1500E+01	-0.3940E+01	0.1211E-03	0.7825E-03	0.1206E-02
0.1000E+01	0.1550E+01	-0.3940E+01	0.1153E-03	0.6383E-03	0.1051E-02
0.1000E+01	0.1600E+01	-0.3940E+01	0.1108E-03	0.5063E-03	0.9097E-03
0.1000E+01	0.1650E+01	-0.3940E+01	0.1076E-03	0.4031E-03	0.7969E-03
0.1000E+01	0.1700E+01	-0.3940E+01	0.1055E-03	0.3280E-03	0.7133E-03
0.1000E+01	0.1750E+01	-0.3940E+01	0.1039E-03	0.2605E-03	0.6378E-03
0.1000E+01	0.1800E+01	-0.3940E+01	0.1029E-03	0.2140E-03	0.5845E-03
0.1000E+01	0.1850E+01	-0.3940E+01	0.1020E-03	0.1708E-03	0.5344E-03
0.1000E+01	0.1900E+01	-0.3940E+01	0.1014E-03	0.1339E-03	0.4905E-03
0.1000E+01	0.1950E+01	-0.3940E+01	0.1010E-03	0.1070E-03	0.4573E-03
0.1000E+01	0.2000E+01	-0.3940E+01	0.1007E-03	0.8618E-04	0.4303E-03
0.1000E+01	0.2100E+01	-0.3940E+01	0.1003E-03	0.5346E-04	0.3852E-03
0.1000E+01	0.2200E+01	-0.3940E+01	0.1002E-03	0.3524E-04	0.3575E-03
0.1000E+01	0.2300E+01	-0.3940E+01	0.1001E-03	0.2227E-04	0.3350E-03
0.1000E+01	0.2400E+01	-0.3940E+01	0.1000E-03	0.1380E-04	0.3175E-03
0.1000E+01	0.2500E+01	-0.3940E+01	0.1000E-03	0.8466E-05	0.3035E-03
0.1000E+01	0.2600E+01	-0.3940E+01	0.1000E-03	0.4942E-05	0.2916E-03
0.1000E+01	0.2700E+01	-0.3940E+01	0.1000E-03	0.2936E-05	0.2818E-03
0.1000E+01	0.2800E+01	-0.3940E+01	0.1000E-03	0.1561E-05	0.2728E-03
0.1000E+01	0.2900E+01	-0.3940E+01	0.1000E-03	0.7892E-06	0.2638E-03
0.1000E+01	0.3000E+01	-0.3940E+01	0.1000E-03	0.3426E-06	0.2559E-03
0.1000E+01	0.3100E+01	-0.3940E+01	0.1000E-03	0.1442E-06	0.2488E-03
0.1000E+01	0.3200E+01	-0.3940E+01	0.1000E-03	0.5803E-07	0.2421E-03
0.1000E+01	0.3300E+01	-0.3940E+01	0.1000E-03	0.7143E-08	0.2356E-03

Time	X co-ord.	Y co-ord.	Damage	Inelastic Strain	Volumetric Strain
(years)	(m)	(m)	(DMAGE)	(DMVOL)	(VOLUM)
0.2000E+01	0.1450E+01	-0.3940E+01	0.1435E-03	0.9684E-03	0.1413E-02
0.2000E+01	0.1470E+01	-0.3940E+01	0.1403E-03	0.9198E-03	0.1363E-02
0.2000E+01	0.1500E+01	-0.3940E+01	0.1352E-03	0.8429E-03	0.1282E-02
0.2000E+01	0.1550E+01	-0.3940E+01	0.1254E-03	0.6883E-03	0.1118E-02
0.2000E+01	0.1600E+01	-0.3940E+01	0.1177E-03	0.5465E-03	0.9668E-03
0.2000E+01	0.1650E+01	-0.3940E+01	0.1125E-03	0.4357E-03	0.8465E-03
0.2000E+01	0.1700E+01	-0.3940E+01	0.1091E-03	0.3549E-03	0.7570E-03
0.2000E+01	0.1750E+01	-0.3940E+01	0.1064E-03	0.2823E-03	0.6756E-03
0.2000E+01	0.1800E+01	-0.3940E+01	0.1048E-03	0.2323E-03	0.6189E-03
0.2000E+01	0.1850E+01	-0.3940E+01	0.1034E-03	0.1857E-03	0.5655E-03
0.2000E+01	0.1900E+01	-0.3940E+01	0.1024E-03	0.1458E-03	0.5182E-03
0.2000E+01	0.1950E+01	-0.3940E+01	0.1017E-03	0.1167E-03	0.4823E-03
0.2000E+01	0.2000E+01	-0.3940E+01	0.1012E-03	0.9403E-04	0.4532E-03
0.2000E+01	0.2100E+01	-0.3940E+01	0.1005E-03	0.5840E-04	0.4051E-03
0.2000E+01	0.2200E+01	-0.3940E+01	0.1003E-03	0.3848E-04	0.3744E-03
0.2000E+01	0.2300E+01	-0.3940E+01	0.1001E-03	0.2428E-04	0.3498E-03
0.2000E+01	0.2400E+01	-0.3940E+01	0.1001E-03	0.1501E-04	0.3311E-03
0.2000E+01	0.2500E+01	-0.3940E+01	0.1000E-03	0.9168E-05	0.3166E-03
0.2000E+01	0.2600E+01	-0.3940E+01	0.1000E-03	0.5325E-05	0.3043E-03
0.2000E+01	0.2700E+01	-0.3940E+01	0.1000E-03	0.3148E-05	0.2941E-03
0.2000E+01	0.2800E+01	-0.3940E+01	0.1000E-03	0.1662E-05	0.2849E-03
0.2000E+01	0.2900E+01	-0.3940E+01	0.1000E-03	0.8350E-06	0.2762E-03
0.2000E+01	0.3000E+01	-0.3940E+01	0.1000E-03	0.3584E-06	0.2683E-03
0.2000E+01	0.3100E+01	-0.3940E+01	0.1000E-03	0.1500E-06	0.2611E-03
0.2000E+01	0.3200E+01	-0.3940E+01	0.1000E-03	0.6044E-07	0.2538E-03
0.2000E+01	0.3300E+01	-0.3940E+01	0.1000E-03	0.8336E-08	0.2464E-03

Time	X co-ord.	Y co-ord.	Damage	Inelastic Strain	Volumetric Strain
(years)	(m)	(m)	(DMAGE)	(DMVOL)	(VOLUM)
0.3000E+01	0.1450E+01	-0.3940E+01	0.1587E-03	0.1022E-02	0.1471E-02
0.3000E+01	0.1470E+01	-0.3940E+01	0.1543E-03	0.9708E-03	0.1419E-02
0.3000E+01	0.1500E+01	-0.3940E+01	0.1473E-03	0.8900E-03	0.1335E-02
0.3000E+01	0.1550E+01	-0.3940E+01	0.1338E-03	0.7274E-03	0.1164E-02
0.3000E+01	0.1600E+01	-0.3940E+01	0.1234E-03	0.5779E-03	0.1003E-02
0.3000E+01	0.1650E+01	-0.3940E+01	0.1164E-03	0.4611E-03	0.8785E-03
0.3000E+01	0.1700E+01	-0.3940E+01	0.1119E-03	0.3759E-03	0.7867E-03
0.3000E+01	0.1750E+01	-0.3940E+01	0.1084E-03	0.2993E-03	0.7033E-03
0.3000E+01	0.1800E+01	-0.3940E+01	0.1063E-03	0.2465E-03	0.6438E-03
0.3000E+01	0.1850E+01	-0.3940E+01	0.1045E-03	0.1972E-03	0.5873E-03
0.3000E+01	0.1900E+01	-0.3940E+01	0.1031E-03	0.1550E-03	0.5371E-03
0.3000E+01	0.1950E+01	-0.3940E+01	0.1022E-03	0.1242E-03	0.4994E-03
0.3000E+01	0.2000E+01	-0.3940E+01	0.1016E-03	0.1001E-03	0.4691E-03
0.3000E+01	0.2100E+01	-0.3940E+01	0.1007E-03	0.6225E-04	0.4191E-03
0.3000E+01	0.2200E+01	-0.3940E+01	0.1004E-03	0.4104E-04	0.3876E-03
0.3000E+01	0.2300E+01	-0.3940E+01	0.1002E-03	0.2588E-04	0.3622E-03
0.3000E+01	0.2400E+01	-0.3940E+01	0.1001E-03	0.1597E-04	0.3427E-03
0.3000E+01	0.2500E+01	-0.3940E+01	0.1000E-03	0.9738E-05	0.3277E-03
0.3000E+01	0.2600E+01	-0.3940E+01	0.1000E-03	0.5640E-05	0.3145E-03
0.3000E+01	0.2700E+01	-0.3940E+01	0.1000E-03	0.3323E-05	0.3039E-03
0.3000E+01	0.2800E+01	-0.3940E+01	0.1000E-03	0.1747E-05	0.2944E-03
0.3000E+01	0.2900E+01	-0.3940E+01	0.1000E-03	0.8741E-06	0.2855E-03
0.3000E+01	0.3000E+01	-0.3940E+01	0.1000E-03	0.3725E-06	0.2774E-03
0.3000E+01	0.3100E+01	-0.3940E+01	0.1000E-03	0.1553E-06	0.2698E-03
0.3000E+01	0.3200E+01	-0.3940E+01	0.1000E-03	0.6262E-07	0.2623E-03
0.3000E+01	0.3300E+01	-0.3940E+01	0.1000E-03	0.9439E-08	0.2549E-03

Time (years)	X co-ord. (m)	Y co-ord. (m)	Damage (DMAGE)	Inelastic Strain (DMVOL)	Volumetric Strain (VOLUM)
0.4000E+01	0.1450E+01	-0.3940E+01	0.1731E-03	0.1068E-02	0.1521E-02
0.4000E+01	0.1470E+01	-0.3940E+01	0.1675E-03	0.1015E-02	0.1466E-02
0.4000E+01	0.1500E+01	-0.3940E+01	0.1585E-03	0.9306E-03	0.1379E-02
0.4000E+01	0.1550E+01	-0.3940E+01	0.1414E-03	0.7610E-03	0.1202E-02
0.4000E+01	0.1600E+01	-0.3940E+01	0.1285E-03	0.6052E-03	0.1038E-02
0.4000E+01	0.1650E+01	-0.3940E+01	0.1199E-03	0.4831E-03	0.9070E-03
0.4000E+01	0.1700E+01	-0.3940E+01	0.1144E-03	0.3940E-03	0.8102E-03
0.4000E+01	0.1750E+01	-0.3940E+01	0.1101E-03	0.3140E-03	0.7231E-03
0.4000E+01	0.1800E+01	-0.3940E+01	0.1076E-03	0.2587E-03	0.6615E-03
0.4000E+01	0.1850E+01	-0.3940E+01	0.1054E-03	0.2072E-03	0.6031E-03
0.4000E+01	0.1900E+01	-0.3940E+01	0.1037E-03	0.1629E-03	0.5513E-03
0.4000E+01	0.1950E+01	-0.3940E+01	0.1026E-03	0.1306E-03	0.5123E-03
0.4000E+01	0.2000E+01	-0.3940E+01	0.1019E-03	0.1054E-03	0.4810E-03
0.4000E+01	0.2100E+01	-0.3940E+01	0.1009E-03	0.6553E-04	0.4295E-03
0.4000E+01	0.2200E+01	-0.3940E+01	0.1004E-03	0.4319E-04	0.3969E-03
0.4000E+01	0.2300E+01	-0.3940E+01	0.1002E-03	0.2722E-04	0.3708E-03
0.4000E+01	0.2400E+01	-0.3940E+01	0.1001E-03	0.1678E-04	0.3511E-03
0.4000E+01	0.2500E+01	-0.3940E+01	0.1000E-03	0.1021E-04	0.3359E-03
0.4000E+01	0.2600E+01	-0.3940E+01	0.1000E-03	0.5899E-05	0.3225E-03
0.4000E+01	0.2700E+01	-0.3940E+01	0.1000E-03	0.3468E-05	0.3118E-03
0.4000E+01	0.2800E+01	-0.3940E+01	0.1000E-03	0.1817E-05	0.3022E-03
0.4000E+01	0.2900E+01	-0.3940E+01	0.1000E-03	0.9067E-06	0.2931E-03
0.4000E+01	0.3000E+01	-0.3940E+01	0.1000E-03	0.3843E-06	0.2848E-03
0.4000E+01	0.3100E+01	-0.3940E+01	0.1000E-03	0.1597E-06	0.2771E-03
0.4000E+01	0.3200E+01	-0.3940E+01	0.1000E-03	0.6450E-07	0.2695E-03
0.4000E+01	0.3300E+01	-0.3940E+01	0.1000E-03	0.1042E-07	0.2619E-03

Time	X co-ord.	Y co-ord.	Damage	Inelastic Strain	Volumetric Strain
(years)	(m)	(m)	(DMAGE)	(DMVOL)	(VOLUM)
0.5000E+01	0.1450E+01	-0.3940E+01	0.1873E-03	0.1110E-02	0.1568E-02
0.5000E+01	0.1470E+01	-0.3940E+01	0.1805E-03	0.1055E-02	0.1511E-02
0.5000E+01	0.1500E+01	-0.3940E+01	0.1695E-03	0.9675E-03	0.1420E-02
0.5000E+01	0.1550E+01	-0.3940E+01	0.1488E-03	0.7915E-03	0.1236E-02
0.5000E+01	0.1600E+01	-0.3940E+01	0.1333E-03	0.6296E-03	0.1065E-02
0.5000E+01	0.1650E+01	-0.3940E+01	0.1231E-03	0.5029E-03	0.9307E-03
0.5000E+01	0.1700E+01	-0.3940E+01	0.1167E-03	0.4103E-03	0.8306E-03
0.5000E+01	0.1750E+01	-0.3940E+01	0.1116E-03	0.3271E-03	0.7398E-03
0.5000E+01	0.1800E+01	-0.3940E+01	0.1087E-03	0.2697E-03	0.6758E-03
0.5000E+01	0.1850E+01	-0.3940E+01	0.1062E-03	0.2161E-03	0.6155E-03
0.5000E+01	0.1900E+01	-0.3940E+01	0.1043E-03	0.1700E-03	0.5622E-03
0.5000E+01	0.1950E+01	-0.3940E+01	0.1030E-03	0.1363E-03	0.5222E-03
0.5000E+01	0.2000E+01	-0.3940E+01	0.1022E-03	0.1100E-03	0.4901E-03
0.5000E+01	0.2100E+01	-0.3940E+01	0.1010E-03	0.6843E-04	0.4370E-03
0.5000E+01	0.2200E+01	-0.3940E+01	0.1005E-03	0.4510E-04	0.4035E-03
0.5000E+01	0.2300E+01	-0.3940E+01	0.1002E-03	0.2840E-04	0.3768E-03
0.5000E+01	0.2400E+01	-0.3940E+01	0.1001E-03	0.1748E-04	0.3565E-03
0.5000E+01	0.2500E+01	-0.3940E+01	0.1000E-03	0.1062E-04	0.3409E-03
0.5000E+01	0.2600E+01	-0.3940E+01	0.1000E-03	0.6119E-05	0.3277E-03
0.5000E+01	0.2700E+01	-0.3940E+01	0.1000E-03	0.3590E-05	0.3171E-03
0.5000E+01	0.2800E+01	-0.3940E+01	0.1000E-03	0.1875E-05	0.3075E-03
0.5000E+01	0.2900E+01	-0.3940E+01	0.1000E-03	0.9329E-06	0.2985E-03
0.5000E+01	0.3000E+01	-0.3940E+01	0.1000E-03	0.3935E-06	0.2904E-03
0.5000E+01	0.3100E+01	-0.3940E+01	0.1000E-03	0.1632E-06	0.2830E-03
0.5000E+01	0.3200E+01	-0.3940E+01	0.1000E-03	0.6607E-07	0.2754E-03
0.5000E+01	0.3300E+01	-0.3940E+01	0.1000E-03	0.1139E-07	0.2678E-03

Time	X co-ord.	Y co-ord.	Damage	Inelastic Strain	Volumetric Strain
(years)	(m)	(m)	(DMAGE)	(DMVOL)	(VOLUM)
0.6000E+01	0.1450E+01	-0.3940E+01	0.2013E-03	0.1148E-02	0.1611E-02
0.6000E+01	0.1470E+01	-0.3940E+01	0.1932E-03	0.1092E-02	0.1552E-02
0.6000E+01	0.1500E+01	-0.3940E+01	0.1803E-03	0.1001E-02	0.1457E-02
0.6000E+01	0.1550E+01	-0.3940E+01	0.1559E-03	0.8196E-03	0.1268E-02
0.6000E+01	0.1600E+01	-0.3940E+01	0.1379E-03	0.6522E-03	0.1092E-02
0.6000E+01	0.1650E+01	-0.3940E+01	0.1262E-03	0.5211E-03	0.9521E-03
0.6000E+01	0.1700E+01	-0.3940E+01	0.1188E-03	0.4252E-03	0.8486E-03
0.6000E+01	0.1750E+01	-0.3940E+01	0.1131E-03	0.3392E-03	0.7547E-03
0.6000E+01	0.1800E+01	-0.3940E+01	0.1098E-03	0.2798E-03	0.6885E-03
0.6000E+01	0.1850E+01	-0.3940E+01	0.1069E-03	0.2243E-03	0.6262E-03
0.6000E+01	0.1900E+01	-0.3940E+01	0.1048E-03	0.1765E-03	0.5714E-03
0.6000E+01	0.1950E+01	-0.3940E+01	0.1034E-03	0.1416E-03	0.5301E-03
0.6000E+01	0.2000E+01	-0.3940E+01	0.1024E-03	0.1143E-03	0.4969E-03
0.6000E+01	0.2100E+01	-0.3940E+01	0.1011E-03	0.7109E-04	0.4425E-03
0.6000E+01	0.2200E+01	-0.3940E+01	0.1006E-03	0.4683E-04	0.4087E-03
0.6000E+01	0.2300E+01	-0.3940E+01	0.1003E-03	0.2947E-04	0.3817E-03
0.6000E+01	0.2400E+01	-0.3940E+01	0.1001E-03	0.1811E-04	0.3614E-03
0.6000E+01	0.2500E+01	-0.3940E+01	0.1000E-03	0.1098E-04	0.3458E-03
0.6000E+01	0.2600E+01	-0.3940E+01	0.1000E-03	0.6313E-05	0.3325E-03
0.6000E+01	0.2700E+01	-0.3940E+01	0.1000E-03	0.3694E-05	0.3218E-03
0.6000E+01	0.2800E+01	-0.3940E+01	0.1000E-03	0.1923E-05	0.3122E-03
0.6000E+01	0.2900E+01	-0.3940E+01	0.1000E-03	0.9547E-06	0.3034E-03
0.6000E+01	0.3000E+01	-0.3940E+01	0.1000E-03	0.4010E-06	0.2953E-03
0.6000E+01	0.3100E+01	-0.3940E+01	0.1000E-03	0.1660E-06	0.2879E-03
0.6000E+01	0.3200E+01	-0.3940E+01	0.1000E-03	0.6736E-07	0.2804E-03
0.6000E+01	0.3300E+01	-0.3940E+01	0.1000E-03	0.1227E-07	0.2729E-03

Time	X co-ord.	Y co-ord.	Damage	Inelastic Strain	Volumetric Strain
(years)	(m)	(m)	(DMAGE)	(DMVOL)	(VOLUM)
0.7000E+01	0.1450E+01	-0.3940E+01	0.2151E-03	0.1184E-02	0.1649E-02
0.7000E+01	0.1470E+01	-0.3940E+01	0.2057E-03	0.1126E-02	0.1587E-02
0.7000E+01	0.1500E+01	-0.3940E+01	0.1908E-03	0.1033E-02	0.1489E-02
0.7000E+01	0.1550E+01	-0.3940E+01	0.1628E-03	0.8459E-03	0.1296E-02
0.7000E+01	0.1600E+01	-0.3940E+01	0.1424E-03	0.6734E-03	0.1115E-02
0.7000E+01	0.1650E+01	-0.3940E+01	0.1291E-03	0.5382E-03	0.9717E-03
0.7000E+01	0.1700E+01	-0.3940E+01	0.1208E-03	0.4392E-03	0.8657E-03
0.7000E+01	0.1750E+01	-0.3940E+01	0.1145E-03	0.3505E-03	0.7695E-03
0.7000E+01	0.1800E+01	-0.3940E+01	0.1108E-03	0.2892E-03	0.7018E-03
0.7000E+01	0.1850E+01	-0.3940E+01	0.1076E-03	0.2319E-03	0.6377E-03
0.7000E+01	0.1900E+01	-0.3940E+01	0.1053E-03	0.1826E-03	0.5811E-03
0.7000E+01	0.1950E+01	-0.3940E+01	0.1037E-03	0.1465E-03	0.5385E-03
0.7000E+01	0.2000E+01	-0.3940E+01	0.1026E-03	0.1182E-03	0.5045E-03
0.7000E+01	0.2100E+01	-0.3940E+01	0.1012E-03	0.7354E-04	0.4487E-03
0.7000E+01	0.2200E+01	-0.3940E+01	0.1006E-03	0.4843E-04	0.4137E-03
0.7000E+01	0.2300E+01	-0.3940E+01	0.1003E-03	0.3045E-04	0.3860E-03
0.7000E+01	0.2400E+01	-0.3940E+01	0.1001E-03	0.1869E-04	0.3652E-03
0.7000E+01	0.2500E+01	-0.3940E+01	0.1000E-03	0.1130E-04	0.3492E-03
0.7000E+01	0.2600E+01	-0.3940E+01	0.1000E-03	0.6486E-05	0.3358E-03
0.7000E+01	0.2700E+01	-0.3940E+01	0.1000E-03	0.3787E-05	0.3253E-03
0.7000E+01	0.2800E+01	-0.3940E+01	0.1000E-03	0.1966E-05	0.3160E-03
0.7000E+01	0.2900E+01	-0.3940E+01	0.1000E-03	0.9738E-06	0.3073E-03
0.7000E+01	0.3000E+01	-0.3940E+01	0.1000E-03	0.4073E-06	0.2993E-03
0.7000E+01	0.3100E+01	-0.3940E+01	0.1000E-03	0.1684E-06	0.2919E-03
0.7000E+01	0.3200E+01	-0.3940E+01	0.1000E-03	0.6847E-07	0.2844E-03
0.7000E+01	0.3300E+01	-0.3940E+01	0.1000E-03	0.1307E-07	0.2770E-03

Time	X co-ord.	Y co-ord.	Damage	Inelastic Strain	Volumetric Strain
(years)	(m)	(m)	(DMAGE)	(DMVOL)	(VOLUM)
0.8000E+01	0.1450E+01	-0.3940E+01	0.2292E-03	0.1219E-02	0.1686E-02
0.8000E+01	0.1470E+01	-0.3940E+01	0.2185E-03	0.1159E-02	0.1624E-02
0.8000E+01	0.1500E+01	-0.3940E+01	0.2015E-03	0.1063E-02	0.1524E-02
0.8000E+01	0.1550E+01	-0.3940E+01	0.1697E-03	0.8709E-03	0.1323E-02
0.8000E+01	0.1600E+01	-0.3940E+01	0.1467E-03	0.6934E-03	0.1136E-02
0.8000E+01	0.1650E+01	-0.3940E+01	0.1319E-03	0.5543E-03	0.9893E-03
0.8000E+01	0.1700E+01	-0.3940E+01	0.1228E-03	0.4525E-03	0.8795E-03
0.8000E+01	0.1750E+01	-0.3940E+01	0.1158E-03	0.3611E-03	0.7804E-03
0.8000E+01	0.1800E+01	-0.3940E+01	0.1118E-03	0.2981E-03	0.7109E-03
0.8000E+01	0.1850E+01	-0.3940E+01	0.1083E-03	0.2392E-03	0.6455E-03
0.8000E+01	0.1900E+01	-0.3940E+01	0.1057E-03	0.1883E-03	0.5875E-03
0.8000E+01	0.1950E+01	-0.3940E+01	0.1040E-03	0.1511E-03	0.5442E-03
0.8000E+01	0.2000E+01	-0.3940E+01	0.1029E-03	0.1220E-03	0.5095E-03
0.8000E+01	0.2100E+01	-0.3940E+01	0.1013E-03	0.7585E-04	0.4527E-03
0.8000E+01	0.2200E+01	-0.3940E+01	0.1007E-03	0.4993E-04	0.4170E-03
0.8000E+01	0.2300E+01	-0.3940E+01	0.1003E-03	0.3136E-04	0.3887E-03
0.8000E+01	0.2400E+01	-0.3940E+01	0.1001E-03	0.1922E-04	0.3677E-03
0.8000E+01	0.2500E+01	-0.3940E+01	0.1000E-03	0.1161E-04	0.3521E-03
0.8000E+01	0.2600E+01	-0.3940E+01	0.1000E-03	0.6647E-05	0.3390E-03
0.8000E+01	0.2700E+01	-0.3940E+01	0.1000E-03	0.3873E-05	0.3284E-03
0.8000E+01	0.2800E+01	-0.3940E+01	0.1000E-03	0.2004E-05	0.3188E-03
0.8000E+01	0.2900E+01	-0.3940E+01	0.1000E-03	0.9905E-06	0.3099E-03
0.8000E+01	0.3000E+01	-0.3940E+01	0.1000E-03	0.4126E-06	0.3019E-03
0.8000E+01	0.3100E+01	-0.3940E+01	0.1000E-03	0.1703E-06	0.2946E-03
0.8000E+01	0.3200E+01	-0.3940E+01	0.1000E-03	0.6938E-07	0.2874E-03
0.8000E+01	0.3300E+01	-0.3940E+01	0.1000E-03	0.1384E-07	0.2803E-03

Time	X co-ord.	Y co-ord.	Damage	Inelastic Strain	Volumetric Strain
(years)	(m)	(m)	(DMAGE)	(DMVOL)	(VOLUM)
0.9000E+01	0.1450E+01	-0.3940E+01	0.2432E-03	0.1251E-02	0.1718E-02
0.9000E+01	0.1470E+01	-0.3940E+01	0.2312E-03	0.1190E-02	0.1655E-02
0.9000E+01	0.1500E+01	-0.3940E+01	0.2121E-03	0.1092E-02	0.1553E-02
0.9000E+01	0.1550E+01	-0.3940E+01	0.1765E-03	0.8947E-03	0.1349E-02
0.9000E+01	0.1600E+01	-0.3940E+01	0.1509E-03	0.7125E-03	0.1157E-02
0.9000E+01	0.1650E+01	-0.3940E+01	0.1347E-03	0.5697E-03	0.1006E-02
0.9000E+01	0.1700E+01	-0.3940E+01	0.1247E-03	0.4652E-03	0.8942E-03
0.9000E+01	0.1750E+01	-0.3940E+01	0.1171E-03	0.3713E-03	0.7925E-03
0.9000E+01	0.1800E+01	-0.3940E+01	0.1127E-03	0.3066E-03	0.7217E-03
0.9000E+01	0.1850E+01	-0.3940E+01	0.1089E-03	0.2461E-03	0.6549E-03
0.9000E+01	0.1900E+01	-0.3940E+01	0.1061E-03	0.1938E-03	0.5959E-03
0.9000E+01	0.1950E+01	-0.3940E+01	0.1043E-03	0.1555E-03	0.5513E-03
0.9000E+01	0.2000E+01	-0.3940E+01	0.1031E-03	0.1255E-03	0.5156E-03
0.9000E+01	0.2100E+01	-0.3940E+01	0.1014E-03	0.7804E-04	0.4570E-03
0.9000E+01	0.2200E+01	-0.3940E+01	0.1007E-03	0.5136E-04	0.4209E-03
0.9000E+01	0.2300E+01	-0.3940E+01	0.1003E-03	0.3223E-04	0.3923E-03
0.9000E+01	0.2400E+01	-0.3940E+01	0.1001E-03	0.1973E-04	0.3709E-03
0.9000E+01	0.2500E+01	-0.3940E+01	0.1001E-03	0.1189E-04	0.3548E-03
0.9000E+01	0.2600E+01	-0.3940E+01	0.1000E-03	0.6796E-05	0.3415E-03
0.9000E+01	0.2700E+01	-0.3940E+01	0.1000E-03	0.3952E-05	0.3310E-03
0.9000E+01	0.2800E+01	-0.3940E+01	0.1000E-03	0.2039E-05	0.3217E-03
0.9000E+01	0.2900E+01	-0.3940E+01	0.1000E-03	0.1006E-05	0.3130E-03
0.9000E+01	0.3000E+01	-0.3940E+01	0.1000E-03	0.4175E-06	0.3051E-03
0.9000E+01	0.3100E+01	-0.3940E+01	0.1000E-03	0.1723E-06	0.2977E-03
0.9000E+01	0.3200E+01	-0.3940E+01	0.1000E-03	0.7037E-07	0.2903E-03
0.9000E+01	0.3300E+01	-0.3940E+01	0.1000E-03	0.1460E-07	0.2829E-03

Time	X co-ord.	Y co-ord.	Damage	Inelastic Strain	Volumetric Strain
(years)	(m)	(m)	(DMAGE)	(DMVOL)	(VOLUM)
0.1000E+02	0.1450E+01	-0.3940E+01	0.2573E-03	0.1282E-02	0.1752E-02
0.1000E+02	0.1470E+01	-0.3940E+01	0.2440E-03	0.1220E-02	0.1687E-02
0.1000E+02	0.1500E+01	-0.3940E+01	0.2227E-03	0.1120E-02	0.1583E-02
0.1000E+02	0.1550E+01	-0.3940E+01	0.1831E-03	0.9174E-03	0.1373E-02
0.1000E+02	0.1600E+01	-0.3940E+01	0.1551E-03	0.7308E-03	0.1177E-02
0.1000E+02	0.1650E+01	-0.3940E+01	0.1374E-03	0.5845E-03	0.1022E-02
0.1000E+02	0.1700E+01	-0.3940E+01	0.1265E-03	0.4773E-03	0.9078E-03
0.1000E+02	0.1750E+01	-0.3940E+01	0.1183E-03	0.3811E-03	0.8046E-03
0.1000E+02	0.1800E+01	-0.3940E+01	0.1136E-03	0.3147E-03	0.7312E-03
0.1000E+02	0.1850E+01	-0.3940E+01	0.1095E-03	0.2526E-03	0.6622E-03
0.1000E+02	0.1900E+01	-0.3940E+01	0.1065E-03	0.1990E-03	0.6020E-03
0.1000E+02	0.1950E+01	-0.3940E+01	0.1046E-03	0.1597E-03	0.5570E-03
0.1000E+02	0.2000E+01	-0.3940E+01	0.1033E-03	0.1289E-03	0.5209E-03
0.1000E+02	0.2100E+01	-0.3940E+01	0.1015E-03	0.8015E-04	0.4614E-03
0.1000E+02	0.2200E+01	-0.3940E+01	0.1008E-03	0.5271E-04	0.4244E-03
0.1000E+02	0.2300E+01	-0.3940E+01	0.1003E-03	0.3305E-04	0.3953E-03
0.1000E+02	0.2400E+01	-0.3940E+01	0.1001E-03	0.2020E-04	0.3736E-03
0.1000E+02	0.2500E+01	-0.3940E+01	0.1001E-03	0.1216E-04	0.3571E-03
0.1000E+02	0.2600E+01	-0.3940E+01	0.1000E-03	0.6933E-05	0.3435E-03
0.1000E+02	0.2700E+01	-0.3940E+01	0.1000E-03	0.4024E-05	0.3331E-03
0.1000E+02	0.2800E+01	-0.3940E+01	0.1000E-03	0.2071E-05	0.3239E-03
0.1000E+02	0.2900E+01	-0.3940E+01	0.1000E-03	0.1020E-05	0.3153E-03
0.1000E+02	0.3000E+01	-0.3940E+01	0.1000E-03	0.4219E-06	0.3074E-03
0.1000E+02	0.3100E+01	-0.3940E+01	0.1000E-03	0.1738E-06	0.3001E-03
0.1000E+02	0.3200E+01	-0.3940E+01	0.1000E-03	0.7113E-07	0.2929E-03
0.1000E+02	0.3300E+01	-0.3940E+01	0.1000E-03	0.1528E-07	0.2858E-03

Federal Agencies

US Department of Energy (4)
Office of Civilian Radioactive Waste Mgmt.
Attn: Deputy Director, RW-2
  Acting Director, RW-10
   Office of Human Resources & Admin.
  Director, RW-30
   Office of Program Mgmt. & Integ.
  Director, RW-40
   Office of Waste Accept., Stor., & Tran.
Forrestal Building
Washington, DC 20585

Attn: Project Director
Yucca Mountain Site Characterization Office
   Director, RW-3
   Office of Quality Assurance
P.O. Box 30307
Las Vegas, NV 89036-0307

US Department of Energy
Albuquerque Operations Office
Attn: National Atomic Museum Library
P.O. Box 5400
Albuquerque, NM 87185-5400

US Department of Energy
Research & Waste Management Division
Attn: Director
P.O. Box E
Oak Ridge, TN 37831

US Department of Energy (5)
Carlsbad Area Office
Attn: G. Dials
  D. Galbraith
  M. McFadden
  R. Lark
  J. A. Mewhinney
P.O. Box 3090
Carlsbad, NM 88221-3090

US Department of Energy
Office of Environmental Restoration and
 Waste Management
Attn: M. Frei, EM-30
Forrestal Building
Washington, DC 20585-0002

US Department of Energy (3)
Office of Environmental Restoration and
 Waste Management
Attn: J. Juri, EM-34, Trevion II
Washington, DC 20585-0002

US Department of Energy
Office of Environmental Restoration and
 Waste Management
Attn: S. Schneider, EM-342, Trevion II
Washington, DC 20585-0002

US Department of Energy (2)
Office of Environment, Safety & Health
Attn: C. Borgstrom, EH-25
  R. Pelletier, EH-231
Washington, DC 20585

US Department of Energy (2)
Idaho Operations Office
Fuel Processing & Waste Mgmt. Division
785 DOE Place
Idaho Falls, ID 83402

US Environmental Protection Agency (2)
Radiation Protection Programs
Attn: M. Oge
ANR-460
Washington, DC 20460

Boards

Defense Nuclear Facilities Safety Board
Attn: D. Winters
625 Indiana Ave. NW, Suite 700
Washington, DC 20004

Nuclear Waste Technical Review Board (2)
Attn: Chairman
  J. L. Cohon
1100 Wilson Blvd., Suite 910
Arlington, VA 22209-2297

State Agencies

Attorney General of New Mexico
P.O. Drawer 1508
Santa Fe, NM 87504-1508

Environmental Evaluation Group (3)
Attn: Library
7007 Wyoming NE
Suite F-2
Albuquerque, NM 87109

NM Energy, Minerals, and Natural
Resources Department
Attn: Library
2040 S. Pacheco
Santa Fe, NM 87505

NM Environment Department (3)
Secretary of the Environment
Attn: Mark Weidler
1190 St. Francis Drive
Santa Fe, NM 87503-0968

NM Bureau of Mines & Mineral Resources
Socorro, NM 87801

Laboratories/Corporations

Battelle Pacific Northwest Laboratories
Battelle Blvd.
Richland, WA 99352

INTERA, Inc. (3)
Attn: G. A. Freeze
1650 University Blvd. NE, Suite 300
Albuquerque, NM 87102

INTERA, Inc.
Attn: J. F. Pickens
9117 Research Bld.
Austin TX 78758

INTERA, Inc.
Attn: W. Stensrud
P.O. Box 2123
Carlsbad, NM 88221

Los Alamos National Laboratory
Attn: B. Erdal, INC-12
P.O. Box 1663
Los Alamos, NM 87544

RE/SPEC, Inc
Attn: Angus Robb
4775 Indian School NE, Suite 300
Albuquerque, NM 87110-3927

RE/SPEC, Inc
Attn: J. L. Ratigan
P.O. Box 725
Rapid City, SD 57709

Tech Reps, Inc. (3)
Attn: J. Chapman (1)
        Loretta Robledo (2)
5000 Marble NE, Suite 222
Albuquerque, NM 87110

Westinghouse Electric Corporation (5)
Attn: Library
        J. Epstein
        J. Lee
        B. A. Howard
        R. Kehrman
P.O. Box 2078
Carlsbad, NM 88221

S. Cohen & Associates
Attn: Bill Thurber
1355 Beverly Road
McLean, VA 22101

National Academy of Sciences,
WIPP Panel

Howard Adler
Oxyrase, Incorporated
7327 Oak Ridge Highway
Knoxville, TN 37931

Tom Kiess
Board of Radioactive Waste Management
GF456
2101 Constitution Ave.
Washington, DC 20418

Rodney C. Ewing
Department of Geology
University of New Mexico
Albuquerque, NM 87131

Charles Fairhurst
Department of Civil and Mineral Engineering
University of Minnesota
500 Pillsbury Dr. SE
Minneapolis, MN 55455-0220

B. John Garrick
PLG Incorporated
4590 MacArthur Blvd., Suite 400
Newport Beach, CA 92660-2027

Leonard F. Konikow
US Geological Survey
431 National Center
Reston, VA 22092

Carl A. Anderson, Director
Board of Radioactive Waste Management
National Research Council
HA 456
2101 Constitution Ave. NW
Washington, DC 20418

Christopher G. Whipple
ICF Kaiser Engineers
1800 Harrison St., 7th Floor
Oakland, CA 94612-3430

John O. Blomeke
720 Clubhouse Way
Knoxville, TN 37909

Sue B. Clark
University of Georgia
Savannah River Ecology Lab
P.O. Drawer E
Aiken, SC 29802

Konrad B. Krauskopf
Department of Geology
Stanford University
Stanford, CA 94305-2115

Della Roy
Pennsylvania State University
217 Materials Research Lab
Hastings Road
University Park, PA 16802

David A. Waite
CH$_2$ M Hill
P.O. Box 91500
Bellevue, WA 98009-2050

Thomas A. Zordon
Zordon Associates, Inc.
3807 Edinburg Drive
Murrysville, PA 15668

Universities

University of New Mexico
Geology Department
Attn: Library
141 Northrop Hall
Albuquerque, NM 87131

University of Washington
College of Ocean & Fishery Sciences
Attn: G. R. Heath
583 Henderson Hall, HN-15
Seattle, WA 98195

Libraries

Thomas Brannigan Library
Attn: D. Dresp
106 W. Hadley St.
Las Cruces, NM 88001

Government Publications Department
Zimmerman Library
University of New Mexico
Albuquerque, NM 87131

New Mexico Junior College
Pannell Library
Attn: R. Hill
Lovington Highway
Hobbs, NM 88240

New Mexico State Library
Attn: N. McCallan
325 Don Gaspar
Santa Fe, NM 87503

New Mexico Tech
Martin Speere Memorial Library
Campus Street
Socorro, NM 87810

WIPP Public Reading Room
Carlsbad Public Library
101 S. Halagueno St.
Carlsbad, NM 88220

Foreign Addresses

Atomic Energy of Canada, Ltd.
Whiteshell Laboratories
Attn: B. Goodwin
Pinawa, Manitoba, CANADA R0E 1L0

Francois Chenevier (2)
ANDRA
Route de Panorama Robert Schumann
B. P. 38
92266 Fontenay-aux-Roses, Cedex
FRANCE

Claude Sombret
Centre d'Etudes Nucleaires de la Vallee Rhone
CEN/VALRHO
S.D.H.A. B.P. 171
30205 Bagnols-Sur-Ceze, FRANCE

Commissariat a L'Energie Atomique
Attn: D. Alexandre
Centre d'Etudes de Cadarache
13108 Saint Paul Lez Durance Cedex
FRANCE

Bundesanstalt fur Geowissenschaften und
Rohstoffe
Attn: M. Langer
Postfach 510 153
D-30631 Hannover, GERMANY

Bundesministerium fur Forschung und
Technologie
Postfach 200 706
5300 Bonn 2, GERMANY

Institut fur Tieflagerung
Attn: K. Kuhn
Theodor-Heuss-Strasse 4
D-3300 Braunschweig, GERMANY

Gesellschaft fur Anlagen und Reaktorsicherheit
(GRS)
Attn: B. Baltes
Schwertnergasse 1
D-50667 Cologne, GERMANY

Shingo Tashiro
Japan Atomic Energy Research Institute
Tokai-Mura, Ibaraki-Ken, 319-11
JAPAN

Netherlands Energy Research Foundation ECN
Attn: J. Prij
3 Westerduinweg
P.O. Box 1
1755 ZG Petten
THE NETHERLANDS

Svensk Karnbransleforsorjning AB
Attn: F. Karlsson
Project KBS (Karnbranslesakerhet)
Box 5864
S-102 48 Stockholm
SWEDEN

Nationale Genossenschaft fur die Lagerung
Radioaktiver Abfalle (2)
Attn: S. Vomvoris
       P. Zuidema
Hardstrasse 73
CH-5430 Wettingen
SWITZERLAND

AEA Technology
Attn: J. H. Rees
D5W/29 Culham Laboratory
Abington, Oxfordshire OX14 3DB
UNITED KINGDOM

AEA Technology
Attn: W. R. Rodwell
044/A31 Winfrith Technical Centre
Dorchester, Dorset DT2 8DH
UNITED KINGDOM

AEA Technology
Attn: J. E. Tinson
B4244 Harwell Laboratory
Didcot, Oxfordshire OX11 0RA
UNITED KINGDOM

Internal

MS	Org.	
1324	6115	P. B. Davies
1320	6831	E. J. Nowak
1322	6121	J. R. Tillerson
1328	6849	D. R. Anderson
1328	6848	H. N. Jow
1335	6801	M. Chu
1341	6832	J. T. Holmes
1395	6800	L. Shephard
1395	6821	M. Marietta
1395	6841	V. H. Slaboszewicz
1324	6115	T. L. Christian-Frear (10)

1324	6115	S. W. Webb (3)
1330	6811	K. Hart (2)
1330	4415	NWM Library (20)
9018	8940-2	Central Technical Files
0899	4414	Technical Library (5)
0619	12690	Review and Approval Desk (2), For DOE/OSTI